# Thermoelectrochemistry
## potential application of gelled electrolytes, gold nanoparticles and novel redox systems

Alzahrani, Hassan

*Awarding institution:*
King's College London

# Thermoelectrochemistry: Potential application of gelled electrolytes, gold nanoparticles and novel redox systems

A thesis submitted in fulfilment of the requirements for the degree of

**PhD of Science in Chemistry**

by

*Hassan Abdullah Alzahrani*

in the

Department of Chemistry

Supervised by

*Dr. Leigh Aldous*

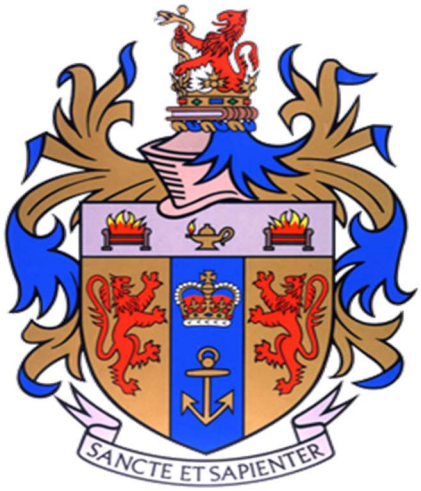


King's College London

London, UK

May, 2019

## *Table of Contents*

## *Preface*

This thesis is a report of original research undertaken by the author and is submitted in partial fulfilment for the degree of **Doctor of Science** (PhD) at King's College London. The work was performed partially in the School of Chemistry at UNSW Sydney and partially in the Department of Chemistry at King's College London, during the period from September 2015 to April 2019. The results presented in this thesis are those of the author, unless otherwise acknowledged.

Hassan Alzahrani

May 2019

## *Acknowledgements*

It was a great experience to study my PhD in two different countries (Australia and UK), with a great understanding of how scientific research is conducted. I would like to thank everyone who I had come across in my PhD's degree.

First, I would like to show my sincere appreciation to my supervisor Dr Leigh Aldous for his patience and tremendous effort taken in planning my PhD project with me, and guiding me throughout during the PhD's degree until its completion. Although there were difficulties accounted, Dr Aldous was always supportive and enthusiastic at answering nicely all my enquiries, which helps the project to be conducted more smoothly. It would not be possible to complete the work without his help support, and encouragement.

Next. I would like to express my appreciation and respect to my colleague Mark Buckingham, for his honest friendship his kindness, help and support that he gave since I have started my study in UK , I'm so proud and happy to know him during my study in UK. I would like too to thank all members in Aldous Group for their help, patience, and guidance. Also I want to send thank and love to all my family and friends for their support, help, and prays for me. A very special shout out goes to people that I have worked with and met in Australia and UK.

Last, but not least, I would deeply extend my thank and condolences too to all soldiers and martyrs in the army of my country, so thank to them for the safety, security, and protect that we see, feel, enjoy and live it in back home.

## ***Journal articles***

- H. A. Alzahrani *et al.,* 'Success and failure in the incorporation of gold nanoparticles inside ferri/ferrocyanide thermogalvanic cells' in *Electrochemistry Communications* **2019**, *102*, 41-45.
- H. A. Alzahrani *et al.,* 'Electrodeposition of vanadium oxide and consequent behaviour as thermogalvanically chargable aqueous sodium ion 'entropy' batteries', submitted for publication
- H. A. Alzahrani *et al.,* 'Gold nanoparticles immobilised in superabsorbent polymer: Synthesis and application for the catalytic removal of toxic compounds', submitted for publication

## ***Conference presentations***

- Poster entitled "Gold Nanoparticle-Containing Super-Adsorbent Gels: Towards Enhanced Charge Propagation", Hassan A. H. Alzahrani, *Electrochemistry at Nano-interfaces: Faraday Discussion",* ***26th-28th June 2018***, Bath, UK
- Presentation entitled "Thermoelectrochemical cells for waste heat harvesting", Hassan A. H. Alzahrani, 3rd *Saudi Scientific Symposium in Sydney*, ***18th August 2018***, Sydney, Australia.
- Discussed results at the "Entrepreneurship & Innovation in Hajj and Umrah" which was held in **20th *Jan 2019***, Jeddah, Kingdom of Saudi Arabia.

Chapter 1

# Introduction

## Energy issues

In the 21st century, it has been discovered that energy reserves (primarily fossil fuels) keep on diminishing at an overwhelming rate. This has been attributed to the increased use of machinery in the motor industry and manufacturing sector. The reserves (of fossil fuels) are burned to release energy which power engines to aid production. Without due regard, the quantities of these energy sources are diminishing rapidly without replenishment, meaning more reliance on 'renewable energy' as a main source of energy.

Fossil fuels provide the main source of energy. Its demand is rated at over seventy per cent of all energy used [1] this implies that continuity in its use - where there is no hope of replenishment - holds the world's economy at risk.

Hydroelectric power, wind, geothermal, are all forms of renewable energy which collectively account for 14.1% of the total world energy supply. Nevertheless, efforts to increase production of renewable energy have been overturned for social-cultural reasons.[1,2] Religious beliefs have also played a major role in a decreased rate of renewable energy technology uptake .[2-4]

A snapshot of the breakdown of the world's primary energy production is shown, by percentages, in Figure 1.

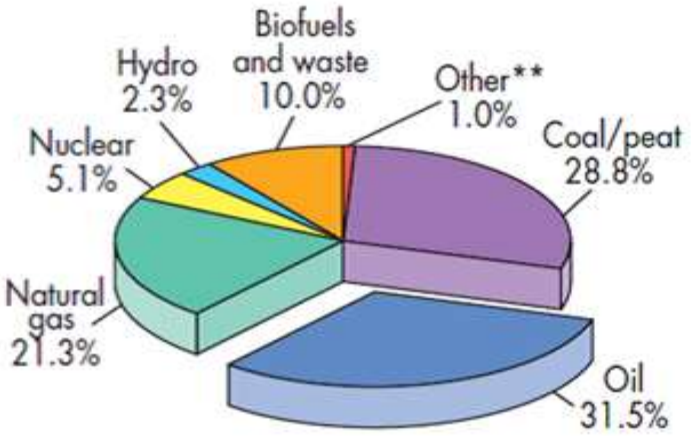


**Fig.1:** *Total world's primary energy production 2014.* [3]

Environmental impact implications of fossil fuels are another important aspect to consider. Methane gas emission and carbon dioxide are both greenhouse gases that foster global warming *via* the greenhouse effect .[5-7]

Ninety five per cent of scientists across the globe believe most of emissions resulting to the greenhouse effect comes from human activities.[8-10] Main industrial human activities accounting to these effects are produced by the energy sector, manufacturing industry (sugar, paper, *etc*),[11,12] and the mining industry.[13,14] This has been agreed to

increase levels of carbon dioxide in the atmosphere exponentially, to levels not seen before in over the past 800,000 years (over several glacial periods) (Figure.2) .[15,16] The main challenge is that carbon dioxide ($CO_2$) does not decompose, and $CO_2$ is well-known to exhibit the greenhouse effect.[6,15] Excess $CO_2$ released by non-natural (*i.e.* human activity) stays in the atmosphere, where a small proportion is absorbed by the oceans and vegetation, but much is retained in the atmosphere. For example, in 2018 $CO_2$ levels jumped to 407.4 parts per million (ppm), after $CO_2$ levels had remained constant at around 280 ppm from 2500 years to 400 years before present. This has stimulated a rise in atmospheric temperatures, this is known global warming.[17]

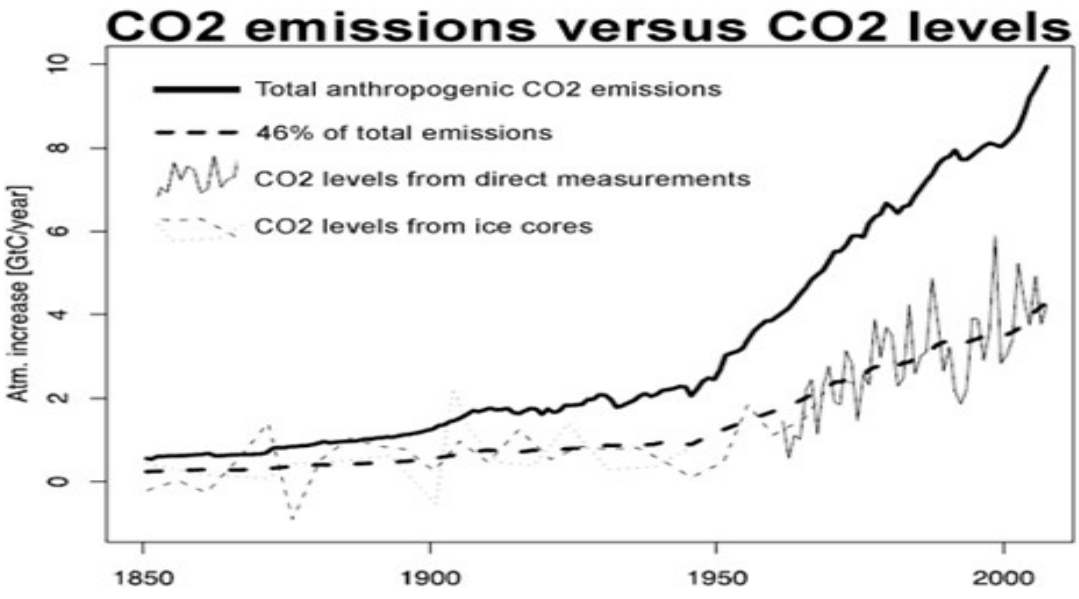


**Fig.2** *Observed increase atmospheric CO2 with time.*[16]

According to NASA Goddard's Institute for Space Studies (GISS), it has been withheld that the concurrently rising temperatures of the atmosphere is the main cause of global surface temperate change.[18-20] This is clarified by the GISS surface temperature analysis (GISTEMP) model (Figure 3). Lowes's smoothing model, also known as LOWESS (Locally Weighted Scatterplot Smoothing), is used to identify overall trends spanning several years from relatively variable annual data. From this the world's record of average ocean-land temperature, temperature has been found to be 0.86 $^{0}$C higher than pre-industrial levels. Basically, Lowess Smoothing is a regression technique that creates to smooth line to help demonstrate the relationship between the variable and foresee trends; its use of near neighbor values is ideal for seasonal data, and it has proven effectiveness for extracting genuine trends from noisy data.

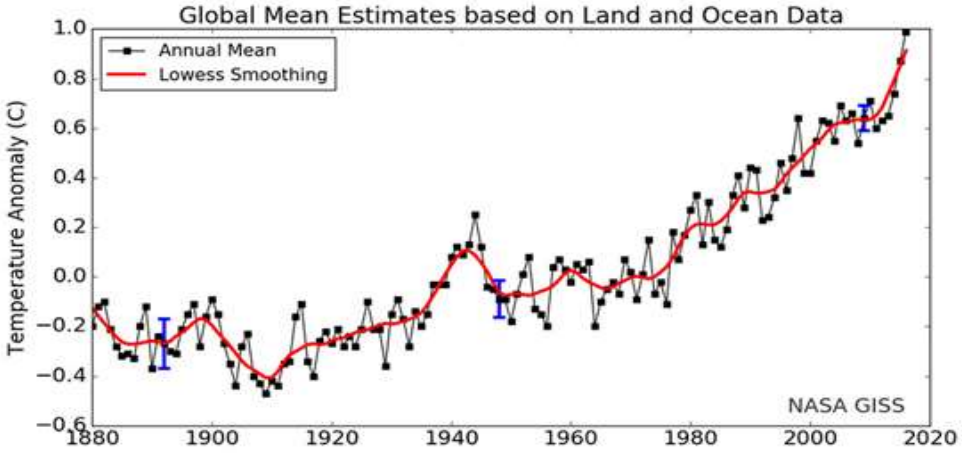


**Fig. 3:** *The world's ocean and land mean temperature data from 1880 to date. The five-year Lowess smooth line is represented by a bold red line and the global annual mean by a thin black line* [19]

During the 21st Conference of the Parties of the United Nations Framework Convention on Climate Change (UNFCCC) in Paris,[4] it was tabled, climatic temperatures should be kept less than 1.5 $^{0}$C above pre-industrial levels,[4] ; any increase at 2 $^{0}$C should not be allowed, the agreement was a benchmark to mitigate against adverse environmental effects of greenhouse gases emission. However, it was found not to be easy to maintain emissions below 2 $^{0}$C to that of pre-industrial levels withholding a negative emission rate. This requires a holistic planet-wide action and commitment of the associated sectors. The reason is that there may be a possibility of delayed action, and high mitigation costs required, this is forecasted to demand a lot from the world economy.[5,6] Also, it means that a requirement to cut down many industrial activities that contribute significantly to the world's economy. Thus it is vital that the world mitigates and curbs the emission of greenhouse gases to at the very least halt global warming.

Identified techniques include harvesting of waste heat from industries,[7,8] and converting this heat into more useful forms of energy such as electricity.[8,9] Sources of waste heat are very diverse. Some emanate from burning of fuels in households or industries, or waste body heat (human body), this waste heat is currently lost to the atmosphere. Due to the many sources of waste heat, and the current lack of utilisation of the potential energy source, its utilisation will not only improve the performance of the world's economies, but also reduce the use of fossil fuels.[9,37]

## Waste heat recovery

The extent to which waste heat energy can be restored will depend on challenges presented by the changing environmental temperatures.[9,10] Typically, the performance of waste heat recovery technology also depends upon the magnitude of the heat source. This gives a basis on which waste heat may be classified.[10] It can thus be grouped or categorised referring to the temperatures of the heat source:

1. Low grade waste heat: 450 ºF [232ºC] and below
2. Medium grade waste heat: 450 ºF [232ºC] to 1200 ºF [650ºC]
3. High grade waste heat: 1200 ºF [650ºC] and above

There are the traditional means of energy generation, but have been developed to generate massive mechanical energy, which is transformed to electrical energy.[10] Mechanical energy has been a pathway in which waste heat energy can be transformed from medium to high grade waste heat. This is undertaken by the waste heat being used to vaporise a fluid, which in turn is used to turn turbines to generate energy.[11] The type of turbine fluid is dependent on the mode and kind of energy to be generated by the system. In the Rankine cycle, water is used as the vaporised fluid,[10] in organic cycles,

silicon oil, toluene and propane are the fluid of choice [10,11] and the Kalina cycle employs a water-ammonia mixture as the fluid. [10]

Recently, increasing effort has been dedicated towards the direct conversion of energy into electrical energy without using mechanical energy. These efforts involve technologies such as thermionic,[21] thermo-photo-voltaic,[22] thermo-electrochemical,[8,23] and thermoelectric generators.[24]

For elevated temperature ranges (800-1000ºC) ThermoPhotoVoltaic (TPV) generators are considered the most efficient. These generators comprise of an emitter (the heat source), a photovoltaic (PV) cell and a radiation filter. [11,22] The radiation is emitted from a heat source; the radiation either passes through a filter to a photovoltaic cell (if the electromagnetic radiation is a photon with appropriate wavelength to be absorbed by the photovoltaic cell) or is reflected by the filter back towards the emitter (i.e. wavelength unable to be absorbed by the photocell).Therefore, the photovoltaic cell converts that radiation into electrical energy and the filter passes the radiation that matches the PV cell while reflection back to the emitter. Thus electricity is generated by the heat source.[21,25]

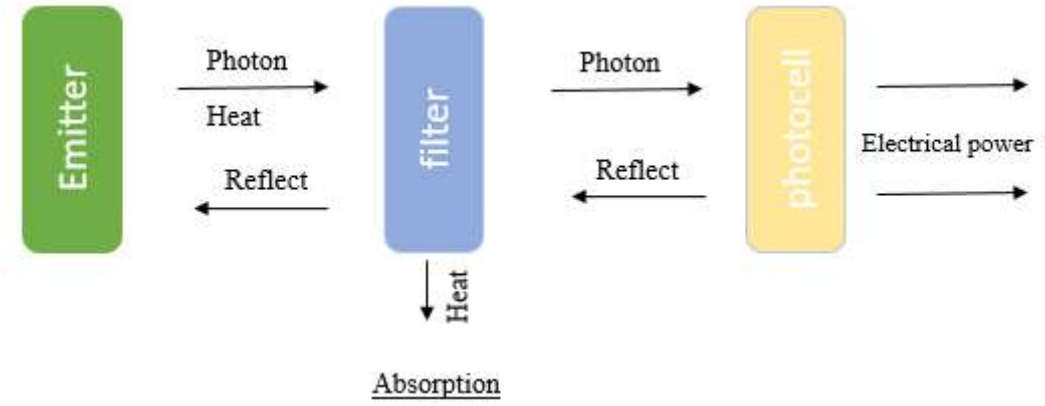


**Fi 4**. *Block diagram of thermophotovoltaics*

## Thermoelectric Generators

Thermoelectric generators are one such device that converts heat into electricity. These are solid state materials that utilise the Seebeck effect [9,26] which is the generation electron-hole pairs to obtain electricity from a temperature gradient (explained in more detail later). However, they suffer from high temperature resistance and high synthetic cost, therefore thermoelectric devices have mostly been restricted to space exploration or probes.[27,28] Research endeavours suggest that thermoelectric generators are more suitable for small end products rather than primary energy generation, based upon a relatively lower efficiency compared to other techniques mentioned above. [27,29] Although their efficiency is low, these thermoelectric generators are still good candidates for thermal energy conversion due to features and characteristics such as scalability, compactness and affordability, and the device size can be tailored to fit the

heat source.[30] These devices display the worthiness for recovering waste heat from various sources. Some have already been manufactured, such as in wristwatches [31,32] that are powered by waste heat from the human body. Thermoelectric generators convert heat into power through a temperature gradient in accord with the Seebeck effect [31,33] *via* the Seebeck coefficient.[8]

## Thermoelectric Effects and the Seebeck coefficient

Like many scientific breakthroughs, the discovery of the thermoelectric phenomenon was the product of many researchers. For thermoelectrics, it took the work of three individuals, Thomas Seebeck, Jean Charles Peltier, and William Thomson to fully describe the observed phenomena of thermoelectric materials. They rationalised three notable effects, which individually are known as the Seebeck Effect,[31] Peltier Effect, [35] and Thomson Effect. [29,35] With these individual effects combined in the Kelvin Relationship, the thermoelectric figure-of-merit was later developed as a means to quantitatively compare thermoelectric materials.[26,36]

The Seebeck effect is the direct conversion of temperature differences to electricity, and is notable by a measurable voltage difference being observed across a temperature difference (discussed more below). Complementing to Seebeck effect, Peltier effect

represents heat transport through electrified conductors. It denotes the amount of heat carried by each charge units. So, both the Seebeck and Peltier effects combine into such state where Seeback effect causes charge transfer and causes heat, and that heat can be deliberately transferred from hot to cold zone by the Peltier effect. The Thomson effect furthers enriches the understanding of the above two effects, as it centers on the concept of introducing spatial gradient for Seebeck effect where temperature keeps fluctuating.

In 1821, the Baltic-German physicist Thomas Johann Seebeck reported his observations of a compass needle placed in the vicinity of a closed loop of two dissimilar conductors, and when one of the junctions was heated, a voltage was produced.[29] While he falsely concluded that the interaction was a magnetic phenomenon, he did go on to investigate a wide variety of other materials that observed the same effect, including materials now classified as semiconductors, [27] ultimately, this interaction was called the Seebeck effect.

Thermoelectrics operate on the principle of Seebeck effect, in other words converting a temperature difference into electricity. They typically contain two types of semiconducting materials; n-type (free electrons) and p-type (free holes). When temperature is applied, the charge carriers can move to diffuse from one temperature

to the other; the tendency of this to occur depends upon both relative mobility and the temperature effect upon the electronic structure of the material; an electric field gradient thus forms across an applied temperature difference, and this is quantified as the Seebeck Coefficient (Eq. 1), such that

$$S_e = \Delta E/\Delta T \quad \textbf{(1)}$$

where $S_e$ is the Seebeck coefficient, $\Delta E$ is the potential difference across two points, and $\Delta T$ is the temperature between these points.[9] In the past this was more broadly defined as the thermoelectromotive force. The current generated by this flow of electrons is proportional to the number and mobility of the charge carriers, which depends upon the degree of doping and bulk electronic structure, respectively.

In a conducting material such as a metal chalcogenide, charge carriers will generally travel from the hot side to the cool side of the material,[8,37] until an equilibrium electrical potential is reached. This effect, illustrated in Figure 5. Further increasing the temperature of the hot side will increase the number of charge carriers that to the cool side, establishing a higher potential difference.

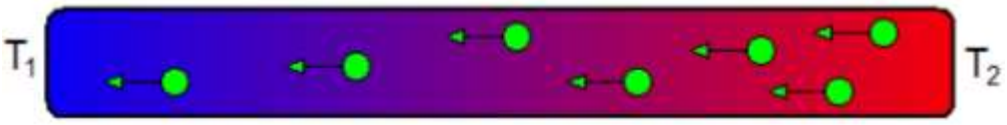


**Fig. 5:** *In this example, the temperature of $T_2$ is higher than that of $T_1$ ($T_2$ hot > $T_1$ cold), and the green circles are the charge carriers. The temperature gradient causes these charge carriers (electrons or holes depending on the material) to move toward the cool side and establish a new equilibrium potential in the material.*

To describe this effect, a mathematical approach was required, therefore the Seebeck coefficient, $S_e$, was derived. [8,9,27,38] This coefficient is defined as the ratio of the electromotive force, with respect to the temperature difference. The Seebeck coefficient for thermoelectric devices are typically between 100-300 μV/K. [9,38] Fundamentally, the Seebeck coefficient measures the entropy transported with a charge carrier as it moves through the material.

The sign of the Seebeck coefficient is determined by the direction of current flow, resulting in 'n-type' and 'p-type' thermoelectric systems,[27,28] where an n-type represents an electron conductor and a p-type a hole conductor. This is an intrinsic property of the system.

However, a direct measurement of the Seebeck coefficient is not routinely undertaken, and when performed and must be performed carefully. This is since all conducting materials exhibit some degree of a thermoelectric effect, with the exception being superconductors below their transition temperature.[28]

## The Thermoelectric Phenomenon: Figure of Merit

At the beginning of the 20th century, the field of thermoelectrics received increasing attention. The physicist Edmund Altenkirch was able to qualify the parameters required for good thermoelectric materials; namely that they should have a low thermal conductivity, to retain and keep the temperature difference across the two junctions, a large Seebeck coefficient, and a low electrical resistance in order to minimise resistive heating.

Broadly, the efficiency of a thermoelectric device is given by the electrical energy supplied by the device, divided by the heat absorbed at the hot junction. However, this requires careful and accurate measurement of both. A quantitative comparison between different materials was thus developed as a means to evaluate materials and compare their (relative) thermoelectric efficiency. This resulted in the introduction of the

dimensionless Figure of Merit (or ZT). It quantitatively characterises a predictor of the performance of a thermoelectric energy generator, based upon a few physical properties. The ZT is calculated by the following Eq. 2 relationship:

$$ZT = \sigma S_e^2 T/\lambda \quad \textbf{(2)}$$

where σ is the ohmic conductivity, $S_e$ is the Seebeck coefficient, T is the temperature, and λ is the thermal conductivity.

Broadly, it has been stated that a ZT > 1 is required to be viable as a commercial device, and a ZT of 2.4 is the highest value ever recorded at room temperature.[8,27,35,39]

## Thermoelectric cell design and potential applications

A key factor of thermoelectric design are the two thermal-to-device interfaces. Here, the role of these thermal-to-device interfaces (called heat exchangers for simplicity) is to positively influence heat absorbency at the intended hotter junction, and encourage rejection of transported heat at the colder junction. If the heat exchangers are bigger than the thermoelectric generators, then the devices efficiency could be compromised. Therefore maximum power generation will typically require device size and heat exchanger to be equal.[39]

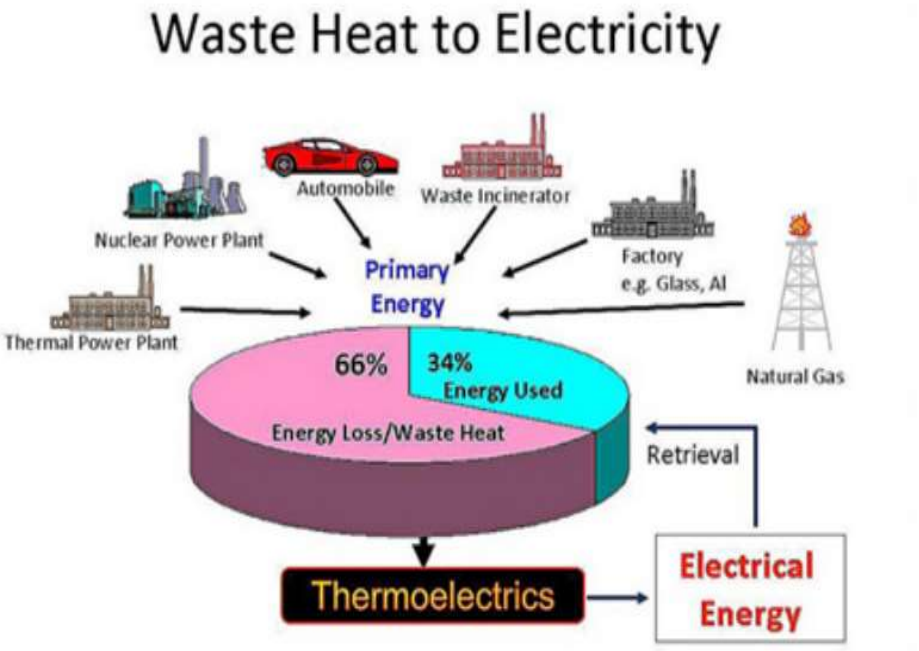


***Fig 6***. *Examples industrial energy usage vs energy loss, primarily as waste heat.* [34]

Recent research into thermal energy harvesting has an emphasis on nanostructured cells, with thin coating and wired systems that will contribute positively the Seebeck effect, while avoiding issues arising from heat conduction and poor heat exchange.

No solid state thermoelectric has ideal physical properties. Furthermore, large-scale power generation requires large quantities of material, which is a significant

disadvantage for thermoelectrics due to the typical cost of the raw materials. Therefore, large scale power generation is unlikely, and thermoelectrics are currently under investigation for small scale applications.[31,33]

Significant positive attributes include the fact that thermoelectric generators are zero sound emission devices. They are also free of mechanical motion, which can render them essentially maintain-free. This triggered numerous application in deep space missions, such as the Voyager probe.[26,40] Space exploration has good conditions for operation of thermoelectric devices, largely due to the strict requirement for low maintenance equipment, the difficulty associated with combustion, and the available temperature differences.[41,42] With the average temperature of space being 2 K, which could theoretically be used in contact with the cold electrode in a thermoelectric device, even modest heat sources in contact with the hot electrode can result in effective power generation.[34,39]

An example of a (terrestrial) thermoelectric application is converting waste heat from the vehicle exhaust to electricity and used to recharge a battery with DC power; by improving the design and fabrication of these harvesters, vehicles will enhance fuel efficiency through power co-generation.[38] If the same application can be extended to

harvesting some of the thermal energy wasted from the household, this could supplement energy within the home. If this development is set on a global scale it will significantly reduce energy consumption.[43]

Apart from the above mentioned, thermoelectric cells hold a unique prospect for portable power sources, although there are challenges to address, such as poor efficiency compared to combustion based engines.

Thermoelectric devices also requires high temperatures, and as mentioned previously design of the exchanger is of paramount importance.[43] A few tested approaches address explore situations, including use of catalytic combustion, which generates heat,[8,44,45]where many studies suggest incorporation of a fuel cell before the catalytic combustion.[35,44]

Recent developments in micro and nanotechnologies for semiconductor and film coating have also been encouraging in wireless sensors,[33,46] medical applications [46] and cell phones development.[46] Recent advancements also include parallel set thermoelectric devices [46] where efficiency loss is recoverable from the length and density of the activated elements and nano-sizing the devices to a level that application

in wristwatches is commercially viable. [31,46,47] This reflects the feasibility of adopting thermoelectric cells in small end applications, providing their production cost is kept to a minimum and can be produced by economy of scale.[31]

Therefore potential and real applications are rife, but ideal systems have yet to be achieved, due to both performance and cost.

## Thermoelectrochemical Cells

Thermoelectrochemical cells, or thermogalvanic cells (both also abbreviated as thermocells),[48,49] are similar in nature to thermoelectric devices,[49] given that their operation also depends significantly upon the Seebeck effect.[31] However, thermoelectrochemistry employs electrochemistry of redox-active ions in solution as the charge carriers within the thermocells.[8,37] As such, they are relatively more complex in their mode of operation, and are sensitive to more parameters that those conventionally associated with thermoelectric devices.

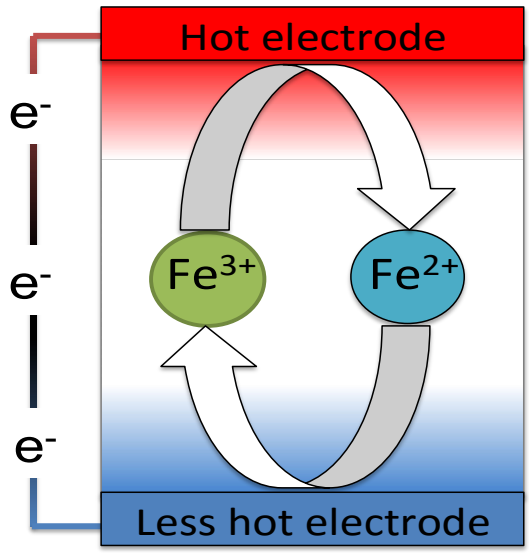


***Fig 7** .A schematic of an example thermoelectrochemical device, utilising the $Fe^{2+}$ and $Fe^{3+}$ redox couple*

Thermocells consist of a redox active electrolyte in simultaneous contact with two electrodes of dissimilar temperatures. Across these two electrodes a potential difference is measurable, and which is commonly referred to as the Seebeck coefficient (*cf.* the discussion above, although this similar observation comes from a different phenomena to that occurring in thermoelectrics). If these two electrodes are electrically connected, reduction and oxidation processes will occur within the cell, and a corresponding current will flow through the external circuit, thus generating electricity. In theory, current is able to flow with until an electrochemical equilibrium is achieved.

However, electrolyte flux (via diffusion) ensures that there is a continuous supply of electrolyte for thermoelectrochemistry to occur. Furthermore, the temperature gradient between two electrodes induces convection into the system, increasing this effect even further, while sometimes deliberate mass transport of the bulk electrolyte is additionally applied. Thus, if all electrochemical reactions are reversible and without side reactions, and as long as the temperature gradient is maintained, electricity production can continue indefinitely.

Investigations into thermocells and thermoelectric devices have demonstrated that both are equally affected by Carnot limitation, as both follow thermodynamics and resembles heat engines. Both do not have moving mechanical parts, and can seeming work indefinitely.[50] However, significantly thermocells do have moving parts; namely they typically possess a fluid electrolyte, involving both the redox couple (the charge carriers) and the solvent. This introduces considerable differences between thermocells and thermoelectrics.

The dimensionless ZT parameter commonly ascribed to thermoelectrics (and discussed above) can also be applied to thermocells, although it is rarely used given the

significantly greater complexity inherent in thermocells. When ZT parameters are determined for thermocells, they are typically two orders of magnitude lower than thermoelectric devices; typically this is because ionic conductivity in these systems are significantly lower than the ohmic conductivities of thermoelectrics Eq.3.[9,34] Typical ZT values for aqueous thermogalvanic cells fall within the range of *ca.* 3 to 700 x $10^{-5}$ $K^{-1}$, with Carnot efficiency between 0.001% and 1%. Conversely ZT values for optimized semiconductor thermocouples can reach 5 x $10^{-2}$ $K^{-1}$, with Carnot efficiencies up to 48%.[51,52]

$$\Delta G = \Delta H - T\,\Delta S = -nFE \qquad \textbf{(3)}$$

$$\Delta E/\Delta T = S_e = -nF/\Delta S$$

where ΔG is Gibbs free energy, ΔH is the enthalpy change of reaction, T is the temperature, ΔS is the standard redox reaction entropy  E is equilibrium electrode potential, n is the number of electrons involved in the reaction, F is the Faraday constant, ΔT  is the temperature difference, and  ΔE is the potential difference.

Nonetheless, thermocells are promising as a means for thermal energy harvesting due to the abundance of waste heat sources, redox species (relative to viable materials for thermoelectric devices) and the solvent is also typically abundant (often being water); all of this enhances affordability and scalability options. Thermocells also offer size

and shape versatility that allows the thermocells to mould to any heat source shape, due to flexible electrode materials; the design and orientation of the system is also modifiable. Finally, they typically possess significantly higher Seebeck coefficients than thermoelectric devices.

The amount of current these thermocells is proportional to how many redox active ions are present (concentration) and how fast they can move from one electrode to the other (*cf.* Figure 7). Ions moving due to the influence of chemical potential which known as diffusion. Diffusion is always present in liquids or gelled media, and can be clearly observed when there is a concentration gradient, as there will be when a thermogalvanic cell generates current. The viscosity of the media effects the diffusion of solutes, *i.e.* the viscosity of ionic liquids is typically higher than that of water, therefore the rate of ion diffusion is typically lower in ionic liquids.

In addition to diffusion, typically thermogalvanic cells have a temperature gradient across them and therefore experience convection. The effectiveness of convection in maintaining solution homogeneity may depend on cell orientation and geometrical design. Moreover that will affect the power generation capabilities of the cell; there is competition in power generation between favourable convection (redox ion transport) and non-favourable convection (heat flux or transport between electrodes). In Figure 8 two types of cell orientations were reported, with either the hot and cold electrodes

either horizontal, or with the cold electrode above the hot. The power output of cell using cold above hot was lower than horizontal, because the nature convection current direction from cathode (hot) to anode(cold) opposed $Cu^{2+}$ cations transport (Figure 8a). However in (Figure 8b) the nature of convection helped to deliver the $Cu^{2+}$ cations from anode (cold) to cathode (hot) cations and also to mix the electrolyte, leading to higher power.[53]

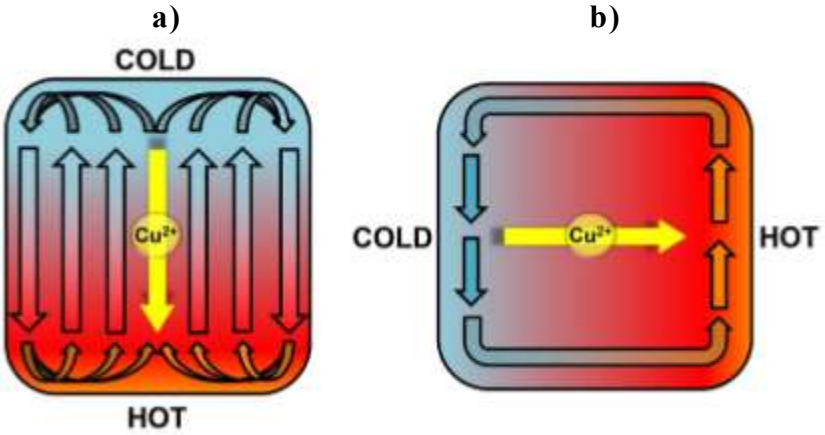


**Fig 8.** *Illustrative image of natural convection within the cell orientation,* ***a)*** *cold above hot,* ***b)*** *horizontal.*[53]

The energy produced through thermoelectrochemistry is related to the redox reaction entropy, which directly relates to the Seebeck coefficient. Researchers continue to explore different redox electrolytes to in an attempt to assess their respective reaction entropies. The resulting entropies are indicative to determine the Seebeck coefficient

of the redox couples. The energy also relates to current, which is directly related to the concentration of the redox active species in the electrolyte.

The redox entropy change (or Seebeck coefficient) is related to the (de)solvation of the ions in their different redox states; therefore different values are observed for different electrolyte systems, such as aqueous *vs* non-aqueous electrolytes.[9] Investigations into introducing gaseous and liquid electrodes can further influence the Seebeck coefficient, but introduce the problem of significant added complexities in cell design.[34]

Research has noted that one of the major limiting factors in thermocells is the solvent. For example, in an aqueous electrolyte the majority of the system is composed of water molecules. Thus, these do not directly enhance ionic conductivity as they are not charge carriers nor redox active, but do contribute towards (unwanted) thermal conductivity. Tests replacing aqueous electrolytes with molten salt based systems did not demonstrate sufficiently improved results that justified that justified the high temperature requirement. Broadly, improved cell designs, for electrode separation, for enhanced electrolyte concentration, and enhanced charge transport and for minimised heat conduction through the system is required.

Some recent attempts to improve the electrolyte have focussed upon replacing water with ionic liquids. Ionic liquids display wider temperature range tolerance than aqueous solvents. Due to their negligible volatility, in theory ionic liquid-based thermocells can work for a long time without evaporation issues.[9]

Other parameters which are key include solvent viscosity, fluid dynamics, series stacking, Ohmic resistance and electrode-kinetics. Due to the fluidity of the electrolyte, even orientation is key, given the orientiation of the temperature gradient with respect to gravity can have a major impact on natural convection. Vertical arrangements, where the cold electrode sits directly above the hot electrode have been determined to be the cell's optimum orientation for enhanced convection; however, this can enhance both charge transport and heat transfer.[51]

Broadly, some items which need to be overcome to enable the further application of thermocells are the relatively low conductivity of conventional electrolytes, the extensive convection of heat by liquid electrolytes, and the risk of leakage in thermocells (*cf.* batteries leaking when exposed to temperature gradients). In this thesis,

some strategies are investigated towards overcoming these issues. For example, in Chapter 2, aqueous vanadium systems are investigated, given their known high solubility, as exemplified by their use in vanadium redox flow batteries; higher concentrations of redox species should enhance ionic conductivity. While not successful in this endeavour, interesting new (thermo)electrochemical processes were observed. In Chapter 3, gelation is initially explored, as a means to overcome leakage and convection issues. In Chapter 4, the use of gelled electrolytes is continued, but now gold nanoparticles are introduced as a potential means of enhancing conductivity. Once again, while not successful in achieving this, novel (thermoelectro)chemistry was observed. Finally, in Chapter 5, these novel systems were explored for other applications.

## References


1. Khan MA, Khan MZ, Zaman K, Naz L. Global estimates of energy consumption and greenhouse gas emissions. *Renewable and Sustainable Energy Reviews*. 2014 1;29:336-44.
2. Petroleum, British. British petroleum statistical review of world energy.*London: British Petroleum Corporate Communications Services* (2001).
3. Makhubela, B. C.; Darkwa, J. The role of noble metal catalysts in conversion of biomass and bio-derived intermediates to fuels and chemicals. *Johnson Matthey Technol. Rev.* 2018, 62,4−31.
4. Rogelj, Joeri, et al. Paris Agreement climate proposals need a boost to keep warming well below 2 C. *Nature* 534.7609 (2016): 631.
5. Peters G. P.,. Andrew R. M, Boden T.,. Canadell, J. G P. Ciais, C. Le Qu´er´e, G.Marland, M. R. Raupach, and C. Wilson, The challenge to keep global warming below 2 c, *Nature Climate Change*, vol. 3, no. 1, pp. 4–6, 2013.
6. Friedlingstein P, Solomon S, Plattner G, R. Knutti, P. Ciais, and M. Raupach,Long-term climate implications of twenty-first century options for carbon dioxide emission mitigation, *Nature Climate Change,* vol. 1, no. 9, pp. 457–461, 2011.
7. Forbes, Gilbert B. Human body composition: growth, aging, nutrition, and activity. *Springer Science & Business Media*, 2012.
8. Abraham TJ, MacFarlane DR, Pringle JM. Seebeck coefficients in ionic liquids–prospects for thermo-electrochemical cells. *Chem Commun*. 2011;47(22):6260-2.

9. Abraham TJ, MacFarlane DR, Baughman RH, Jin L, Li N, Pringle JM. Towards ionic liquid-based thermoelectrochemical cells for the harvesting of thermal energy. *Electrochimica Acta*. 2013;113:87-93.

10. Goldstick R. , A. Thumann Principles of waste heat recovery *The Fairmont Press, Inc* (1986).

11. Turner W. C.. S. Doty, Energy management handbook. *The Fairmont Press,Inc*., 2012.

12. Bernstein L, P. Bosch, O. Canziani, Z. Chen, R. Christ, and O. Davidson, Climate change 2007: Synthesis report. summary for policymakers,in Climate change 2007: *Synthesis report. Summary for policymakers*, *IPCC*, 2007.

13. Rehan R, M. Nehdi. Carbon dioxide emissions and climate change: policy implications for the cement industry. *Environmental Science & Policy*, 8 (2005), pp. 105-114

14. Mikulčić H, Vujanović M, Duić N. Reducing the $CO_2$ emissions in Croatian cement industry. *Applied Energy*, 101 (2013), pp. 41-48

15. Oreskes N (2007) The scientific consensus on climate change: How do we know we're not wrong? In: DiMento JF, Doughman P (eds) Climate change: What it means for us, our children, and our grandchildren. *MIT Press, Cambridge*, pp 65–99

16. Fischer, Hubertus, et al. The role of Southern Ocean processes in orbital and millennial $CO_2$ variations–A synthesis. *Quaternary Science Reviews* 29.1-2 (2010): 193-205.

17. Knorr W. Is the airborne fraction of anthropogenic $CO_2$ emissions increasing? *Geophys Res Lett*, 36 (2009), pp. L21710, 10.1029/2009 GL040613

18. Russell G.L, Rind D. Response to $CO_2$ transient increase in the GISS coupled model: regional coolings in a warming climate. *J. Climate*, 12 (1999), pp. 531-539

19. Rahmstorf, Stefan, Grant Foster, and Niamh Cahill. Global temperature evolution: recent trends and some pitfalls. *Environmental Research Letters* 12.5 (2017):054001.

20. Hansen J, Ruedy R, M. Sato, and K. Lo, Global surface temperature change, *Reviews of Geophysics*, vol. 48, no. 4, 2010.

21. Anchukaitis, Kevin J., et al. Tree-ring-reconstructed summer temperatures from northwestern North America during the last nine centuries. *Journal of Climate* 26.10 (2013): 3001-3012.

22. Murphy E L and Good R H 1956 Thermionic emission, field emission, and the transition region. *Phys. Rev*. 102 1464–73.

23. Baldasaro P. F., Brown E. J., Depoy D. M, Campbell B. C, and J. R. Parrington,Experimental assessment of low temperature voltaic energy conversion, in The first NREL conference on thermophotovoltaic generation of electricity, *AIP Publishing, vol*. 321, 1995, pp. 29–43.

24. Zhou H, Yamada T, and Kimizuka N.Supramolecular thermo-electrochemical cells: Enhanced thermoelectric performance by host–guest complexation and saltinduced crystallization, *Journal of the American Chemical Society, vol.* 138, no.33, pp. 10 502–10 507, 2016.

25. Bennett G. L. Skrabek E. Power performanceof us space radioisotope thermoelectric generators, in Thermoelectrics, 1996., *Fifteenth International Conference on*, IEEE, 1996,pp. 357–372.

26. A Datas and A Mart´ı, Thermophotovoltaic energy in space applications: Reviewand future potential, *Solar Energy Materials and Solar Cells*, vol. 161, pp. 285–296, 2017.

27. Snyder GJ, Toberer ES. Complex thermoelectric materials. *Nature materials*. 2008;7(2):105-14.

28. Vining CB. An inconvenient truth about thermoelectrics. *Nature Materials.* 2009;8(2):83-5.

29. Biswas K, He J, Blum ID, Wu C-I, Hogan TP, Seidman DN, et al. High-performance bulk thermoelectrics with all-scale hierarchical architectures. *Nature.* 2012;489(7416):414-8.

30. Martin J, Tritt T, Uher C. High temperature Seebeck coefficient metrology. *Journal of Applied Physics*. 2010;108(12):121101.

31. Lay-Ekuakille, A.; Vendramin, G.; Trotta, A.; Mazzotta, G. Thermoelectric generator design based on power from body heat for biomedical autonomous

devices. *In Proceedings of 2009 IEEE International Workshop on Medical Measurements and Applications*, Cetraro, Italy, 29–30 May 2009; pp. 1–4

32. Snyder GJ. Small thermoelectric generators. *The Electrochemical Society Interface.* 2008;17(3):54.

33. Im H, Moon HG, Lee JS, Chung IY, Kang TJ, Kim YH. Flexible thermocells for utilization of body heat. *Nano Research*. 2014;7(4):1-10.

34. Romano MS, Li N, Antiohos D, Razal JM, Nattestad A, Beirne S, et al. Carbon Nanotube - Reduced Graphene Oxide Composites for Thermal Energy Harvesting Applications. *Advanced Materials*. 2013; 25(45): 66026.

35. Alzahrani, H.AH, et al. Combining thermogalvanic corrosion and thermogalvanic redox couples for improved electrochemical waste heat harvesting. *Electrochemistry Communications* 58 (2015): 76-79.

36. Hicks L, Dresselhaus M. Effect of quantum-well structures on the thermoelectric figure of merit. *Physical Review B*. 1993;47(19):12727.

37. Altenkirch WWE, Gehlhoff GR. Thermo-electric heating and cooling body. *Google Patents;* 1914.

38. Quickenden T. Vernon C. Thermogalvanic conversion of heat to electricity, *Solar Energy*, vol. 36, no. 1, pp. 63–72, 1986.

39. Yang J. Potential applications of thermoelectric waste heat recovery in the automotive industry. *In International conference on thermoelectrics* 2005: 155-159.

40. Paul, Douglas. Thermoelectric energy harvesting. *ICT-Energy-Concepts Towards Zero-Power Information and Communication Technology. InTech* 20 (2014): 21.

41. Yuen, Joseph H., ed. Deep space telecommunications systems engineering. *Springer Science & Business Media*, 2013.

42. Kivelson, Atmo. Introduction to space physics. *Cambridge university press*, 1995.

43. Gazis, P. R., et al. Solar wind velocity and temperature in the outer heliosphere. *Journal of Geophysical Research: Space Physics* 99.A4 (1994): 6561-6573.

44. Graves, Christopher, et al. Sustainable hydrocarbon fuels by recycling $CO_2$ and H2O with renewable or nuclear energy. *Renewable and Sustainable Energy Reviews* 15.1 (2011): 1-23.

45. Sheldon R. Catalytic reactions in ionic liquids. *Chemical Communications*. 2001(23):2399-407.

46. Alvarado U, Juanicorena A, Adin I, Sedano B, Gutiérrez I, Nó J. Energy harvesting technologies for low-power electronics. *Transactions on Emerging Telecommunications Technologies*. 2012;23(8):728-41.

47. Leonov V. Thermoelectric energy harvesting of human body heat for wearable sensors. *Sensors Journal, IEEE*. 2013;13(6):2284-91.

48. Mitcheson PD. Energy harvesting for human wearable and implantable bio-sensors. *In: Proceedings of the annual international conference of the IEEE engineering in medicine and biology society*; 2010. p. 3432–6..

49. Maier J. Nanoionics: ion transport and electrochemical storage in confined systems. *Nature materials.* 2005;4(11):805-15.

50. MacFarlane DR, Tachikawa N, Forsyth M, Pringle JM, Howlett PC, Elliott GD, et al. *Energy applications of ionic liquids. Energy & Environmental Science.* 2014;7(1):232-50.

51. Ross, Robert T. Thermodynamic limitations on the conversion of radiant energy into work. *The Journal of Chemical Physics* 45.1 (1966): 1-7.

52. Quickenden, T. I.; Mua, Y., A review of power generation in aqueous thermogalvanic cells. *Journal of the Electrochemical Society* **1995,** *142* (11), 3985-94.

53. Venkatasubramanian R, Siivola E, Colpitts T, and O'quinn B. "Thin-film thermoelectric devices with high room-temperature figures of merit," *Nature, vol.* 413, no. 6856, pp. 597–602, 2001.

54. Gunawan A, Li H, Lin C.-H, Buttry D.A, Mujica V, Taylor R.A, Prasher, R.S, Phelan P.E. The amplifying effect of natural convection on power generation of thermogalvanic cells Int. *J. Heat Mass Transfer,* 78 (2014), pp. 423-434.

Chapter 2

# Vanadium

The majority of the contents of this chapter has been submitted for publication under the title of '*Electrodeposition of vanadium oxide and consequent behaviour as thermogalvanically chargeable aqueous sodium ion 'entropy' batteries'*

## Abstract

This chapter describes a thermogalvanic investigation of the electrochemistry of the V(IV) / V(V) redox couple, and the significant differences observed in acidic *vs* neutral conditions.

The sustainable harvesting, storage and release of electrical energy is a key challenge. In this context, the thermogalvanic conversion of waste heat into electricity, and the storage and release of electrical energy using water-based batteries are two growing areas of investigation. In this study, we have investigated the thermoelectrochemistry of the V(IV) / V(V) redox couple widely employed in all-vanadium redox flow batteries, using acidified $VOSO_4$ and $NaVO_3$. These have scope for converting a temperature gradient into electricity, but both poor thermodynamics and kinetics w

ere observed. Investigation of this same vanadium redox couple in neutral aqueous solution resulted in the facile electrodeposition of vanadium oxide deposits, which readily underwent reversible Faradaic insertion (or intercalation) and release of sodium ions. When these were employed within thermoelectrochemical cells, the thermogalvanic 'charging' of these aqueous sodium ion-based systems was observed, generating a flow of current as sodium ions migrated from the colder electrode to the hotter electrode. When the temperature gradient was removed, current flowed in the

opposite direction as these ‘charged’ batteries discharged to balance the sodium content, thus demonstrating both thermogalvanic conversion and even storage and release of energy harvested from a temperature gradient.

# Introduction

Both the human population and each individuals' daily utilisation of technology are increasing rapidly; energy efficiency and sustainability has become one of the biggest challenges in our age.[1] Importantly, solar irradiation, human industry and humans themselves all radiate vast quantities of energy as low grade waste heat.[2]

The thermoelectric (or Seebeck) effect is known to convert a temperature gradient into electricity with zero moving parts.[3] It has been known since 1821, but is typically based upon relatively expensive and fragile semiconductor materials.[3] An electrochemical equivalent which uses solid or liquid electrolytes and redox chemistry also exists and is widely referred to as thermoelectrochemistry, or the thermogalvanic effect.[4-6] Using this latter approach, scalable, flexible, inexpensive systems can be developed where even comparatively small temperature differences (*e.g.* a 5°C difference) can be effectively converted into a useful electrical current.[7]

A characteristic of such systems is the Seebeck coefficient ($S_e$, in mV $K^{-1}$), namely the potential difference, $\Delta E$, generated by the temperature difference, $\Delta T$, across two electrodes.[6] In thermoelectrochemistry, this parameter is proportional to the entropy change associated with the redox chemistry occurring in the electrochemical cell, $\Delta S$.[8]

High values of ΔS corresponds to high values of $S_e$, but this typically requires small ions with high valence charges.[9] The ΔS is the underlying thermodynamic driving force; however, the kinetics of the electron transfer, concentration of the redox species and their diffusivity all also strongly influence the current output of thermogalvanic cells (or thermocells).[5, 10] Thermal energy transduction into electrical energy in thermocells is therefore favoured by a high temperature difference, favourable thermodynanics and ionic conductivity, and frustrated thermal conduction.[5, 11]

As opposed to thermocells, which are a means of energy conversion, redox flow batteries (or RFBs) are methods of energy storage. RFB's have been proposed as a form of large-scale electrochemical energy storage.[12] Energy is stored by redox reactions by species dissolved in electrolyte solutions; these solutions flow through an electrochemical cells during both charge and discharge.[12] They are targeted as energy storage devices for periodic renewable energy sources, and have few moving parts, typically no noise and require minimal maintenance.[13] The concept is relatively old, but successful demonstration and commercial development was not achieved until the 1980's.[14] This was achieved by Prof. Maria Skyllas-Kazacos and co-workers, who developed an 'all-vanadium RFB', using a sulfuric acid electrolyte, and was patented in 1986.[14-15] The all-vanadium system was possible as vanadium has four common

oxidation states; +2, +3, +4 and +5.[16] This is now an area of major commercial and practical development in Germany, the USA and Japan.[16-17]

There are several critical parameters for both a successful all-Vanadium RFB and a good thermocell, notably that (i) the solubility of the redox species needs to be high, (ii) when in solution it should be (thermally and chemically) stable, (iii) the electrodes should have a high surface area, and (iv) at these electrodes the rate of electron transfer should be rapid (*i.e.* electrocatalysis).

One half of the all-vanadium RFB relies upon the 2+ and 3+ states, whereas the other half relies upon the 4+ and 5+ states; the latter are generally found as their oxy species when dissolved in aqueous media.[18] These two are represented by the equilibria 1 & 2. These combine to produce the full-cell reaction shown in equilibria 3.

$$V^{3+} + e^- \rightleftharpoons V^{2+} \quad \textbf{(1)}$$

$$VO_2^+ + 2H^+ + e^- \rightleftharpoons VO^{2+} + H_2O \quad \textbf{(2)}$$

$$V^{2+} + VO_2^+ + 2H^+ \rightleftharpoons V^{3+} + VO^{2+} + H_2O \quad \textbf{(3)}$$

A ‘Vanadium thermocell’ has not been previously reported. Conversely, a tremendous amount of effort has been devoted towards optimising all-Vanadium RFBs. Despite this, only limited values of $\Delta E/\Delta T$ (or $S_e$ values) have been published, and these are often from calculated values; they vary between +0.4 and *ca.* +1.5 mV $K^{-1}$ for Eq. 1, under standard conditions, between -0.2 and -0.9 mV $K^{-1}$ for Eq. 2, and between -1.2 and -2.4 mV $K^{-1}$ for Eq. 3.[18]

Hudak experimentally investigated an all-Vanadium redox flow battery, prepared initially from *ca.* 2 M $VOSO_4$ and 6 M HCl.[18] The entire battery was heated (between 22ºC and 80ºC), and the trend in open circuit potential *vs* temperature gave $\Delta E/\Delta T$ values that varied between *ca.* -0.2 and -1.7 mV, as a function of the state of charge of the battery.[18]

Notably, the thermoelectrochemistry of lithium-ion battery intercalation materials[19-21] and lithium metal-based systems[22-24] has also been reported recently. Here, temperature gradients across the battery can alter the cell potential, and even encourage thermally driven (re)charging[20] of these battery assemblies. However, all of these relied upon non-aqueous electrolytes. Conversely, aqueous rechargeable lithium and sodium ions batteries have many desirable attributes and applications.[25] In particular, vanadium-

based anodes have been reported for use in aqueous electrolyte-based sodium ion batteries, employing compounds such as $V_2O_5$, $Na_{1+x}V_3O_8$ and $Na_2V_6O_{16}.nH_2O$.[25]

In this study we have investigated the thermoelectrochemistry of the aqueous V(IV)/V(V) redox couple, using acidified electrolytes directly analogous to those found in all-vanadium redox flow batteries; the first such 'thermocell' based upon this system has therefore been prepared and investigated. Additionally, the unexpected but facile electrodeposition of a vanadium-based sodium ion intercalation material from neutral aqueous solutions has been observed. This was applied in a 'one-pot' process to electrodeposit this material on two sides of a commercial battery casing; application of a temperature gradient across this aqueous battery resulted in thermogalvanic power being generated due to migration of sodium ions from the cold to the hot electrode, for entropic reasons. This also resulted in these two intercalation electrodes no longer being equal, and removal of the temperature gradient resulted in electrical power being generated (with the current flowing in the opposite direction) due to the rebalancing of the sodium ion intercalation materials, for enthalpic reasons. Therefore, this system could act as a thermogalvanically-chargeable aqueous sodium ion 'entropy' battery.

## Experimental

Ultrapure water (resistivity 18.2 MΩ $cm^{-1}$) was used throughout. All chemical reagents were purchased from Sigma–Aldrich (Castle Hill, NSW, Australia) and used as received.

Conventional electrochemical measurements such as cyclic voltammetry (CV) was performed in a three-electrode cell, using a glassy carbon working electrode (GC, 3 mm diameter), Pt counter and Ag/AgCl (3 M KCl) reference electrode (all BASi Analytical, USA) and a μAutolab PGSTAT 101 (Ecochemie, The Netherlands)

For acidic electrolytes, thermoelectrochemical measurements were performed in a homemade glass cell, which consisted of two screw thread autosampler vials. These were cut in half and fused, to create a single vessel with two screw thread lids. The septa was removed, and the lids super-glued to slabs of glassy carbon, to have a symmetrical corrosion-resistant cell with glassy carbon electrodes at either end.

Neutral solutions were measured in 304 stainless steel CR2032 battery button cells (MTI Corporation, CA, USA), which were crimped using an MSK-110 hydraulic

crimping machine (also MTI Corporation) and thus measurements were made in hermitically sealed casings. Prior to crimping, the two halves of the cell has vanadium oxide electrodeposited into the interior of the casing, as described in more detail in the main text; this was achieved by securing the half of the cell at the bottom of a plastic tube, such that it consisted of the bottom of an electrochemical cell, and could be used as a working electrode and cycled repeatedly between +1 V and -1 V *vs* Ag/AgCl.

Thermoelectrochemical measurements were performed using a Keysight B2900A Source Measurement Unit, using either Quick IV measurement software or a custom Excel Macro program. Temperature was controlled using the below assembly:

HE | Peltier | ACP | Cell | ACP | Peltier | HE

where HE is a copper heat exchanger, Peltier is a peltier heater/cooler and ACP is an aluminium cold plate (all purchased from Custom Thermoelectric, MD, USA), where the latter had an embedded thermistor. The temperature was thus controlled and maintained to within 0.1 °C, using an Arduino microprocessor. The cell is either the sealed CR2032 casing or the glass-based cell.

## X-Ray photoelectron Spectroscopy (XPS)

XPS was performed using a ThermoScientific ESCALAB 250Xi spectrometer with a monochromatic Al Ka X-ray source (hv = 1486.68 eV) under a pressure of less than 2 $x10^{-9}$ mbar. The Al twin Anode was powered at 150W (13 kV x 12 mA). The photoelectron take-off angle was 90° in respect to the sample surface normal with a sample diameter of 500µm. The pass energy for survey scans and region scans were 100 eV and 20 eV respectively and survey scans were performed at 1eV steps and regions scans at 0.1 eV steps for higher resolution. The spectrometer was calibrated relative to Au 4f7 = 83.96 eV, Ag 3d5 = 368.21 eV, Cu2p3 = 932.62 eV, and scans were performed without ion beam surface cleaning. Empirical sensitivity factors were taken into account for each element and Advantage software was used for data processing (XPS spectra were treated by a Shirley-type background). Binding energies were referenced to the C 1s (284.8 eV). Assignation of the signals to specific structures or given oxidation state of elements analysed was done by comparison with data reported by NIST Standard Reference Database 20, Version 3.5.

# Results & Discussion

## Cyclic voltammetry of V(V) / V(IV) in acidic aqueous media

Most research into the electrochemistry of the vanadium redox states have been performed in relatively concentrated acid solutions,[26-27] therefore this was used for the preliminary investigation of vanadium thermoelectrochemistry.

The electrolytes employed in typical all-vanadium RFBs were prepared as reported in the literature.[14] Figure 1(a) displays CVs recorded for V(IV) and V(V) individually (introduced as $VOSO_4$ and $NaVO_3$, respectively) and when mixed. It clearly displays that the redox chemistry is chemically reversible, but the extremely large separation between the peaks is indicative of very slow electron transfer constants. Enhancing the electrode kinetics typically involves either (i) electrochemically oxidising the carbon electrode (*cf.* [28]), (ii) heating the carbon electrode in air to oxidise (*cf.* [29-30]), (iii) changing from bulk electrodes to nanostructured electrodes, and (iv) altering the acidic electrolyte (*cf.* [18, 31]). Notably, extending the scan beyond +1.5 V resulted in oxidation of the glassy carbon electrode and decreases in the peak-to-peak separation, but these modifications were removed by extended exposure to the electrolyte.

Oxidation of carbon electrodes is known to effect the vanadium electrochemistry and various routes have been used to deliberately oxidise carbon electrodes. Electrochemically oxidising graphite felt electrodes in sulfuric acid solution increased the molar ratio of O to C from 0.085 to 0.15, mainly by the introduction of –COOH groups.[28] Boiling graphite felt electrodes in concentrated sulphuric acid for about 5 h also increased the O to C ratio,[18,31] as did heating to 400 ºC in an oxygen-enriched environment (42% oxygen and 58% nitrogen).[29,30] In all cases, they were tested for effectiveness in a redox flow battery, and the most significant effect was improved hydrophilicity and therefore an increase in the electrochemically wetted surface area, e.g. from 0.24 to 51.22 m2/g.[30] Such effects dominate the observed response, but potentially there is also an increase in the rate of electron transfer between vanadium and carbon by virtue of the new oxygen functionality at the carbon surface.

In order to evaluate the effect of other electrode materials, graphite was also investigated, as shown in Figure 1(b). Here the peak to peak separation of the V(V)/V(IV) redox couple was significantly reduced, the V(IV)/V(III) process was also observed at *ca.* 0 V, and the V(III)/V(II) process was partially observed within the hydrogen evolution region (below -0.5 V).

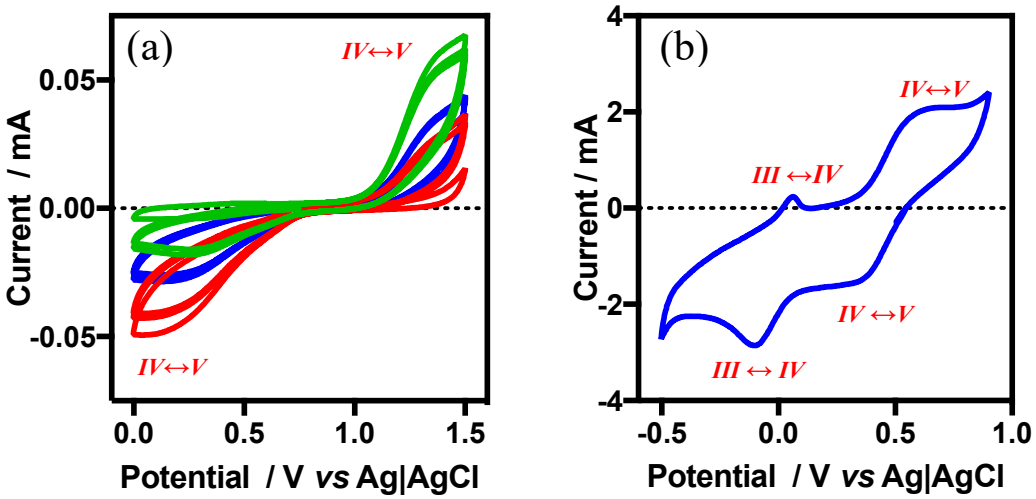


***Fig 1:*** *Cyclic voltammetry (all in aqueous 2 M $H_2SO_4$) recorded at (a) a glassy carbon electrode and (b) graphite rod, for 1 M $NaVO_3$ (red), 1 M $VOSO_4$ (green), and both 0.5 M $NaVO_3$ and 0.5 M $VOSO_4$ (blue).*

## Thermoelectrochemistry of V(V) / V(IV) in acidic aqueous media

Our previously reported thermoelectrochemical setup[21-22, 24, 32] is based upon stainless steel housings, so is incompatible with even dilute acids. Therefore a glass-based thermoelectrochemical cell with glassy carbon electrodes was prepared to contain the corrosive electrolyte; this is shown in Figure 2(a). Thermocouples were introduced directly into the electrodes, and this apparatus was demonstrated to resist corrosion.

Near ideal thermoelectrochemistry was recorded in this setup for ferri/ferrocyanide, yielding a seebeck coefficent of -1.39 mV $K^{-1}$, in good agreement with the literature.[6] Having developed this cell, it was possible to investigate an 'all-vanadium thermocell', and benchmark its performance against a conventional ferri/ferrocyanide thermocell.

The trend in voltage *vs.* temperature for the V(IV)/V(V) thermocell as a function of temperature; here the Seebeck coefficient of the V(IV)/V(V) was found to be -0.14 mV $K^{-1}$; significantly lower than that of the -1.39 mV $K^{-1}$ for the $[FeCN_6]^{3-}/[FeCN_6]^{4-}$ system. Initially, one might expect a more significant Seebeck coefficient for the V(IV)/V(V) system, and a positive Seebeck coefficient, *e.g.* as $V^{4+}$ and $V^{5+}$. However, the actual species in solution for V(IV) and V(V) are typically reported as $VO^{2+}$ and $VO_2^{+}$, respectively.[6] The observed negative sign and magnitude of the Seebeck coefficient is entirely consistent with these being the redox active system, given that a negative Seebeck coefficient corresponds to an oxidation occurring at the hotter electrode. Notably, this is at the very bottom end of published values for the aqueous V(IV)/V(V) system, which have largely been calculated using thermodynamic values for standard conditions rather than experimentally measured, and vary between -0.18 mV $K^{-1}$ and -0.901 mV $K^{-1}$.[18] Hudak experimentally measured an entire vanadium redox flow battery to have values between *ca.* -0.2 and *ca.* -1.7 mV (as a function of

state of charge), relative to reported (largely calculated) values between -1.2 and -2.4 mV $K^{-1}$.[18]

Despite the poor Seebeck coefficient, the power output of the all-vanadium thermocell was also evaluated. Figure 2(b) displays the power curve generated by the thermocell at $\Delta T$ = 20 K ($T_{cold}$ = 20°C; $T_{hot}$ = 40°C); the expected potential was generated, and the associated current density (and therefore power density) was extremely low; this is a combination of both the low Seebeck coefficient (and therefore weak thermodynamic driving force) and the extremely slow rate of electron transfer, as demonstrated by the cyclic voltammetry shown in Figure 1. As a result, only minor quantities of power could be generated by acidified aqueous V(IV) / V(V); therefore investigation moved to other vanadium systems.

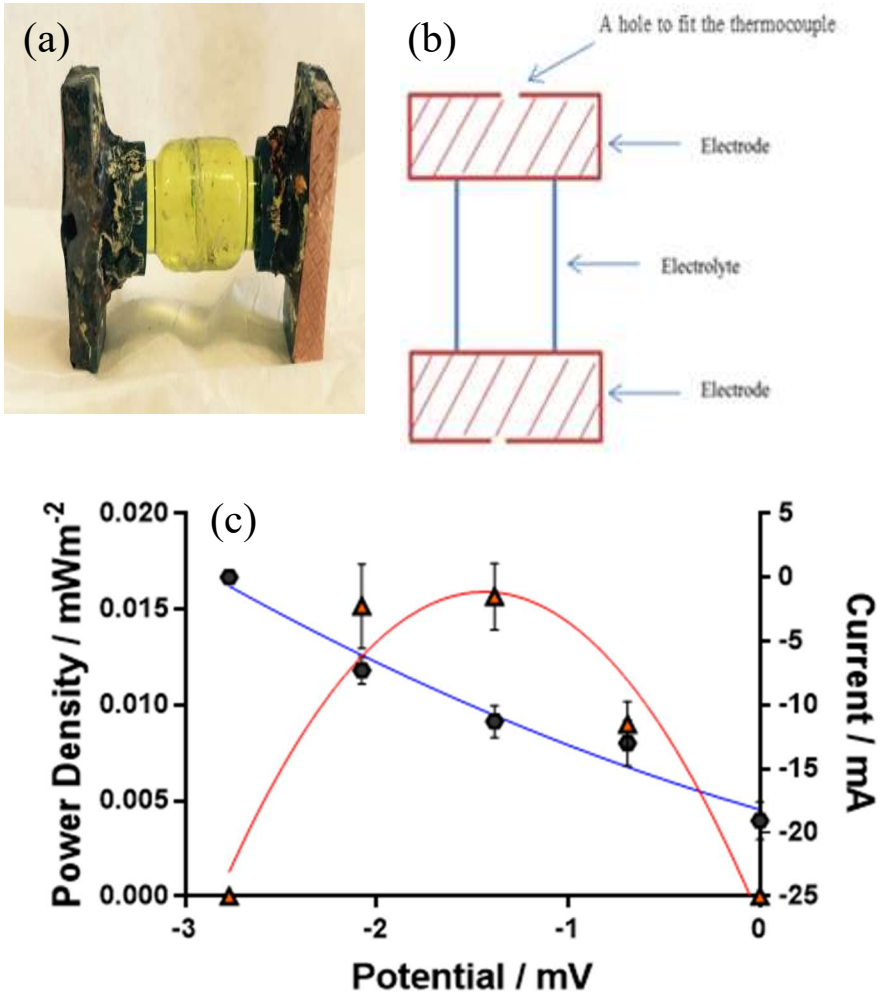


**Fig 2**: ***(a)*** *Photograph of the glass-based cell, containing the acidic V(IV)/V(V) electrolyte, and* ***(b)*** *A schematic of the glass-based cell.* ***(c)*** *a typical I-V plot and associated power curve for 0.1 M each of V(IV) and V(V) (introduced as* $VOSO_4$ *and* $NaVO_3$*, respectively) in 2 M* $H_2SO_4$*, and measured at* $\Delta T = 20$ *K.*

## Cyclic voltammetry of just V(IV) / V(V) in water: Electrodeposition of vanadium oxide

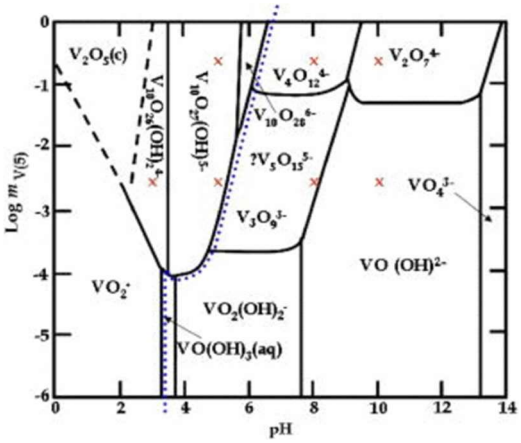


Vanadium has extremely rich redox chemistry. Furthermore, it has extremely rich speciation as a function of concentration and pH. The figure to the left displays the predominant solution-phase species for V(V) in water as a function of pH.[33] As noted above, vanadium RFB research has limited investigation to a narrow region (pH 0 to 1) due to the necessity of employing a proton exchange membrane to separate the anolyte and catholyte, and because protons and proton exchange is used to ensure charge neutrality during charging and discharging.[12, 17]. For thermoelectrochemistry, any pH can be used and therefore a wide variety of vanadium species can be investigated. The highly charged polyoxovanadates (*e.g.* $[V_{10}O_{28}]^{6-}$ ) found at high concentrations and neutral pH's could be of particular interest. However, preliminary investigation of vanadium electrochemistry at higher pH values ( >9) demonstrated that oxidation was completely irreversible, indicating that it cannot be employed as a redox couple in a thermocell. While higher charge clusters are formed at higher pH values,[33] these clusters also appear to have even slower electron transfer constants than those found under highly acidic conditions.

A notable exception was when high concentrations of V(IV) and V(V) were dissolved in un-buffered water, in the absence of supporting electrolyte, and exposed to cyclic voltammetry. While un-buffered and lacking supporting electrolyte, the high concentration of the inherently acidic metal oxides resulted in the solution having a pH of *ca.* 2. This system is consistent with most thermoelectrochemical investigations where no excess supporting electrolyte is added, and only the redox couple of interest is added. Here, radically altered voltametric results were observed if both redox states were dissolved together.

Figure 3(a) displays a CV of just V(V) (as $NaVO_3$) dissolved in pure water; no redox chemistry was observed within the available electrochemical window. Conversely, just V(IV) (as $VOSO_4$) in pure water displayed complex voltammetry, with oxidation of the V(IV) to presumably V(V) resulting in a deposition process (as demonstrated by the cross-over in the voltamogram) followed by reduction of the oxidised species on the reverse scan. Extended electrolysis of V(IV) has been used to supersaturate the electrode with V(V) as a method to electrodeposit $V_2O_5$ at the electrode; the electrode was then rapidly removed from the solution to avoid redissolution.[34]

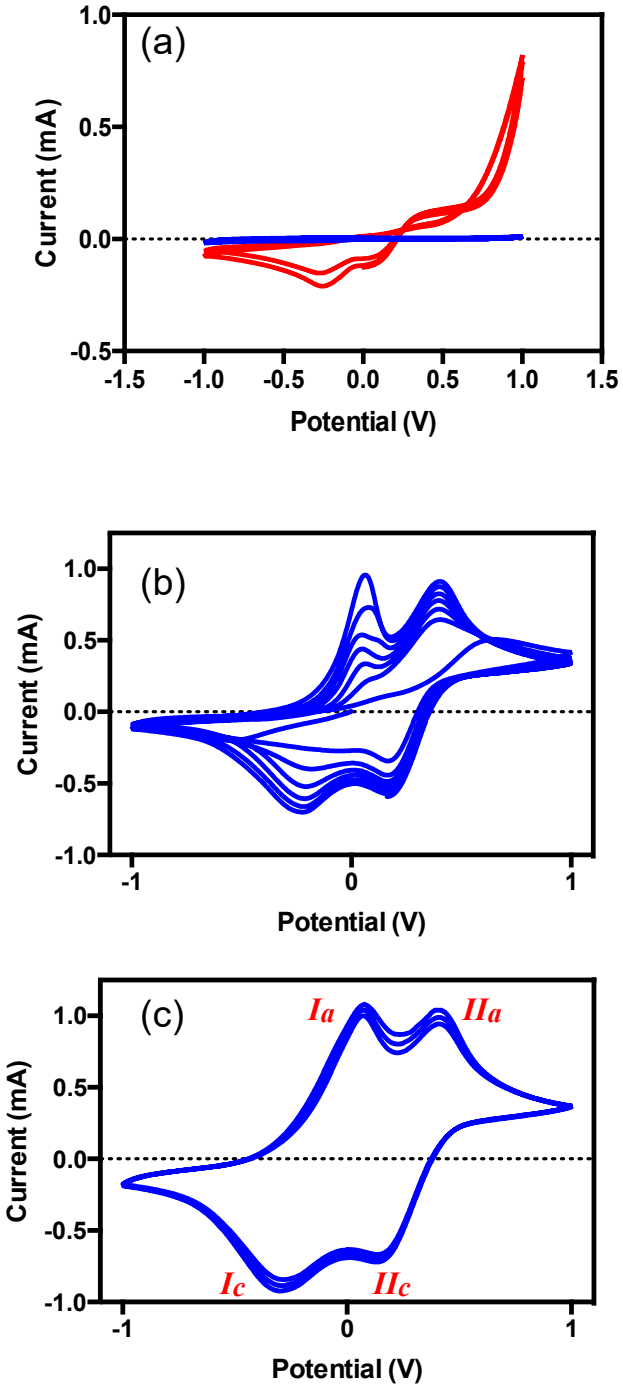


**Fig 3**: *Cyclic voltammograms recorded at a glassy carbon electrode, in an un-buffered aqueous solution containing only vanadium salts (i.e. no other supporting electrolyte present) for (**a**) either just 0.26 M $NaVO_3$ (blue line) or 0.26 M $VOSO_4$ (red line), and (**b**) the first 7 scans recorded in a solution containing both 0.26 M $NaVO_3$ and 0.26 M $VOSO_4$, showing the increase in current with scans, and (**c**) the same system, showing scans 50 to 55. Scan rate = 5 mV $s^{-1}$.*

*In fig (c): Subscript a and c stand for anodic and cathodic, respectively.*

The situation was significantly different when both V(IV) and V(V) (as $VOSO_4$ and $NaVO_3$, respectively) were dissolved in the same solution. Here, scanning oxidatively demonstrated an oxidation peak at *ca.* +0.75 V, after which two reduction features appeared, with two resulting oxidation peaks; this is shown in Figure 3(a). Successive scanning within the +1 V to -1 V potential range resulted in a successive growth of two reversible redox couples. The peaks grew rapidly, but beyond the $10^{th}$ scan the peaks typically stabilised and grew relatively more slowly, as shown in Figure 3(c). Repeated scanning resulted in these peaks gradually growing, before occasional sharp decreases in current, followed by the current growing again; drops in current corresponded with physical delamination of a layer of black deposit from the surface of the glassy carbon electrode.

These features are analogous to $Li^+$ insertion and removal,[35] and therefore correspond to $Na^+$ insertion and removal (introduced via the $NaVO_3$) in a layer of electrodeposited and electroactive vanadium oxide. Taking the amorphous vanadium oxide as $V_yO_z$, $Na^+$ insertion and removal would follow a two process such that;

**Peak I:** $Na_xV_yO_z + Na^+ + e^- \rightarrow Na_{x+1}V_yO_z$

**Peak II:** $Na_{x+1}V_yO_z + Na^+ + e^- \rightarrow Na_{x+2}V_yO_z$

Two peaks observed in such voltammograms are typically associated with there being two distinct Na-intercalation sites present in the $V_yO_z$ lattice.[36] The initial deposition of this vanadium oxide species, followed by reversible intercalation of the sodium cation, is displayed schematically in Figure 4.

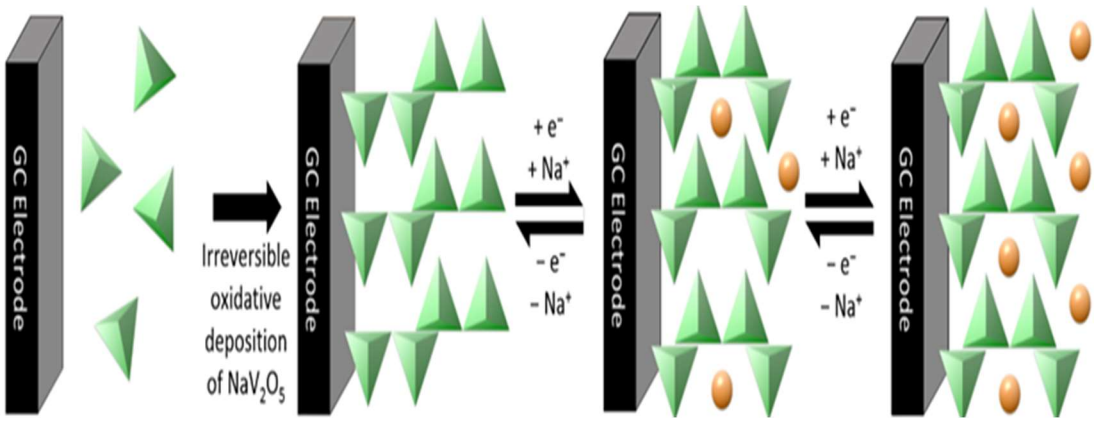


**Fig 4.** *This illustration displaying Vanadium deposition onto the graphite electrode surface by electrodeposition, and subsequent Sodium-ion intercalation*

The fact that this was $Na^+$ insertion and removal was further confirmed by altering the $Na^+$ concentration; when half of the $NaVO_3$ was replaced with $0.5V_2O_5$ (as an alternate V(V) source) the peak size was decreased by half. Conversely, when the $Na^+$ concentration inherent in the system was doubled by the deliberate addition of $Na_2SO_4$ to the system, the peak current increased, albeit by only *ca.* 20%.

Electrodeposition of a well-adhered layer of black deposit was achieved on glassy carbon. In addition, this was also achieved on stainless steel, specifically CR2032 battery casings. Figure 5(a) shows a photo of half of a CR2032 casing; Figure 5(b) displays the same cell casing after electrodepositing the material on the stainless steel surface by preforming repeated cyclic voltammograms using the cell casing as the working electrode. A similar black precipitate was observed after the mixed V(IV) and V(V) solutions were left for several days; coating of the steel was therefore attempted by simply leaving the solution for several days. As shown in Figure 5(c), this was partially successful but the deposits rapidly dried out and delaminated from the steel surface.

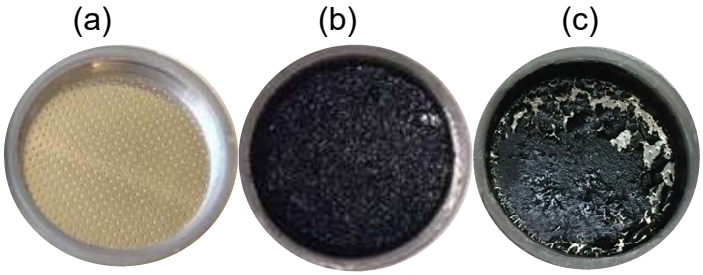


**Fig 5***: **(a)** Displays a photo of an unused CR2032 casing; **(b)** shows the same cell casing after coating vanadium onto the stainless steel by performing repeated cyclic voltammograms using the cell casing as the working electrode; **(c)** shows the cell casing if the vanadium solution was simply drop-cast and allowed to evaporate to coat the stainless steel; the poor adhesion and spontaneous delamination of the deposit from the stainless steel in this case is clearly seen.*

The vanadium oxide material was assumed above to be $V_2O_5$. However, a range of sodium-intercalated vanadium oxides are known, such as $Na_xV_2O_5$, $Na_{1+x}V_3O_8$ and $Na_2V_6O_{16}.nH_2O$.[25] X-ray Diffraction characterisation of the deposits achieved by both electrodeposition and by allowing graduation chemical deposition over a period of days demonstrated both to be amorphous in nature. X-ray Photoelectron Spectroscopy (XPS) of deposits upon glassy carbon (Figure 6a) had a broad peak in the vanadium V 2p region as in Figure 6b, which could not be quantitatively deconvoluted but did correspond largely to V(IV) oxide.

## X-ray photoelectron spectroscopy (XPS) of vanadium –coated on a flat GC electrode

X-ray photoelectron spectroscopy (XPS) it is a type of a spectroscopic technique which is used as a quantitative surface-element probe. It can determine the various elements present at or near a surface, as well as quantify their relative abundance. It is only suitable for solid, non-volatile samples (such as metals) as it must be performed

in vacuum. A flat glassy carbon electrode then was coated with vanadium oxide by cycling in 0.26 M V(V)/V(IV); the spectra is shown in Figure 6.

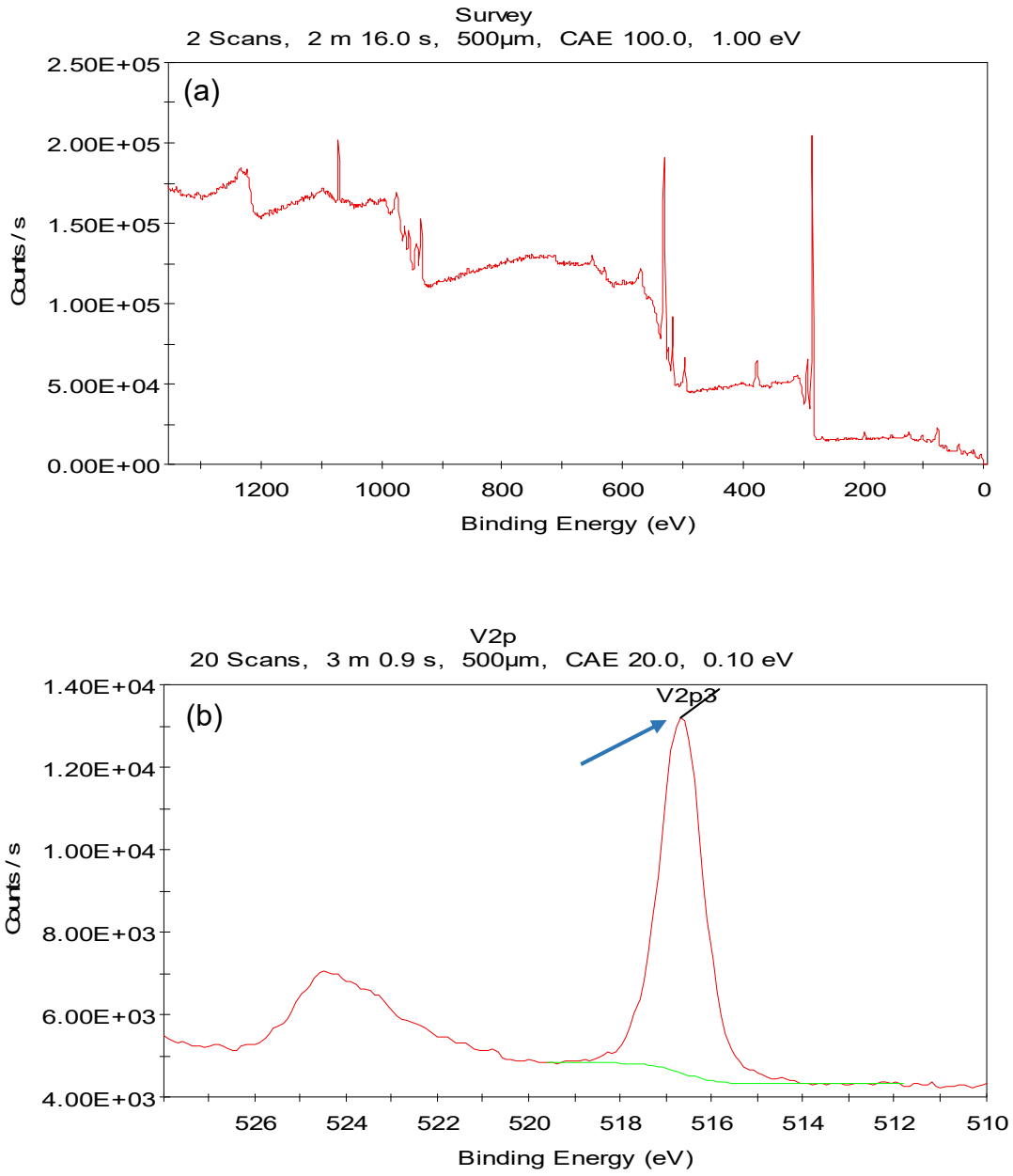


**Fig 6.** *XPS spectra for **a)** survey 0.26 M V(V)/V(IV) for vanadium coated on the flat glassy carbon .**b)** Showing the vanadium V 2p region.*

## Thermoelectrochemistry of the unbuffered, unsupported, aqueous V(IV)/V(V) system

The thermoelectrochemistry of the unbuffered, unsupported, aqueous V(IV)/V(V) system was initially highly unstable. However, if the electrode was first coated with a layer of electrodeposited $[Na_xV_2O_5]^{x+}$, reproducible thermoelectrochemistry was observed. Additionally, measurements of this system were more stable and reproducible if a smaller temperature difference was employed, therefore all subsequent results relate to using $\Delta T = 5$ K ($T_{cold} = 25°C$; $T_{hot} = 30°C$). Notably, this type of temperature range is highly relevant to waste body heat harvesting.

Figure 7(a) summerises the overall results observed; two halves of a CR2032 casing were electrodeposited with $Na_xV_2O_5$, the battery filled with fresh 0.2 M V(IV) / V(V) aqueous solution (as 0.1 M $NaVO_3$ and 0.1 M $VOSO_4$) and exposed to a temperature difference of 5 K. Measuring the short circuit current generated by the thermogalvanic cell, an initial spike of current lasting *ca.* 300 seconds was observed, before dropping to a steady-state current. When the temperature difference was removed, the current eventually dropped to zero (as would be expected) but only after a flow of current in the opposite direction was observed, of a similar magnitude and duration to the initial thermogalvanic spike in current. These features could be observed by repeatedly

applying and removing a temperature difference, as clearly shown in Figure 7(a) for the successive application and removal of a 5 K temperature difference three times. The high spike in the first peak is partially due to initial fluctuations in temperature (in our set up) when starting from everything being at room temperature to reach the required temperature ($\Delta T = 5$ K), relative to the further scans where the setup was fully thermally equilibrated. Additionally, some restructuring of the electrodeposited material also likely occurred, but only on the first cycle.

It was therefore speculated that the initial spikes in current under non-isothermal conditions corresponded to the migration of $Na^+$ from $Na_xV_2O_{5(cold)}$ to $Na_xV_2O_{5(hot)}$; since insertion of $Na^+$ will release water of hydration, this process increases entropy to the system. The subsequent steady state current then corresponds to the migration of vanadium from $Na_xV_2O_5$(cold) to $Na_xV_2O_5$(hot); once again the electrodissolution of vanadium will decrease entropy whereas its electrodeposition will increase it, via the associated water of solvation.

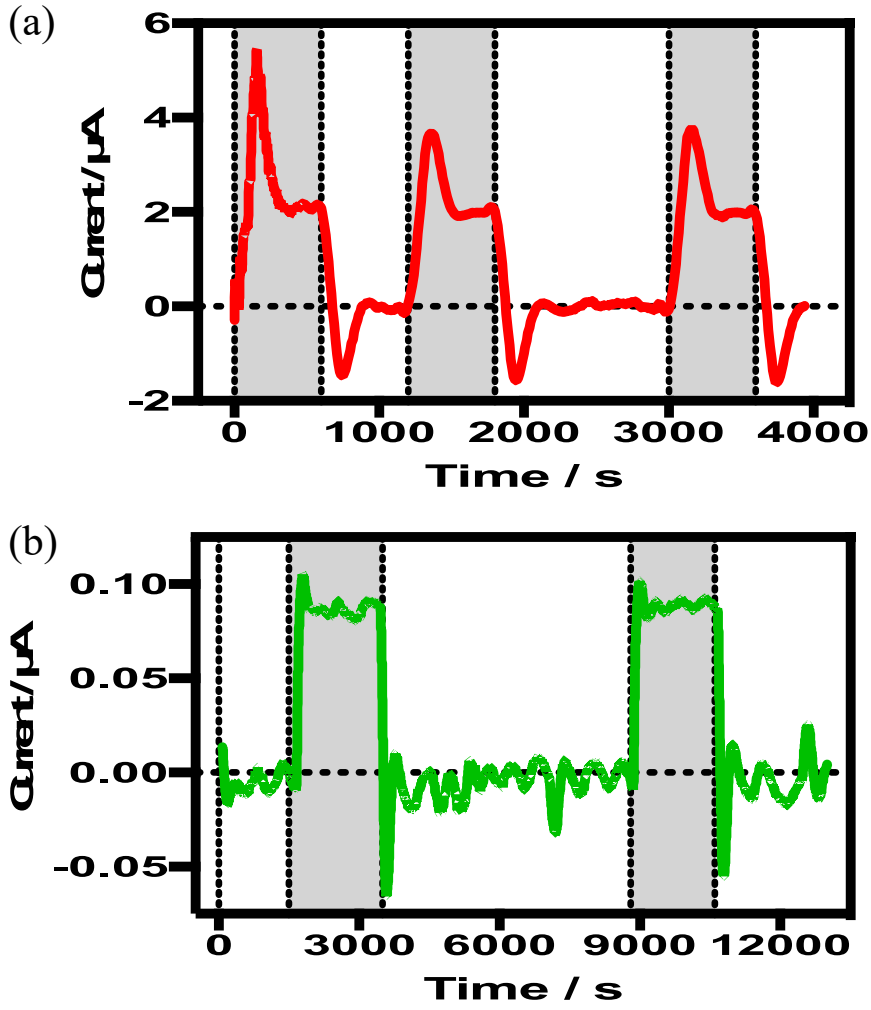


***Fig 7:*** *Graphs displaying the short-circuit current produced by battery casings which were alternately exposed to temperature gradients of ΔT= 5 K ($T_{hot}$ = 30°C, $T_{cold}$ = 25°C), as represented by the grey shaded area, or no temperature gradient ($T_{both}$ = 25°C). The battery casings were exposed to cyclic voltammetry in, and then crimped to contain 0.2 M V(IV) / V(V), composed of (a) 0.1 M $VOSO_4$ and 0.1 M $NaVO_3$ (i.e. Na-containing electrolyte) and (b) 0.1 M $VOSO_4$ and 0.05 M $V_2O_5$ (i.e. Na-free electrolyte).*

The migration of $Na^+$ from $Na_xV_2O_{5(cold)}$ to $Na_xV_2O_{5(hot)}$ is a finite process, since eventually the cold side will be sufficiently $Na^+$-deficient (*i.e.* $x < 0.5$) and the hot side corresponding $Na^+$-rich (*i.e.* $x > 0.5$) such that further migration of $Na^+$ is unfavourable. Removal of the temperature difference then results in enthalpically different electrodes; migration of $Na^+$ in the reverse direction, with associated redox chemistry, results in a flow of current and $Na^+$ in the opposite direction, until $x_{(hot)} = x_{(cold)}$ once again, as shown in Figure 8.

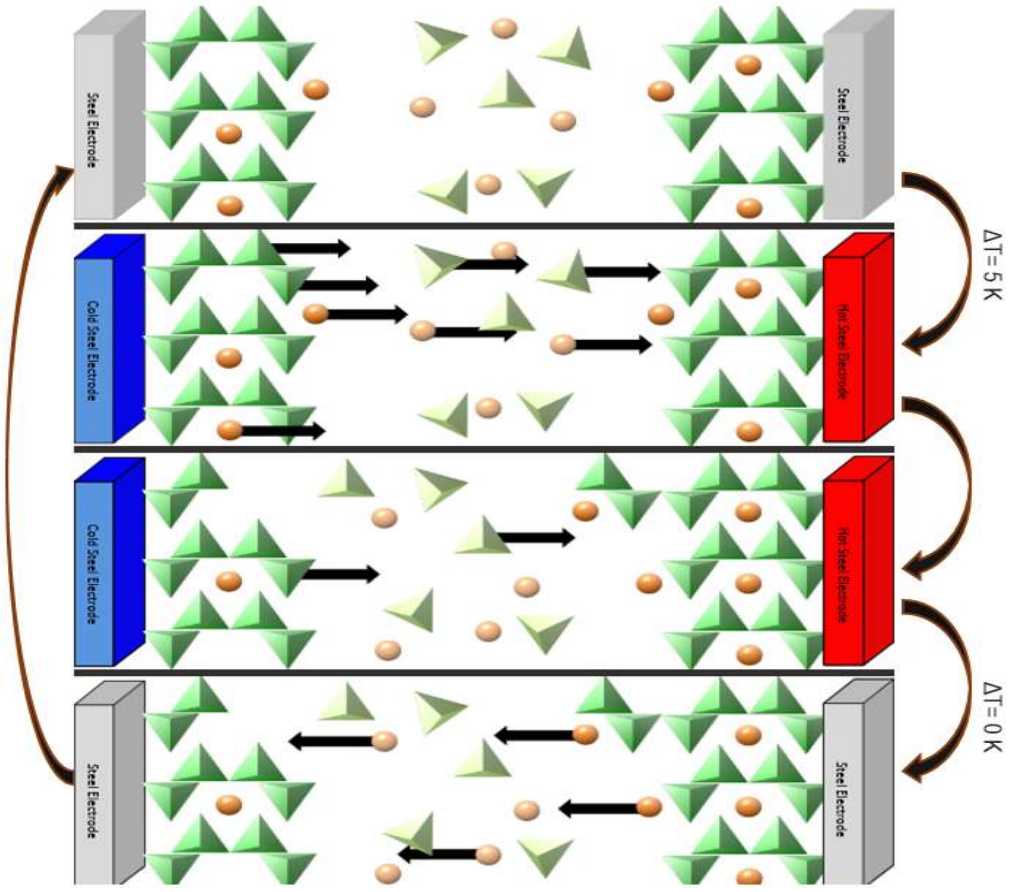


**Fig 8.** *Illustration displaying the Sodium-ion traveling from the cold electrode to the hotter side, when the temperature (T) applied, and the reversible process when T removed.*

Further confirmation was sought by investigating an analogous $Na^+$-free system. This was achieved by cycling the potential for a mixture of $V_2O_5$ and $VOSO_4$ (rather than $NaVO_3$ and $VOSO_4$). Measuring the thermogalvanic current for this system (Figure 7b) resulted in the expected response for a simple system; positive, steady current was generated when a temperature difference was applied, and the current rapidly dropped to zero in the absence of a temperature gradient. As such, this further confirmed the steady-state current was the migration of vanadium, while the presence of $Na^+$ resulted in transient current being generated in both directions. Minor current spikes are observed, but this is due to background noise, *cf.* the low currents recorded for the poor quality deposits achieved by this system.

As such, this demonstrates simultaneous thermogalvanic redox reactions (vanadium and sodium migration) being employed together to generate higher current. It also demonstrates a route by which a system can be 'buffered' against sudden removal of a temperature gradient. For example, a wearable system containing this thermogalvanic system could generate power continuously in the presence of a temperature gradient (at least until the vanadium on the cold electrode is exhausted), and when removed would continue to generate power (until the imbalance in x is corrected).

The migration of vanadium was found to be a reversible process (i.e. inverting the temperature gradient inverts the current) but a system containing only an 'entropy battery' effect is also desirable.

Attempts were made to suppress the migration of vanadium by increasing the pH, and by replacing the aqueous electrolyte with a non-aqueous electrolyte, namely NaPF6 in a 1:1 mixture of ethylene carbonate and propylene carbonate; neither were successful, and resulted in a complete loss of thermogalvanic chemistry. Therefore stable and reproducible systems could only be prepared by employing a 1-pot process where the CR2032 casing was electrochemically coated with the vanadium oxide deposit, and was subsequently filled with either the same vanadium-containing electrolyte (either from the cell used during electrodeposition, or with fresh vanadium-containing electrolyte of the same composition). The application of a one-pot process and using neutral aqueous solution is in fact highly advantageous, but expansion of this system to high surface area materials, e.g. carbon nanotubes, could achieve even more significant quantities of stored and released charges from these 'entropy batteries'.

## Conclusions

This study has noted that an acidic V(IV) / V(V) system (conventionally used in all-Vanadium redox flow batteries) demonstrates the expected thermogalvanic response consistent with these species being $VO^{2+}$ and $VO_2^{+}$, respectively. Ultimately, this system demonstrates a small Seebeck coefficient and slow electron transfer kinetics, resulting in relatively little thermogalvanic power being generated.

However, when the same system was investigated in neutral, unbuffered aqueous solution, facile electrodeposition of a vanadium oxide deposit could be achieved, on glassy carbon and stainless steel. Facile intercalation of Na+ ions was observed, and when investigated thermogalvanically two methods of current generation was observed. Firstly, Na+ ions migrated from the colder electrode to the hotter electrode, generating a follow of current. Secondly, when the temperature gradient was removed the flow of current was reversed, as the Na+ ions concentration was re-balanced across the two intercalation electrodes. This therefore demonstrates both waste thermal energy harvesting and waste heat energy storage opportunities.

## References


1. Hall, P. J.; Bain, E. J., Energy-storage technologies and electricity generation. *Energy Policy* **2008,** *36* (12), 4352-4355.
2. Snyder, G. J., Small thermoelectric generators. *The Electrochemical Society Interface* **2008,** *17* (3), 54.
3. Vining, C. B., An inconvenient truth about thermoelectrics. *Nature Materials* **2009,** *8* (2), 83-85.
4. Al Maimani, M.; Black, J. J.; Aldous, L., Achieving pseudo-'n-type p-type' in-series and parallel liquid thermoelectrics using all-iron thermoelectrochemical cells with opposite Seebeck coefficients. *Electrochemistry Communications* **2016,** *72*, 181-185.
5. Burrows, B., Discharge Behavior of Redox Thermogalvanic Cells. *Journal of the Electrochemical Society* **1976,** *123* (2), 154-159.
6. Quickenden, T. I.; Mua, Y., A review of power generation in aqueous thermogalvanic cells. *Journal of the Electrochemical Society* **1995,** *142* (11), 3985-94.
7. Buckingham, M. A.; Marken, F.; Aldous, L., The thermoelectrochemistry of the aqueous iron(ii)/iron(iii) redox couple: significance of the anion and pH in thermogalvanic thermal-to-electrical energy conversion. *Sustainable Energy & Fuels* **2018,** *2* (12), 2717-2726.

8. Aldous, L.; Black, J. J.; Elias, M. C.; Gélinas, B.; Rochefort, D., Enhancing thermoelectrochemical properties by tethering ferrocene to the anion or cation of ionic liquids: altered thermodynamics and solubility. *Physical Chemistry Chemical Physics* **2017,** *19* (35), 24255-24263.
9. Hupp, J. T.; Weaver, M. J., Solvent, ligand, and ionic charge effects on reaction entropies for simple transition-metal redox couples. *Inorganic Chemistry* **1984,** *23* (22), 3639-3644.
10. Salazar, P. F.; Kumar, S.; Cola, B. A., Design and optimization of thermo-electrochemical cells. *Journal of Applied Electrochemistry* **2014,** *44* (2), 325-336.
11. Wu, J.; Black, J. J.; Aldous, L., Thermoelectrochemistry using conventional and novel gelled electrolytes in heat-to-current thermocells. *Electrochimica Acta* **2017,** *225*, 482-492.
12. Weber, A. Z.; Mench, M. M.; Meyers, J. P.; Ross, P. N.; Gostick, J. T.; Liu, Q., Redox flow batteries: a review. *Journal of Applied Electrochemistry* **2011,** *41* (10), 1137-1164.
13. Tokuda, N.; Kumamoto, T.; Shigematsu, T.; Deguchi, H.; Ito, T.; Yoshikawa, N.; Hara, T., Development of a redox flow battery system. *SEI Technical Review* **2000**, *50,* 88-94.

14. Sum, E.; Rychcik, M.; Skyllas-Kazacos, M., Investigation of the V (V)/V (IV) system for use in the positive half-cell of a redox battery. *Journal of Power Sources* **1985,** *16* (2), 85-95.
15. Chung, S.-L.; Li, X., Materials Science and Energy Engineering (CMSEE 2014): *Proceedings of the 2014 International Conference*. *World Scientific*: 2015.
16. Bartolozzi, M., Development of redox flow batteries. A historical bibliography. *Journal of Power Sources* **1989,** *27* (3), 219-234.
17. Kear, G.; Shah, A. A.; Walsh, F. C., Development of the all-vanadium redox flow battery for energy storage: a review of technological, financial and policy aspects. *International Journal of Energy Research* **2012,** *36* (11), 1105-1120.
18. Hudak, N. S., Practical thermodynamic quantities for aqueous vanadium- and iron-based flow batteries. *Journal of Power Sources* **2014,** *269*, 962-974.
19. Fukuzumi, Y.; Hinuma, Y.; Moritomo, Y., Temperature coefficient of redox potential of LixFePO4. *AIP Advances* **2018,** *8* (6).
20. Hudak, N. S.; Amatucci, G. G., Energy Harvesting and Storage with Lithium-Ion Thermogalvanic Cells. *Journal of the Electrochemical Society* **2011,** *158* (5), A572-A579.
21. Black, J. J.; Harper, J. B.; Aldous, L., Temperature effect upon the thermoelectrochemical potential generated between lithium metal and lithium ion

intercalation electrodes in symmetric and asymmetric battery arrangements. *Electrochemistry Communications* **2018,** *86*, 153-156.

22. Black, J. J.; Murphy, T.; Atkin, R.; Dolana, A.; Aldous, L., The thermoelectrochemistry of lithium-glyme solvate ionic liquids: towards waste heat harvesting. *Physical Chemistry Chemical Physics* **2016,** *18* (30), 20768-20777.
23. Kim, K.; Lee, H., Thermoelectrochemical cells based on Li+/Li redox couples in LiFSI glyme electrolytes. *Physical Chemistry Chemical Physics* **2018,** *20* (36), 23433-23440.
24. Black, J. J.; Dolan, A.; Harper, J. B.; Aldous, L., Kamlet-Taft solvent parameters, NMR spectroscopic analysis and thermoelectrochemistry of lithium-glyme solvate ionic liquids and their dilute solutions. *Physical Chemistry Chemical Physics* **2018,** *20* (24), 16558-16567.
25. Kim, H.; Hong, J.; Park, K. Y.; Kim, H.; Kim, S. W.; Kang, K., Aqueous Rechargeable Li and Na Ion Batteries. *Chemical Reviews* **2014,** *114* (23), 11788-11827.
26. Rahman, F.; Skyllas-Kazacos, M., Solubility of vanadyl sulfate in concentrated sulfuric acid solutions. *Journal of Power Sources* **1998,** *72* (2), 105-110.
27. Skyllas-Kazacos, M.; McCann, J., Vanadium redox flow batteries (VRBs) for medium- and large-scale energy storage. In Menictas, C. Skyllas-Kazacos, M.,

Lim T. M. (eds), *Advances in Batteries for Medium and Large-Scale Energy Storage: Types and Applications* **2014**.

28. Li, X.-G.; Huang, K.-L.; Liu, S.-Q.; Ning, T.; Chen, L.-Q., Characteristics of graphite felt electrode electrochemically oxidized for vanadium redox battery application. *Transactions of Nonferrous Metals Society of China* **2007,** *17* (1), 195-199.
29. Sun, B.; Skyllas-Kazacos, M., Modification of graphite electrode materials for vanadium redox flow battery application—I. Thermal treatment. *Electrochimica Acta* **1992,** *37* (7), 1253-1260.
30. Pezeshki, A. M.; Clement, J. T.; Veith, G. M.; Zawodzinski, T. A.; Mench, M. M., High performance electrodes in vanadium redox flow batteries through oxygen-enriched thermal activation. *Journal of Power Sources* **2015,** *294*, 333-338.
31. Sun, B.; Skyllas-Kazacos, M., Chemical modification of graphite electrode materials for vanadium redox flow battery application—part II. Acid treatments. *Electrochimica Acta* **1992,** *37* (13), 2459-2465.
32. Alzahrani, H. A. H.; Black, J. J.; Goonetilleke, D.; Panchompoo, J.; Aldous, L., Combining thermogalvanic corrosion and thermogalvanic redox couples for improved electrochemical waste heat harvesting. *Electrochemistry Communications* **2015,** *58*, 76-79.

33. Ralston, K.; Chrisanti, S.; Young, T.; Buchheit, R., Corrosion inhibition of aluminum alloy 2024-T3 by aqueous vanadium species. *Journal of The Electrochemical Society* **2008,** *155* (7), C350-C359.
34. Lee, J.-K.; Kim, G.-P.; Song, I. K.; Baeck, S.-H., Electrodeposition of mesoporous V 2 O 5 with enhanced lithium-ion intercalation property. *Electrochemistry Communications* **2009,** *11* (8), 1571-1574.
35. Liu, C.; Gillette, E. I.; Chen, X.; Pearse, A. J.; Kozen, A. C.; Schroeder, M. A.; Gregorczyk, K. E.; Lee, S. B.; Rubloff, G. W., An all-in-one nanopore battery array. *Nature Nanotechnology* **2014,** *9* (12), 1031-1039.
36. Braithwaite, J. S.; Catlow, C. R. A.; Gale, J. D.; Harding, J. H. *Chem. Mater*. 1999, 11, 1990.

Chapter 3

# Agar Agar gel: Food-grade materials as potentially benign gelling agents for thermogalvanic systems

## Abstract

Electrolyte systems have widely been developed for many systems. One interesting approach is gelling the electrolytes, which is aiming to help to overcome difficulties in liquid electrolytes (such as leakage) while aiming to maintain desirable properties. In this chapter, the thermoelectrochemical behaviour of two types of electrolytes gelled by agar agar were investigated, and were compared with liquid-electrolytes equivalents. Part of this study involved developing a thermoelectrochemical cell suitable cell for use with the gelled systems, and to overcome corrosion issues identified by application of the iodide/triiodide redox couple. Results demonstrated that gelling different redox systems with agar agar was possible, but required different techniques for the different systems. Ultimately, thermoelectrochemically active gelled electrolytes were achieved, but an alternative gelling system was further explored in the following chapter.

# Introduction

Liquid electrolytes are typical in the majority of electrochemical studies. However, gelling electrolytes is known to have clear benefits in certain systems, and in particular in functional devices.[1, 2] Known potential benefits are;

- Overcoming safety issues by significantly reducing the likelihood of leakage of electrolytes
- Allows the development of novel solid-type electrolytes, which could have properties different to that of the liquid state analogue
- Can have good flexibility, which facilitates application to a variety of geometries, which would come with increased leakage risks in liquid-state systems

## Agar agar and carrageenan

Agar agar is known as a hydrophilic extract from certain seaweeds and red algae, and was found in 1658 by Minoya Tarozaemon.[3] Agar agar powder is a mixture of polysaccharides whose basic monomer is galactose.[4,5] The powder is widely commercial available, and agar agar gels are widely consumed.

Agar agar powder is soluble in boiling water, and upon cooling the solution to around 35 °C it forms a firm gel, and it will stay as a gel as long as the temperature does not exceed 85°C.

Carrageenan is another hydrophilic extract from certain seaweeds, and is significantly more heavily sulfonated than agar agar.[6] As such, it is significantly more water soluble, and gelation is triggered by the addition of calcium or potassium salts, where ionic interactions trigger gelation.[7]

Notably, both represent edible, safe, widely available gelling agents, one of which is thermally triggered and largely neutral (agar agar) and the other is heavily charged and triggered by the presence of appropriate cations (carrageenan). As such, they could have potential applications in large-scale or wearable thermogalvanic devices.

## Thermogalvanic corrosion

Galvanic corrosion is a well-established issue, whereby the more reactive component of a electrochemical system will corrode (anode) when connected electrically to a less reactive part (cathode) in the same electrolyte.[3] This is clearly noticed in the case of dissimilar metals, if there are conductive and corrosive electrolytes in the system; the combination of copper (as cathode) and stainless steel (as anode) is well established.[8] A key accelerating factor in corrosion processes is increasing temperature.[9,10] Moreover, fluid velocity and viscosity are also linked to corrosion damage in metals..[8,11]

Thermogalvanic systems typically use two electrodes composed of identical material, and therefore such corrosion should not be an issue. However, if these electrodes are at dissimilar temperatures then they can have dissimilar reactivity, and those thermogalvanic corrosion can occur. This was previously demonstrated when the thermogalvanic properties of the aqueous iodide/triiodide ($I^-/[I_3]^-$) redox couple was investigated in a stainless steel battery casing; thermogalvanic corrosion was observed to dominate the observed thermoelectrochemistry of the system.[11] It is reasonable to assume that almost all systems will undergo thermogalvanic corrosion to some extent, if the system is investigated for long enough, therefore metal systems such as stainless steel or even precious metals such as platinum and gold should ideally be avoided.

In this chapter, the gelation of both aqueous potassium ferri/ferrocyanide and aqueous potassium iodide/triiodide electrolytes was investigated. A novel thermogalvanic cell devoid of metal components was developed in order to investigate the thermogalvanic properties of this system, and remove the risk of thermogalvanic corrosion interfering.

# Experimental

Milli-QTM water (resistivity of 18.2 $M\Omega cm^{-1}$) was used throughout. Stainless steel CR2032 battery cells (plasma sputtered, both MTI Corporation, CA, USA) were crimped using a hydraulic press, and thus measurements were made in hermitically sealed casings. All reagents were purchased from Sigma–Aldrich (Castle Hill, NSW, Australia) and used as received.

## Gel preparation

Food-grade agar agar powder was obtained from a local supermarket. Agar agar gel was made by combining the specified wt% of agar agar powder with either water or the specified liquid electrolyte; this sample was simmered for 20 min in a covered beaker before being placed in a 4 °C fridge to set. Each prospective agar agar powder was mixed at five different ratios (1 wt% to 10 wt%) with both ultrapure water and the electrolyte.

Electrochemical measurements were performed using a Keysight B2900A Source Measurement Unit, using either Quick IV measurement software or a custom Excel Macro program. Temperature was controlled using the below assembly:

HE|Peltier|ACP| Cell |ACP|Peltier|HE

where HE is a copper heat exchanger, Peltier is a peltier heater/cooler, and ACP is an aluminum cold plate (all purchased from Custom Thermoelectric, MD, USA), the latter containing an embedded thermocouple. The temperature was thus controlled and maintained to within 0.1 °C, using an Arduino microprocessor.

All current–voltage data points were recorded by steady-state measurements over a 10 min period; the last 5 min was averaged to generate the relevant data points.

For gelled-electrolytes, a 3D printed nylon thermocell, was designed to have the same dimensions as the CR2032 battery casing. Glassy Carbon (vitreous carbon) plates were positioned on either side of the gel as electrodes (as anode and cathode).

## Results & Discussion

The thermogalvanic properties of two redox-active aqueous electrolytes were investigated; 0.2M potassium ferricyanide and 0.2 M potassium ferrocyanide dissolved in water, and 0.4 M iodine and 0.8 M potassium iodide. In the latter case, equimolar equivalents of iodine and iodide are expected to combine, in order to form 0.4 M potassium iodide and 0.4 M potassium triiodide. These were initially investigated in conjunction with agar agar.

### Gelled electrolyte preparation

Initially, the preparation of the agar agar gels had to be optimised, given that the introduction of either 0.2M potassium ferricyanide and 0.2 M potassium ferrocyanide, or 0.4 M iodine and 0.8 M potassium iodide (to form 0.4 M potassium iodide and 0.4 M potassium triiodide) was observed to alter the gelation properties of the agar agar.

This was achieved by following the standard protocol of mixing agar agar powder with the aqueous electrolyte, the solution was heated rapidly on a hot plate until visibly boiling, and then allowed to cool to room temperature. After cooling to room temperature, the samples were inverted, and if the solution was still a solid mass sticking to the top of the inverted vessel after 5 minutes, it was considered ‘gelled’ as

it had passed the inversion test. This was optimised for water, and then also performed under identical conditions for the redox active electrolytes, with the wt% values of the agar agar varied from 1 wt% up to 10 wt%. As shown in the Table 1, all water-only samples within this range gelled. The lowest loading (1 wt%) failed to gel in the presence of potassium ferri/ferrocyanide, but from 2 wt% upwards, strong and firm gels could be obtained; as such, gelled potassium ferri/ferrocyanide could be easily obtained. However, for the iodide/triiodide electrolyte, gelation could not be achieved, even after the addition of 10 wt% agar agar powder.

| Wt% agar agar powder | Mass agar agar powder added (mg) | Volume of water added (µl) | Result for pure water | Result for 0.4M ferri/ferrocyanide | Result for 0.4M $I_2$ + 0.8M KI |
|---|---|---|---|---|---|
| **10** | 200 | 1800 | Gel | Gel | Not gelled |
| **6.6** | 132 | 1868 | Gel | Gel | Not gelled |
| **3.3** | 66 | 1934 | Gel | Gel | Not gelled |
| **2** | 40 | 1960 | Gel | Gel | Not gelled |
| **1** | 20 | 1980 | Gel | Not gelled | Not gelled |

**Table 1.** *Different wt% values of the agar agar that added to water and other redox couple*

In an effort to achieve agar agar gel containing the redox active iodide/triiodide redox couple, agar agar gels were initially synthesised in pure water. Then, these pre-prepared gels were soaked in an aqueous solution of iodide/triiodide for a period of several hours; upon removal of the gels from the aqueous electrolyte, the penetration of the iodine-based electrolyte was clearly observed. Figure 1 displays the gelled ferri/ferrocyanide electrolyte achieved by heating agar agar powder added directly to

the ferri/ferrocyanide electrolyte. A high quality, homogenous gel structure could consistently be achieved, where the structure of the gel mirrored the size and shape of the vessel in which the gel was cooled. Figure 2 displays the resulting gel when it was prepared by heating and cooling 6.6 wt% agar agar gel in pure water, and then soaking the aqueous gel in a significantly larger volume of aqueous electrolyte containing 0.4 M iodine and 0.8 M potassium iodide for 2-3 hours. Upon removal of the gel from the electrolyte, penetration of the dark iodide/triiodide electrolyte into the gel was clearly observed. These gels were prepared in a mould such that they would fit within the interior cavity of a CR2032 battery casing; these were then taken subjected to thermogalvanic analysis.

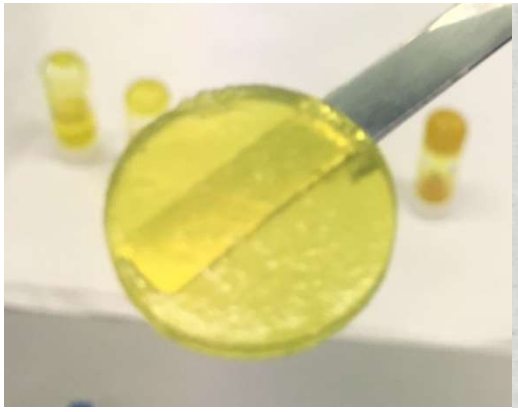

**Fig 1.** *This photograph for Ferri/ferrocyanide gelled electrolyte: Dissolve agar agar powder into electrolyte to form gel*

**Fig 2.** *This photograph for Iodine gelled electrolyte : Necessary to make agar gel then soak in a solution of Iodide/triiodide for a few hours*

## Thermogalvanic measurement of the liquid electrolytes

Initially the thermogalvanic properties of the ferri/ferrocyanide electrolyte and the iodide/triiodide electrolyte were investigated in stainless steel CR2032 casings. Figure 3 displays the resulting power curve for 0.4 M potassium ferri/ferrocyanide at $\Delta T$ = 30°C; the power curve gave the expected parabola. The apparent Seebeck coefficient was recorded as -1.2 mV $K^{-1}$; literature values for the Seebeck coefficient of 0.4 M ferri/ferrocyanide span from -1.2 to -1.6 mV $K^{-1}$ .[12.13]

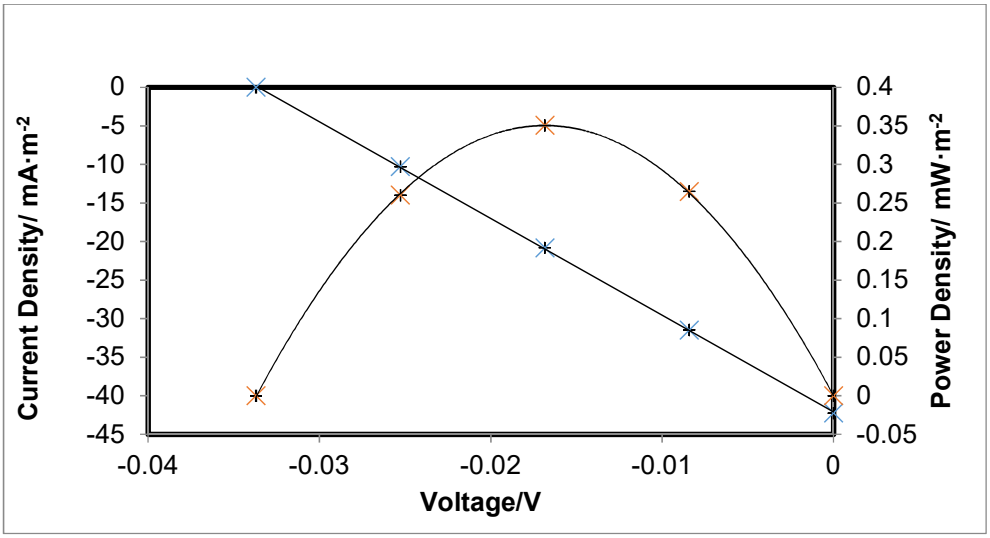


***Fig 3.*** *Shows current &power density plots recorded for 0.4 M of Ferri-ferrocyanide in a stainless steel battery casing at ΔT =30°C*

The open circuit potential and short circuit current density for this system was stable as a function of time, indicating the stainless steel casing was appropriate for measuring such systems.

The same experiment was performed, but using the aqueous electrolyte containing 0.4 M iodine and 0.8 M potassium iodide. In this case, the open circuit potential and short circuit current density were observed to be unstable in the stainless steel battery casing. For example, Figure 4 displays the thermogalvanic power curve for the same system when (a) measured after being prepared, (b) the same system 24 hours later, and (c) 72 hours later (all at $\Delta T = 30°C$). This was determined to correspond to thermogalvanic corrosion of the stainless steel casing occurring (full details published elsewhere[9]) and this demonstrated that the iodine-containing gels could not be investigated in the stainless steel cell casing. As such, the preparation of a metal-free thermogalvanic cell with similar internal dimensions to that of the CR2032 was investigated.

.

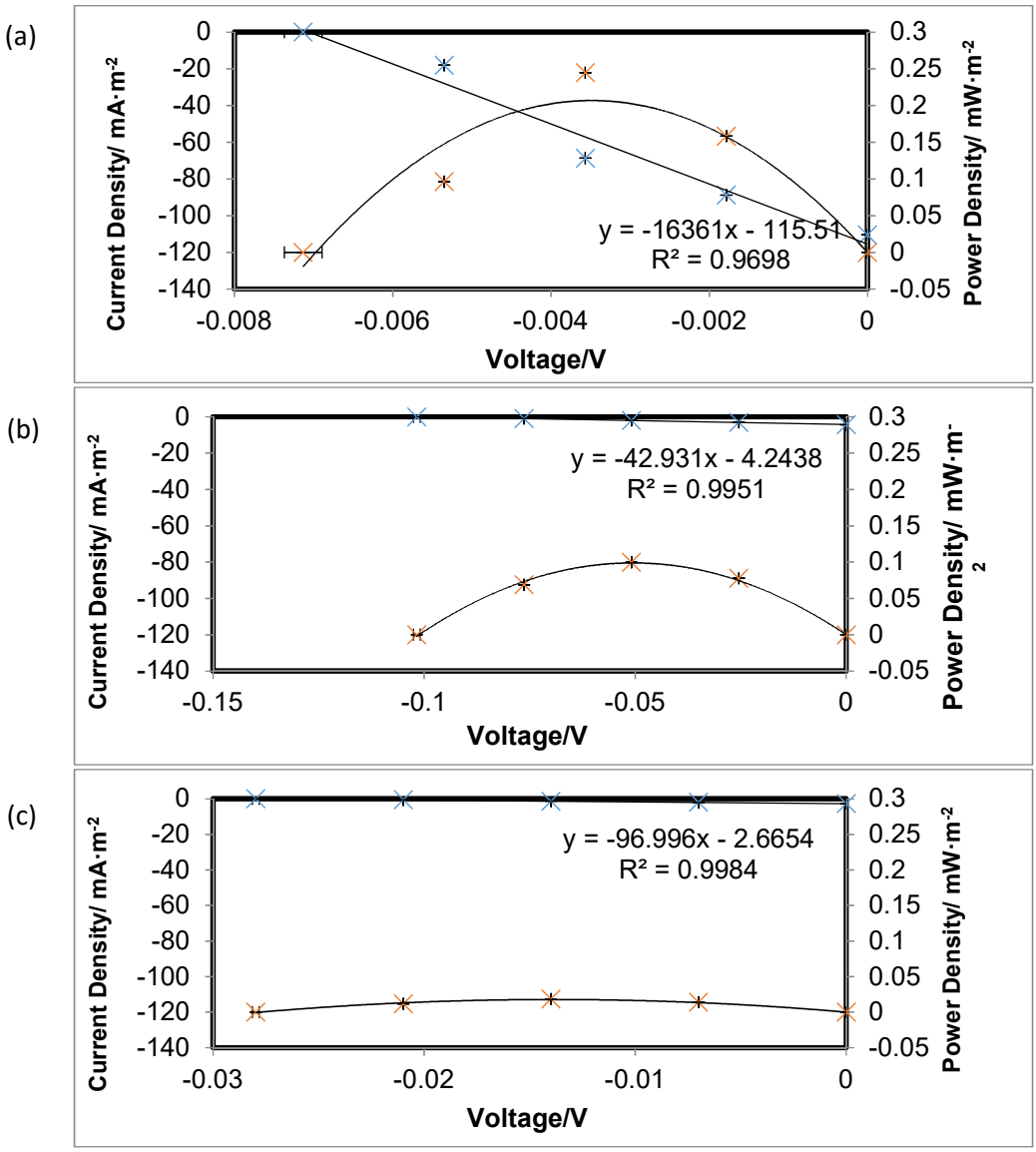


***Fig 4.*** Current & *power density plots recorded for 0.4M of $I^-/[I_3]^-$ in a stainless steel battery casing at $\Delta T$ values of 30°C($T_{cold}$=15°C), for 72hr.* ***(a)*** *first measuring power before starting.* ***(b)*** *second power in 24 hours.* ***(c)*** *measuring power in 72hr.*

### The metal-free thermogalvanic set-up

Since the CR2032 stainless steel battery casings were not a viable housing, and precious metal sputtered versions were also unstable, entirely carbon-based alternatives were investigated. Ultimately, the most effective cell developed was based upon a 3D printed nylon holder, with a circular cavity through it with the same dimensions as that of the CR2032 casing. Glassy Carbon (vitreous carbon) plates were positioned on top and bottom as electrodes (as anode and cathode); Figure 5 displays a schematic of this cell, as well as a photograph of the cell and the gelled electrolyte it could measure. Temperature control was achieved by placing Peltier devices in contact with the glassy carbon plates; holes in the side of the glassy carbon plates allowed the insertion of thermistors, such that the temperature could be monitored and controlled. While this cell was unable to investigate liquid electrolyte (given that there is no firm seal, or o-ring or equivalent, which is required to make the cell completely liquid-tight), it was able to measure the gelled electrolyte with no leakage issues.

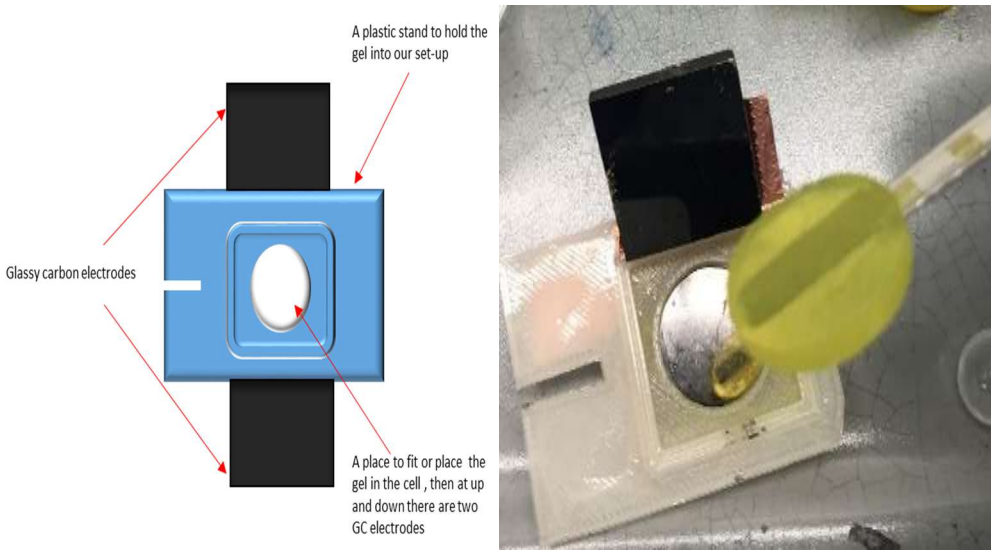


**Fig 5.** *Experimental apparatus set up, this 3D printed nylon holder cell is showing how the gelled is taking place in-between two glassy carbon electrodes.*

## Thermogalvanic measurement of the gelled electrolytes

Having developed an appropriate cell, and methods to prepare the two gelled electrolytes, the corresponding gels were investigated for their thermogalvanic properties. Firstly, 0.05 M ferri/ferrocyanide gelled-electrolyte was investigated. Glassy carbon was used as an electrode, and the expected power curve was recorded (Figure 6). This therefore demonstrated that the new cell assembly was operating successfully, and gelling the ferri/ferrocyanide did not prevent the thermoelectrochemistry occurring.

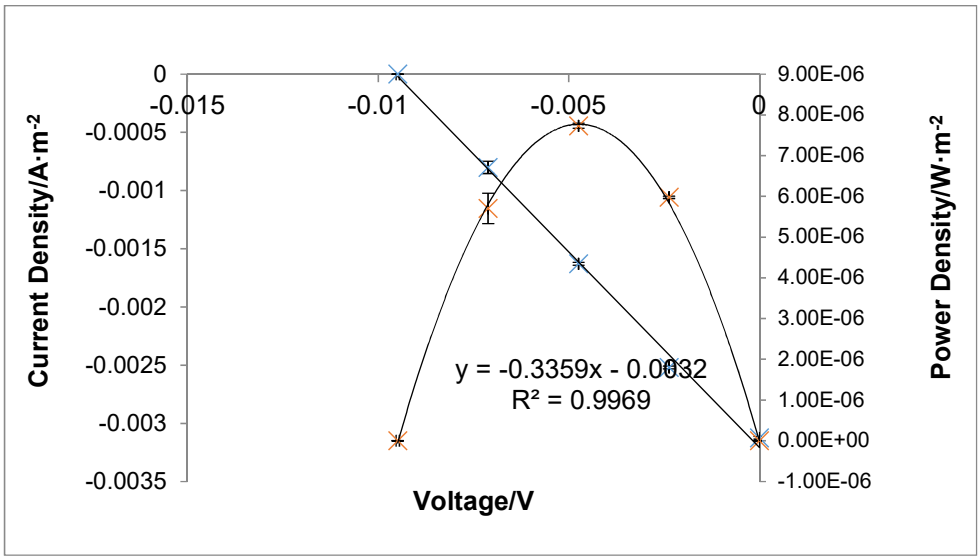


**Fig 6.** *Shows current &power density plots recorded for gelled 0.05M of Ferri-ferrocyanide in a stainless steel battery casing at ΔT = 10K.*

The iodide/triiodide-based agar agar gels were also investigated, after soaking the pre-made gels in the solution, as described above. Unlike the case of the aqueous iodide/triiodide-based system in the stainless steel system, the gelled electrolyte in the metal-free cell resulted in typical thermogalvanic power curves, and measurements did not change with time. As shown in Figure 7(a), when exposed to ΔT = 20 K, an apparent Seebeck coefficient of +0.5 mV $K^{-1}$ was measured.

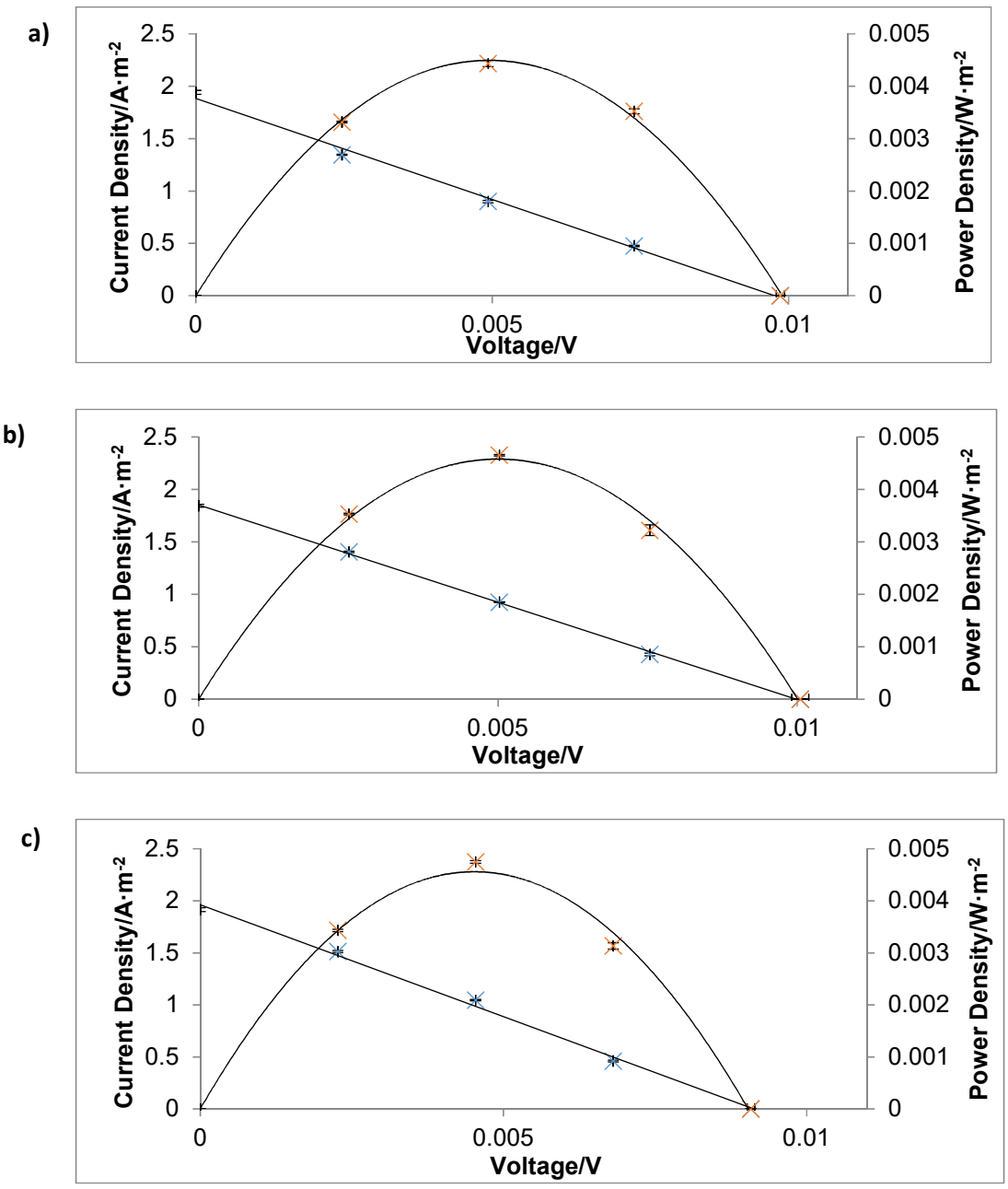


**Fig 7.** *Typical I-V plots and associated power curves for agar agar gel after being soaked in (a) 0.4 M I2 in 0.8 M KI (or 0.4 M [I3]- and 0.4 M I-) (b) 0.2 M I2 in 0.6 M KI (or 0.2 M [I3]- and 0.4 M I-), and (a) 0.2 M I2 in 0.8M KI (or 0.2 M [I3]- and 0.6 M I-). All were measured at ΔT = 20 K*

Given that the iodide/triiodide redox couple was now able to be probed, the ratio and concentration of the two redox states were varied, in order to investigate their effect upon the overall power output. However, as shown in Figure 7, even when (b) the concentration of both was reduced in the aqueous solution, or (c) the concentration of just the iodine was reduced, the Seebeck coefficient, current output and power output was still essentially the same as that of the original ratio. This indicates that it's likely that the agar agar is extracting a fixed quantity of iodide and triiodide from the aqueous solution, and in an unknown ratio. This was likely a relatively low quantity of material, given that it was relatively insensitive to the concentration of the two in the surrounding aqueous solution. Therefore, while it's positive that a relatively reproducible system can be prepared each time (despite variations in the soaking solution) is also noted that the composition inside the gel is unknown. Future work could focus upon analysing these separately, *e.g.* using UV-Vis to monitor the concentration of triiodide in solution before and after contacting it with the gel, in order to calculate how much was taken up. However, this would remain a relatively low concentration, which is not ideal for a gelled thermogalvanic cell, cf. attempts to make the gel in the solution containing reasonable concentrations of electrolyte always failed. Therefore, the gelled electrolyte is not a suitable for a fundamental investigation of the iodide/triiodide system without extensive further work, and this system is not anticipated to be able to support reasonable concentrations of redox active material.

## Conclusions

Thermoelectrochemical cells can in theory generate power indefinitely, but leakage is one potential route of failure. Given the temperature difference such cells are exposed to, leakage is an unfortunately common issue. This Chapter has successfully reported gelling of two thermoelectrochemically active electrolytes, using benign agar agar. However, while effective for the ferri/ferrocyanide redox couple, for the iodide/triiodide redox couple one-pot formation was not possible, and soaking in the electrolyte was required to generate a redox-active gel. This demonstrated some insensitivity with respect to the solution-phase concentration, hence in the next Chapter, agar agar was abandoned in favour of super-adsorbent polymer gels.

## References


1. Liyu, Jin, et al. Redox-active quasi-solid-state electrolytes for thermal energy harvesting. *ACS Energy Letters* 1.4 (2016): 654-658.
2. Jimmy,Wu, Black, J J, and Aldous, L. Thermoelectrochemistry using conventional and novel gelled electrolytes in heat-to-current thermocells. *Electrochimica Acta* 225 (2017): 482-492.
3. Tooru A, Izumi Sei-ichi. Sulfate Groups of the Mucilage of Red Seaweeds (Rhodopheceae). *Agricultural and Biological Chemistry* 40.2 (1976): 285-289.
4. Allan GG, Johnson PG, Lai YZ, Sarkanen KV. Marine polymers: part I. A new procedure for the fractionation of agar. *Carbohydrate Research*. 1971 Mar 1;17(1):234-6.
5. Araki CH. Acetylation of agar like substance of Gelidium amansii. *J. Chem. Soc.* 1937;58:1338-50.
6. Bhattacharjee, SS., Yaphe W., Hamer GK.. Study of agar and carrageenan by 13 C nuclear magnetic resonance spectroscopy. *Proc. int. Seaweed Symp.* Vol. 9. 1979.
7. DiNinno V, McCandless EL. The chemistry and immunochemistry of carrageenans from Eucheuma and related algal species. *Carbohydrate research*. 1978 Oct 1;66(1):85-93.

8. Kuzminskii Y, Zasukha V, Kuzminskaya G. Thermoelectric effects in electrochemical systems. Nonconventional thermogalvanic cells. *Journal of power sources.* 1994;52(2):231-42.

9. Gerasimov V, Rozenfeld I. Thermogalvanic corrosion. *Bulletin of the Academy of Sciences of the USSR, Division of chemical science*. 1957;6(1):29-31.

10. Kritzer P. Corrosion in high-temperature and supercritical water and aqueous solutions: a review. *The Journal of Supercritical Fluids*. 2004;29(1):1-29.

11. Alzahrani, H. A. H.; Black, J. J.; Goonetilleke, D.; Panchompoo, J.; Aldous, L., Combining thermogalvanic corrosion and thermogalvanic redox couples for improved electrochemical waste heat harvesting. *Electrochemistry Communications* **2015,** *58*, 76-79.

12. Romano MS, Li N, Antiohos D, Razal JM, Nattestad A, Beirne S, et al. Carbon Nanotube - Reduced Graphene Oxide Composites for Thermal Energy Harvesting Applications. *Advanced Materials*. 2013;25(45):6602-6.

13. Hu R, Cola BA, Haram N, Barisci JN, Lee S, Stoughton S, et al. Harvesting waste thermal energy using a carbon-nanotube-based thermo-electrochemical cell. *Nano letters*. 2010;10(3):838-46.

Chapter 4

# AuNP thermoelectrochemistry

This majority of the results presented in this chapter has been published as '*Success and failure in the incorporation of gold nanoparticles inside ferri/ferrocyanide thermogalvanic cells*' in Electrochemistry Communications.

(Alzahrani, Hassan AH, et al. "*Success and failure in the incorporation of gold nanoparticles inside ferri/ferrocyanide thermogalvanic cells*." Electrochemistry Communications 102 (2019): 41-45.)

## Abstract

In this chapter, gelled electrolytes were also employed, following on from Chapter 3. However, in this case commercial material was employed, and novel ways of integrating gold nanoparticles with the gelled electrolyte was explored.

Thermogalvanic systems represent a means to convert a temperature gradient into electricity, using only redox chemistry. However, the kinetics of electron transfer and physical mass transport of the redox couples are known limitations. In this study we present self-contained gelled thermogalvanic cells (or thermocells) containing the ferricyanide/ferrocyanide redox couple, which additionally have gold nanoparticles either immobilised at the gel/electrode interface, or distributed throughout the entire gel. Both methods of introducing the gold nanoparticles results in an apparent electrocatalytic improvement, as demonstrated by significant decreases in the electron transfer resistance. However, when used as thermogalvanic cells, only minor improvements were observed in power generation, and relatively rapid dissolution of

the gold nanoparticles was observed, to yield passivating gold analogues of Prussian Blue. Therefore successful preparation and short-term improvements have been demonstrated, but are offset by long-term stability issues. The relatively surprising instability of the generally inert gold nanoparticles in the presence of ferricyanide/ferrocyanide, particularly under thermogalvanic conditions, is of particular note.

Additionally, since stable gels were formed, these were investigated in detail without AuNP being present. Notably, significantly restricted mass transport of the electrochemical products away from the two electrodes resulted in a significant decrease in performance vs time; this was conclusively demonstrated, and also recovery of the systems, albeit after extended periods without discharging.

## Introduction

Thermogalvanic energy conversion has been receiving increasing attention, given its ability to convert waste heat, in the form of a temperature gradient, into a flow of electrical current.[1] This occurs without moving mechanical parts, and is achieved by an entropy-driven redox reaction, or 'electrochemical Seebeck effect',[2] which was first noted more than 120 years ago.[1,3] Recently, attention has been drawn to maximising the current output, by the development of thermogalvanic cells, or thermocells. Here, the redox couple, solvent, electrode material, cell dimensions and even cell orientation are all critical features.[3,4]

Arguably the most commonly employed system in thermogalvanic investigations is the aqueous potassium ferricyanide / potassium ferrocyanide redox couple.[1–3] This system benefits from the relatively high solubility of the redox couple, relative ease of availability, and a relatively high temperature-dependence upon the cell potential (or "Seebeck coefficient").[2] While typically employed in liquid form, recently it has been investigated in a range of gelled media.[5–7] Given that such devices typically operate at low over-potentials (mV-range), significant electrocatalytic effects have been observed, such as a 60-fold increase in current and power output from an aqueous ferri/ferrocyanide thermogalvanic cell upon moving from bare stainless steel to

platinum-sputtered electrodes.[8] The use of nanomaterials, largely in the form of graphene and carbon nanotubes, has also been explored extensively and has been reviewed elsewhere.[9]

While the application of nanoparticles at the electrode surface in thermogalvanic cells has not been widely reported, the application of nanoparticles *inside* liquid thermogalvanic cells has, in the form of nanofluids. Huang *et al.* reported that maghemite nanoparticles in dimethylsulfoxide undergo "thermodiffusion or thermophoresis" in a temperature gradient, generating a measurable Seebeck coefficient; they demonstrated that this is more than simple thermal gradient introduced convention.[10] The same groups also demonstrated that maghemite nanoparticle addition to an aqueous ferri/ferrocyanide thermogalvanic cell increased the apparent Seebeck coefficient, and thus the thermogalvanic power output.[11] Others have investigated the addition of alumina nanoparticles to aqueous ferri/ferrocyanide thermogalvanic cells; while an increase in ionic conductivity and decrease in thermal conductivity was demonstrated, the Seebeck coefficient remained unchanged and power generation was not investigated.[12]

Gold nanoparticles (AuNP) have been widely reported (although not in the context of thermogalvanic cells) and can be produced through various methods.[13–15] One conventional method involves heating $Au_{(III)}$ in the presence of citrate, to produce an aqueous colloid of citrate-capped AuNP.[16] The electrocatalytic ability of gold has been widely explored,[17] and the homogeneous (electro)catalysis of redox reactions by AuNP has also been noted, *e.g.* the presence of AuNP in solution resulted in a *ca.* $10^4$ rate enhancement in the reduction of $[Fe(CN)_6]^{3-}$ to $[Fe(CN)_6]^{4-}$ by $Na[BH_4]$.[18] However, the effective immobilisation of such nanoparticles at electrode surfaces is challenging,[19] and preparation of reasonably mechanically robust systems often requires direct covalent linkage to the electrode surface,[20] composite preparation (such as using polymers)[20] or even the application of magnetic fields.[19] This is especially challenging for thermogalvanic cells, given the extensive convection expected.[21]

AuNP synthesis inside gelled media has also been reported, such as inside agarose gels,[22,23] chitosan films,[24] in the presence of molecular gelators,[25,26] *etc.* While used for sensing and catalysis, they have not been investigated for electrochemical systems in general, nor thermogalvanic cells in particular. An exception was the *in situ* preparation of AuNP in agrose hydrogels; exposure of the hydrogel to 0.5 M $HAuCl_4$, followed by $NaBH_4$ reduction, followed by partial dehydration, demonstrated conductivity and I-V properties consistent with a percolation network forming.[27]

In this investigation, we have firstly investigated the application of single sodium poly(acrylate) superadsorbent spheres (or gel) soaked in aqueous ferri/ferrocyanide as a facile means for forming a standalone thermogalvanic cell. We have then investigated the application of AuNP to the interface between the electrode and the gel, whereby immobilisation is achieved without the use of any other binders. Finally, we have investigated the application of immobilised AuNP inside and throughout the gel-based thermogalvanic cell. As a consequence, this investigation reports successful electrocatalysis, and thus improvements in the power output of the gel-based thermogalvanic cells, but also long-term stability issues, by virtue of AuNP dissolution in the redox active electrolyte.

## Experimental

### Chemicals

All reagent were ordered from UK suppliers, and used as received. These were sodium tetrachloroaurate hydrate, ($NaAuCl_4$, 98%, Acros Organics), sodium citrate tribasic dihydrate (>99%, Sigma Aldrich), potassium hexacyanoferrate(II) trihydrate ($K_4[Fe(CN)_6]$, ≥99.5%, Sigma Aldrich), potassium hexacyanoferrate(III), ($K_3[Fe(CN)_6]$, ≥99%, Honeywell), and commercial sodium polyacrylate spheres (Sungpunet, China).

### Gel and Gold Nanoparticle (AuNP) synthesis

Commercial sodium polyacrylate spheres (*ca.* 2.5 mm diameter when dry) were soaked in an excess volume of aqueous 0.2 M $K_3[Fe(CN)_6]$ / 0.2 M $K_4[Fe(CN)_6]$ for 24 hours; during this period the gels swelled to have a diameter of *ca.* 8 mm.

Gold nanoparticle (AuNP) colloids in water were synthesised by the Turkevich method,[16] by bringing a 1 mM $NaAuCl_4$ and 5 mM sodium citrate to the boil, and boiling until the expected burgundy-coloured solution was obtained. After cooling, 10 µL of the colloid was dropcast onto the graphite electrode surface and allowed to dry before use.

AuNP colloids immobilised inside a sodium polyacrylate matrix was achieved as reported in detail elsewhere.[28] Briefly, this involved soaking a sodium polyacrylate sphere in a 4 mM $NaAuCl_4$ aqueous solution for ~1 hour, then bringing to the boil and refluxing for ~30 minutes; this resulted in a deep burgundy colour, with the swollen gel now containing uncapped immobilised AuNP.. Figure 1 displays the size distribution of the AuNPs in the gel, as quantified by cryo-TEM analysis (more details in Chapter 5). These were then transferred to 0.2 M $K_3[Fe(CN)_6]$ / 0.2 M $K_4[Fe(CN)_6]$ and soaked for 24 hours.

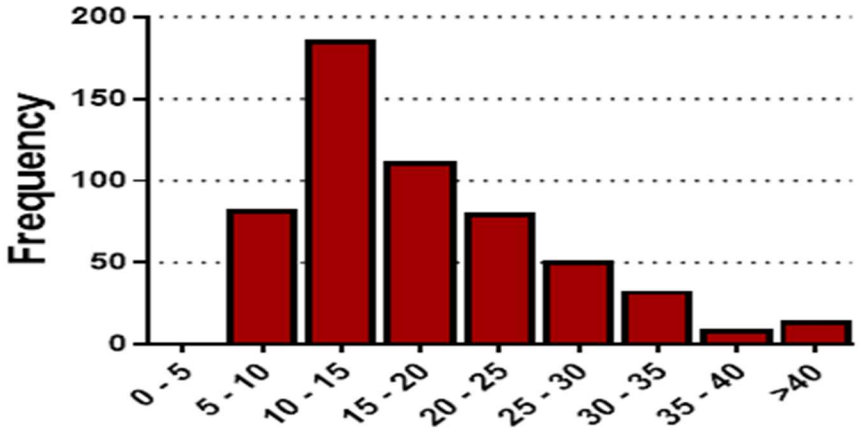


**Fig 1**: *Distribution plot of gold nanoparticle in gel diameters.*

## Thermoelectrochemical Measurements

The thermoelectrochemical cell consisted of a Nylon 6,6 tube with an outer diameter of 20 mm, an inner diameter of 10.5 mm, and an inter-electrode separation of 8 mm (RS Components Ltd, UK). This was placed between two graphite electrodes, which were in contact with copper heat exchangers connected to RS-TX150 thermostatic circulator baths (Grant Instruments Ltd, UK). This is shown schematically in Figure 2a ,and the entire setup shown visually in Figure 2b. The contact area between the gel and electrode was fixed by covering the graphite with an adhesive polyethylene label (P12/64 R MWPE) into which a 6 mm diameter hole had been punched. The electrode material consisted of 0.017 mm thick Pyrolytic Graphite Thermal Interface Material (1750 W $m^{-1}$ $K^{-1}$ thermal conduction, RS components). Experimental measurement conditions were the same as those reported elsewhere.[29]

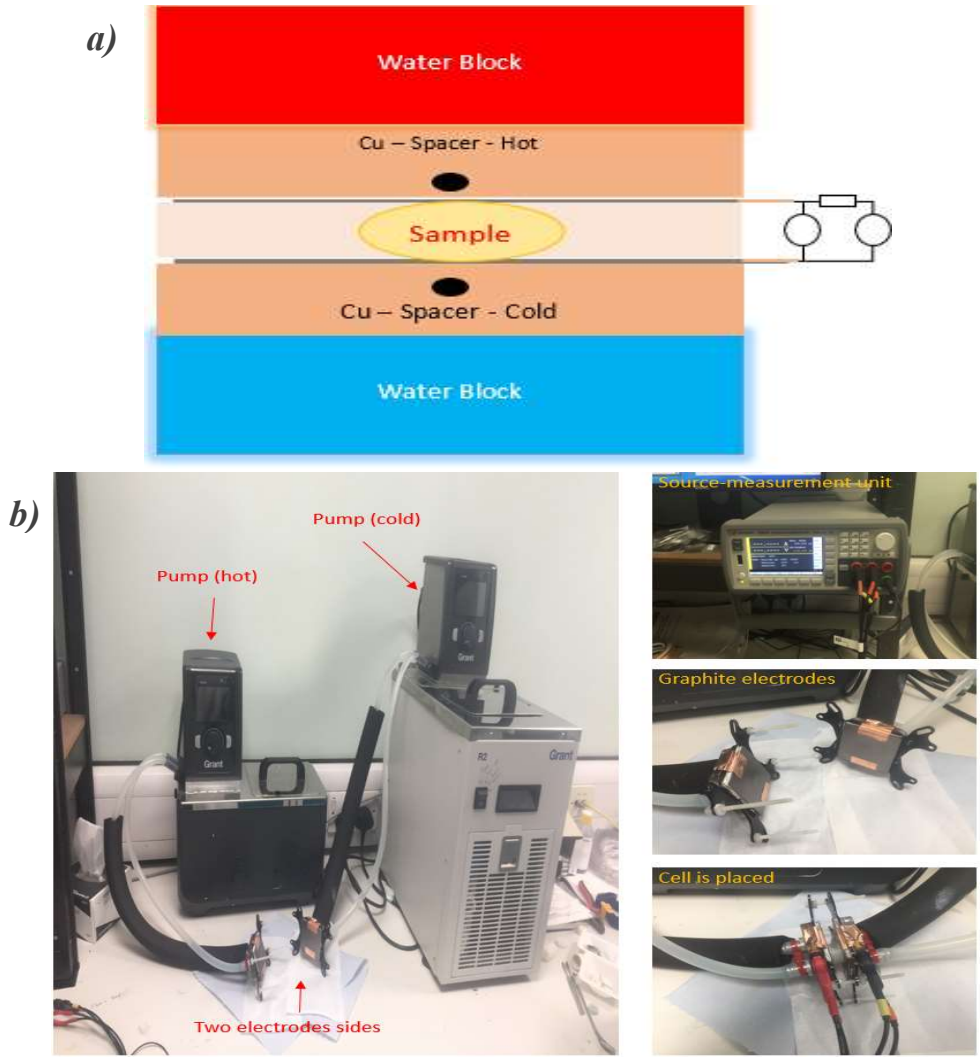


**Fig 2. a)** *Schematic of the experimental setup,* ***b)*** *Photos showing the complete experimental setup*

## Electrochemical Impedance Spectroscopy

Electrochemical Impedance was performed on liquid and gelled systems (all containing 0.2 M $K_3[Fe(CN)_6]$ / 0.2 M $K_4[Fe(CN)_6]$) in the same setup as thermoelectrochemical measurements. The impedance measurements were performed using an Ivium compact potentiostat. The impedance spectra were obtained at the equilibrium potential with a frequency range from 50,000 Hz to 0.05 Hz and with an amplitude of 50 mV.

## Results & Discussion

### Electrochemical Impedance Spectroscopy

Initially, the systems were characterised under isothermal conditions using impedance spectroscopy; aqueous 0.2 M $K_3[Fe(CN)_6]$ / 0.2 M $K_4[Fe(CN)_6]$ (henceforth referred to as "**liquid cell**") was compared with gelled spheres swollen with the same electrolyte (referred to as "**gel-cell**"). Two systems containing gold nanoparticles (or AuNP) were also evaluated; the first involved AuNP dropcast onto the electrode surface ("**AuNP@surface**"). The second involved gel spheres where AuNP had been grown inside of the gel ("**AuNP@gel**"). Figure 3 displays a schematic highlighting the resulting thermocells prepared by these three gel sphere systems.

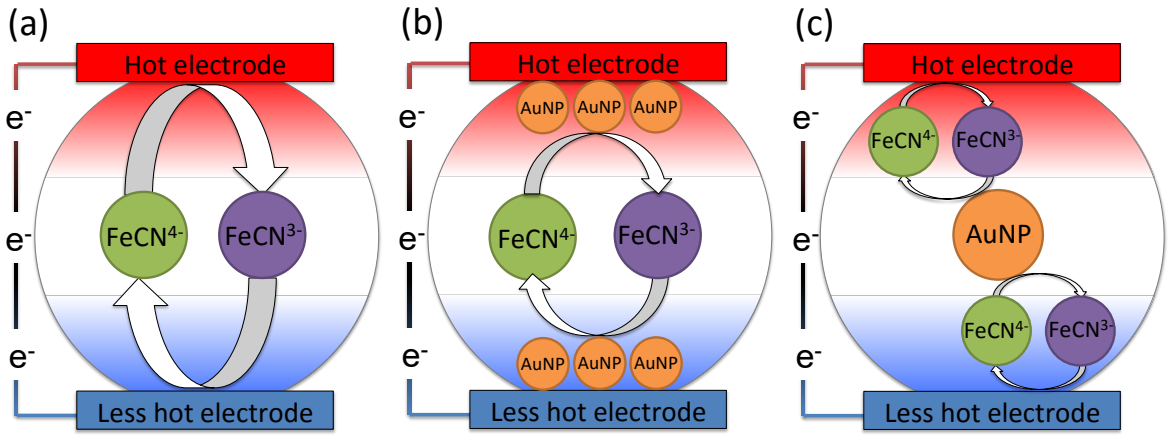


***Fig 3:*** *Schematics highlighting;* ***(a)*** *a spherical super-adsorbent polymeric sphere containing* $[Fe(CN)_6]^{3-/4-}$*, allowing it to act as a thermogalvanic cell, referred to as "****gel-cell****"; **(b)** the same system where gold nanoparticles (AuNP) have been physically sandwiched between the gel and electrode, for improved electrocatalysis in the thermogalvanic cell ("****AuNP@surface****"); **(c)** the same system where AuNP have been formed and immobilised throughout the gel ("****AuNP@gel****"), potentially allowing charge transfer through the AuNP, thus facilitating ionic charge propagation when there is a concentration imbalance between* $[Fe(CN)_6]^{3-}$*, and* $[Fe(CN)_6]^{4-}$*, either side of the AuNP.*

Notably, use of a single gelled sphere (in **gel-cell**) results in an easily prepared, robust and self-contained thermocell system, once in contact with two electrodes. Sandwiching dropcast AuNP between the gel sphere and the electrode (in **AuNP@surface**) means that the no binder is required to immobilise the AuNP, in theory resulting in a simple to prepare but mechanically robust system which will display electrocatalytic improvements with respect to $[Fe(CN)_6]^{3-/4-}$ electrolyte. Finally, immobilising the AuNP throughout the gel (in **AuNP@gel**) means that a high concentration of AuNP can be employed, without any salt-induced aggregation issues.

Furthermore, this latter system opens the possibility of charge propagation through the AuNP; electron transfer through AuNP is known to occur over multi-nm dimensions, even through dense organic layers.[30] Drawing a current from the thermogalvanic cell will result in a concentration gradient; if a concentration gradient exists either side of an AuNP, it is possible that AuNP-facilitated charge propagation could occur, whereby charge migration would occur faster than physical diffusion of the individual ions could allow.

In order to investigate these novel systems, they were initially prepared and measured under isothermal conditions using impedance spectroscopy. The impedance values are summarised in Figure 4. The solution resistance, $R_s$, for all four systems were relatively similar (Figure 4(a)). $R_s$ was lowest for the aqueous system, and $R_s$ for the three gelled systems were only slightly higher; notably, these are polyanionic gels containing immobilised carboxylate anions and free $Na^+$ cations at molar levels, hence lack of mobility is offset by a larger number of charge carriers. Notably, there is no evidence of AuNP-facilitated charge propagation in **AuNP@gel**, with this system in fact having the highest $R_s$ value.

More significant differences were observed in the electron transfer resistance, $R_{ET}$ (Figure 4(b)). A value of *ca.* 32 ± 1 ohms was observed for the aqueous system, which doubled to 58 ± 2 ohms in the **gel-cell** system. However, introduction of AuNP, both at the surface and inside the gel, displayed an electrocatalytic effect, dropping the $R_{ET}$ value by roughly 4-fold for **AuNP@surface**, and *ca.* 5-fold for **AuNP@gel** to 16 ± 1 and 12 ± 1 ohms, respectively. This is consistent with the work of Liu *et al*., who reported a very significant reduction in $R_{ET}$ for the $[Fe(CN)_6]^{3-/4-}$ redox couple upon immobilisation of AuNP at 4-phenyl-modified glassy carbon electrodes.[31]

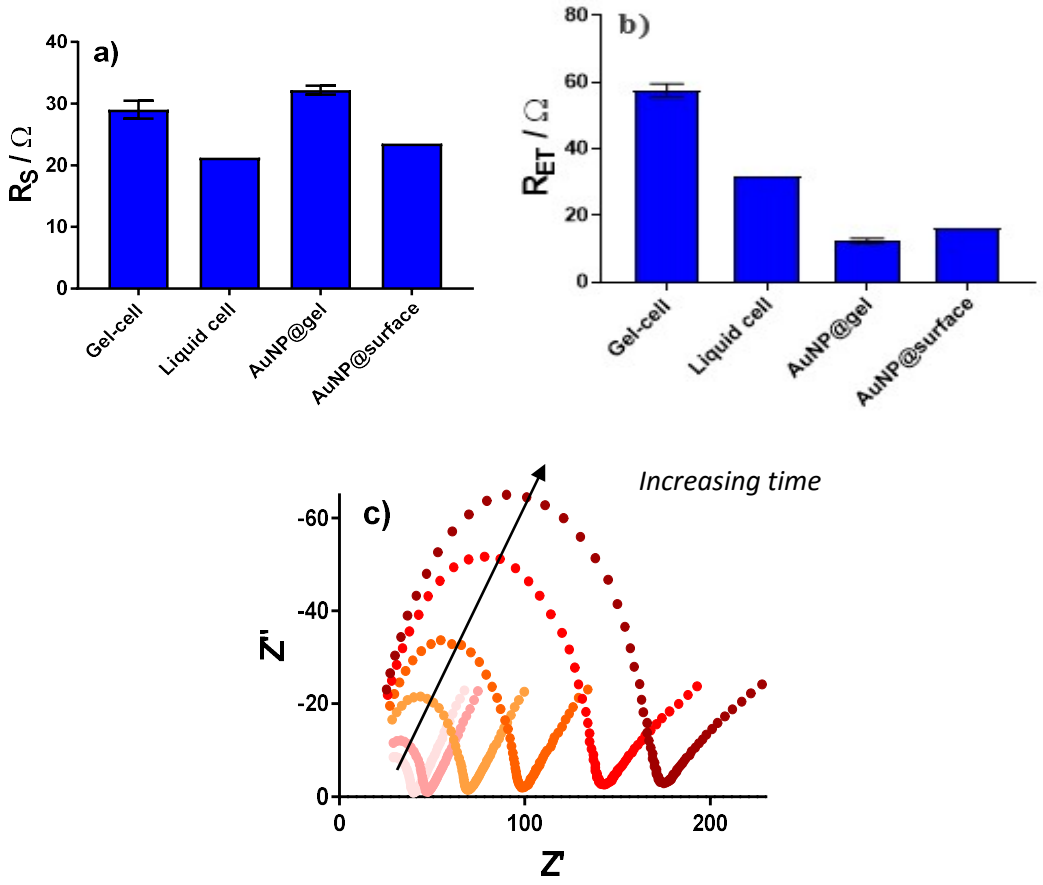


**Fig *4.*** *Impedance spectroscopy was used to investigate the four systems (containing 0.4 M $[Fe(CN)_6]^{3-/4-}$) under isothermal conditions; fitting on the Nyquist plots (using the model described elsewhere[29]) quantified the systems, and shown is* ***a)*** *the solution resistance, $R_s$ and* ***b)*** *the electron transfer resistance, $R_{ET}$. Also shown is* ***c)*** *the Nyquist plot for a* ***AuNP@surface*** *system, measured every 3 min.*

Given these highly promising results, the three gel systems were investigated for their thermogalvanic conversion of a temperature gradient into a flow of current. The **liquid cell** could not be compared, since dropcast AuNP were rapidly lost from the electrode

surface (due to no binder being applied) and AuNP inside the electrolyte were immediately aggregated due to the systems' extremely high ionic strength.

Figure 5(a) displays representative power curves for the three gelled systems, and Figure 5(b) their associated I-V lines. Figure 5(c) displays average maximum power density from testing multiple fresh systems. The average open circuit voltage (or "Seebeck coefficient") was equal in all cases, as expected, since the thermodynamics of the 0.4 M $[Fe(CN)_6]^{3-/4-}$ redox couple should not be altered by the presence of AuNP. In general, slightly more current was generated by the **AuNP@surface** system, demonstrating some electrocatalysis by the AuNP at the electrode surface. Interestingly, the **AuNP@gel** system was indistinguishable from the AuNP-free **gel-cell**, in contrast to the impedance results under isothermal conditions. In addition, clear colour changes were observed, either after extended time or directly after thermogalvanic measurements.

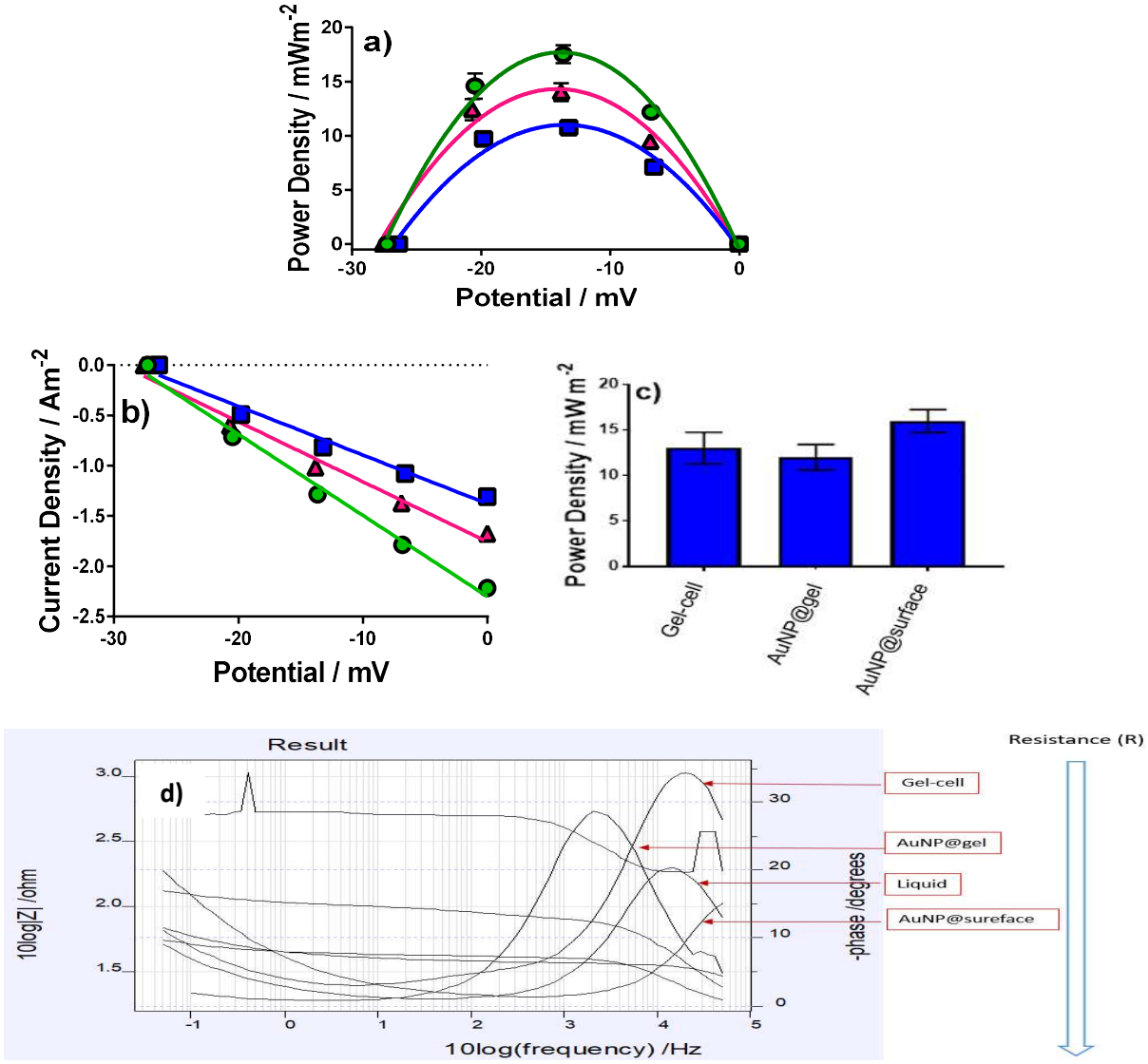


**Fig 5**. *Graphs showing representative* ***a)*** *power curves and* ***b)*** *I-V plots for (pink)* ***gel-cell****, (green)* ***AuNP@surface*** *and (blue)* ***AuNP@gel*** *systems.* ***c)*** *summarised the average power density for triplicate measurements of these three systems, where the error bar represents one standard deviation.* ***d)*** *Raw impedance spectra recorded for these systems under various conditions. Showing the resistance force of each systems is dropping down*

Figure 6 (a) displays a photograph of the "**gel-cell**" system (*i.e.* containing only 0.4 M $[Fe(CN)_6]^{3-/4-}$), (b) shows the **AuNP@gel** system before soaking in 0.4 M $[Fe(CN)_6]^{3-/4-}$, which displays the expected rich burgundy colouration expected for an AuNP colloid, and (c) displays the AuNP@gel system after extended soaking in 0.4 M $[Fe(CN)_6]^{3-/4-}$, after which the entire system became green; this clearly indicates long term stability issues.

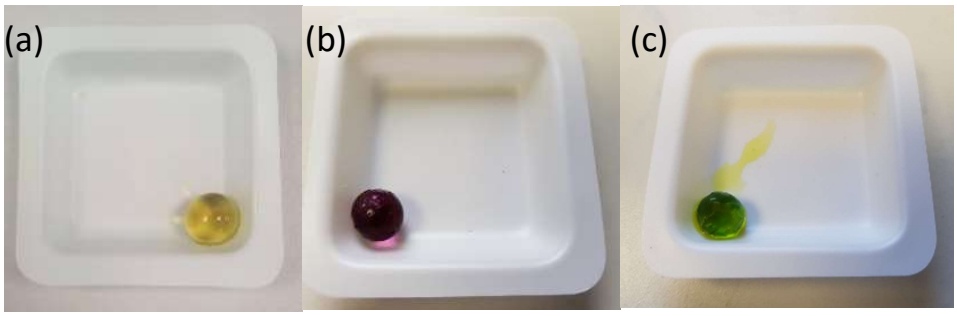


**Fig 6.** *Photos of **(a)** the gel sphere after being soaked in 0.4 M [Fe(CN)6]3-/4-), showing the expected yellow colour (gel-cell), **(b)** a gel sphere containing immobilised AuNP (AuNP@gel), showing the expected burgundy colour, and **(c)** the AuNP@gel after extended exposure to 0.4 M [Fe(CN)6]3-/4- and/or thermogalvanic measurement, highlighting the deep green colouration consistent with formation of a gold analogue of Prussian blue.*

As noted in the introduction, Susana *et al.* reported that AuNP had a very significant 1st order catalytic effect (*ca.* $10^4$ rate enhancement) upon the homogenous reduction of $[Fe(CN)_6]^{3-}$ to $[Fe(CN)_6]^{4-}$, by $Na[BH_4]$.[18] However, Zhai *et al.* reported partial dissolution of AuNP by $[Fe(CN)_6]^{3-}$, with AuNP decreasing from *ca.* 14 nm to *ca.* 12 nm over a 3-hour period; this was attributed to release of $[CN]^-$ by the $[Fe(CN)_6]^{3-}$, to

yield $[Au(CN)_2]^-$.[32] Finally, Harish *et al.* reported that $HAuCl_4$ reacted with $[Fe(CN)_6]^{4-}$ (but not $[Fe(CN)_6]^{3-}$) to form an intense green product attributed to a gold analogue of Prussian blue, namely $KFe_x[Au(CN)_2]_y$.[33] Therefore, it is likely that the relatively high concentration of $[Fe(CN)_6]^{3-/4-}$ was responsible for the relatively rapid and complete dissolution of the uncapped AuNP suspended within the gel matrix, to yield the reported green-coloured Au(I) analogue of Prussian blue. This accounts for why short-term measurements of the **AuNP@gel** system under isothermal conditions (*cf.* Figure 4) gave results consistent with an AuNP-induced electrocatalytic effect, but attempts to measure thermogalvanic power output resulted in loss of the AuNP.

The citrate-capped AuNP were expected to be more stable, but subsequent results demonstrated that even these gradually underwent dissolution. Figure 4(c) displays the Nyquist plots for the same **AuNP@surface** system measured over time; consecutive scans highlight a gradual increase in $R_{ET}$ associated with dissolution of the citrate-capped AuNP at the electrode/gel interface, resulting in an 0.1 $\Omega$ $s^{-1}$ increase in $R_{ET}$. This could not be visually confirmed, given the very small quantity of AuNP at the interface, but the observed impedance results are consistent with what was visually observed in the **AuNP@gel** systems (*cf.* Figure 6(c)). Eventually $R_{ET}$ for the **AuNP@surface** system exceeded the $R_{ET}$ of the AuNP-free **gel-cell**, consistent with passivation occurring at the electrode interface.

Therefore, clear improvements have been demonstrated by the combination of AuNP with the gelled $[Fe(CN)_6]^{3-/4-}$ systems, both via isothermal impedance spectroscopy and, to a lesser extent, in genuine thermogalvanic electricity production. However, these improvements are short-lived, and in fact result in poorer performance of the systems over longer timescales. Replacement of the $[Fe(CN)_6]^{3-/4-}$ redox active electrolyte with another electrolyte could overcome these issues, but notably most redox couples are actually positively charged,[34] and multi-valent cations trigger the collapse of sodium polyacrylate gels. A notable exception is the negatively charged iodide/triiodide redox couple, but this this is known to have even more severe (thermogalvanic) corrosion issues.[35]

## A comparison of liquid and gelled electrolyte systems

A detailed comparison of $Fe(CN)^{-3/-4}$ aqueous solution was investigated, by comparing this liquid system with a sodium polyacrylate sphere soaked in this system.

Figure 8 highlights an initial comparison of the effect of the concentration of $[Fe(CN)_6]^{3-/4-}$ in the solution phase, for 0.05 M, 0.1 M, and 0.2 M of each redox state. This clearly demonstrates a variation in power output with concentration; the power

does not directly scale with concentration, since the potential is not constant; larger potentials are known to generate significantly higher current densities (due to a larger driving force) and the combination of higher potential and larger-than-expected current results in proportionately higher power at lower concentrations.

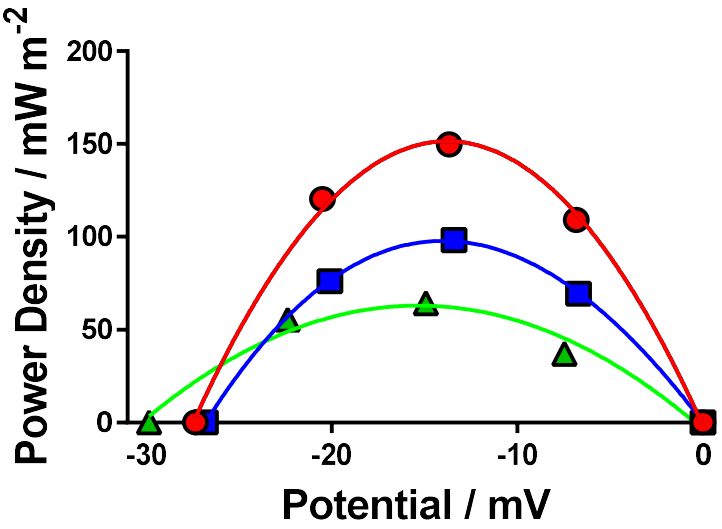


**Fig 8.** *Power curves showing the effect of different concentrations of* $[Fe(CN)_6]^{3-/4-}$*, for 0.2 M (red), 0.1M (blue) and 0.05 M (green) of each redox state. This clearly demonstrates that power output was related to concentration.*

Then, the power output for 0.4 M $[Fe(CN)_6]^{3-/4-}$ was compared for the liquid *vs* gelled systems. Figure 9 displays this, and highlights significantly lower power was generated for the gelled system, relative to the liquid system. This difference is far lower than even that for 0.1 M $[Fe(CN)_6]^{3-/4-}$ indicating that this must be due to significantly

reduced mobility of the redox species, rather than any concentration imbalance. For this reason, the current output as a function of time was investigated in more detail.

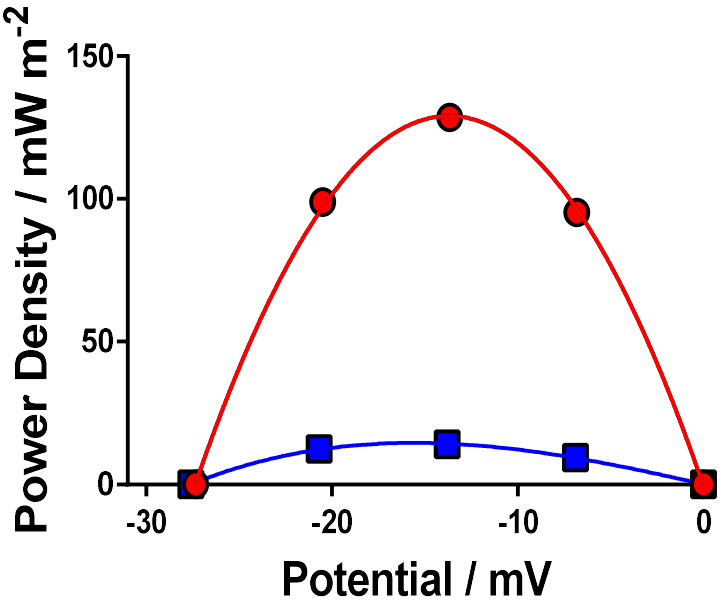


**Fig 9**. *Displays the power output at ΔT = 20°C for aqueous 0.4M ferri/ferrocyanide li quid (red, circles) and the gelled 0.4M ferri/ferrocyanide system (blue, squares).*

Figure 10 displays the short circuit current output for 0.4 M $[Fe(CN)_6]^{3-/4-}$ over time, for both liquid and gelled systems. The liquid system rapidly approached steady state output, and was able to sustain a constant power output. However, for the gelled system, the current was initially relatively high for the gelled system, but rapidly

decreased with time; even after >6,000 seconds, a steady current output was not achieved. Therefore this indicates that while the redox material close to the electrode surface is likely relatively accessible, as more and more current is drawn, it is locally exhausted and this depletion layer goes deeper and deeper into the gel.

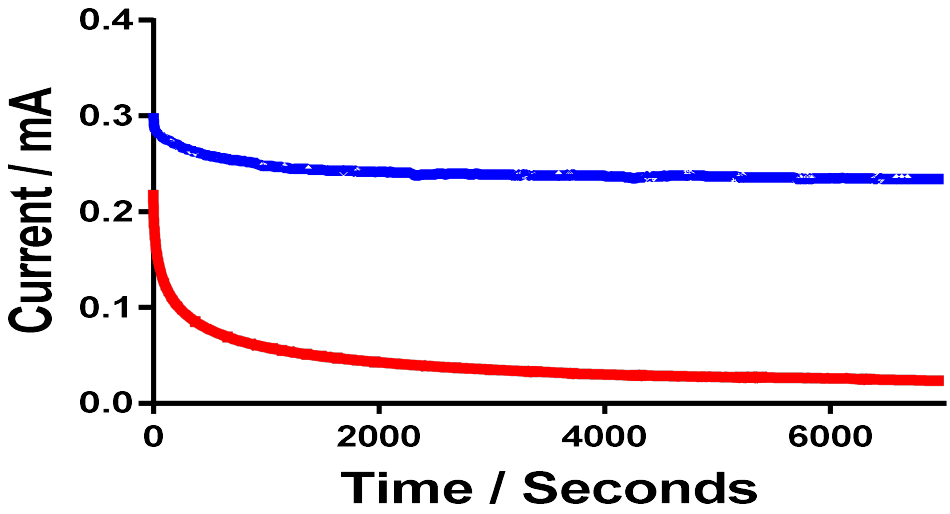


**Fig 10**. *Plot of current as function of time (2.30 h) for 0.4M* $Fe(CN)_6^{3-/4-}$ *liquid (blue), gel (red).*

This was further confirmed by measuring the power output from gelled 0.4 M $[Fe(CN)_6]^{3-/4-}$ three times in a row. This is shown in Figure 11, and demonstrates that the first power curve gave the expected result, whereas the second power curve was significantly smaller, demonstrating a significant drop in the open circuit potential. The third was smaller again. Exhaustion of material or passivation should result in a current drop, and therefore a drop in power, but in this case the potential drop is clearly significant; this is consistent with an imbalance of the redox states accumulating at the surface of the

electrode, given that electron transfer occurs but the resulting products are not diffusing away on the timescale (*ca.* 30 min) of the measurement.

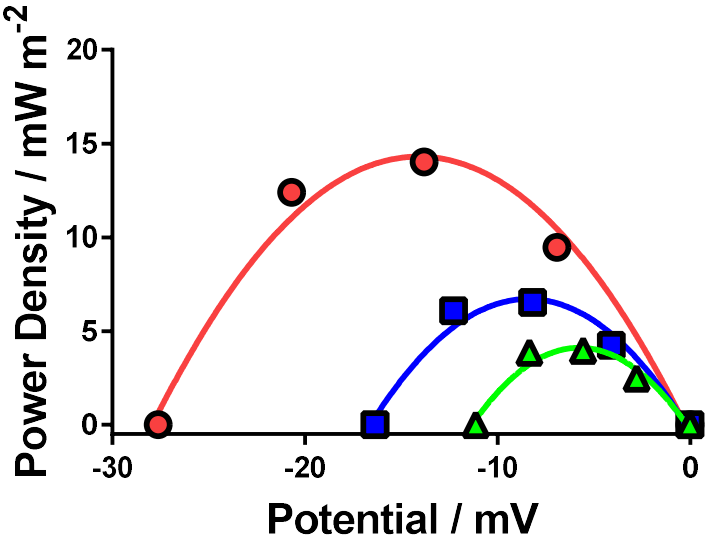


**Fig 11.** *Showing the recovering & stability 0.4M $Fe(CN)_6^{3-/4-}$ sphere, these three runs show clearly the power curve is decreasing with each run. Red was the first run, blue the second, green the third run*

Finally, if this was the case, then recovery should be gradual and could be demonstrated by measuring the open circuit potential *vs* time. This was tested by measuring a power curve, then recording the open circuit potential *vs* time (Figure 12). This demonstrated that the process was reversible.

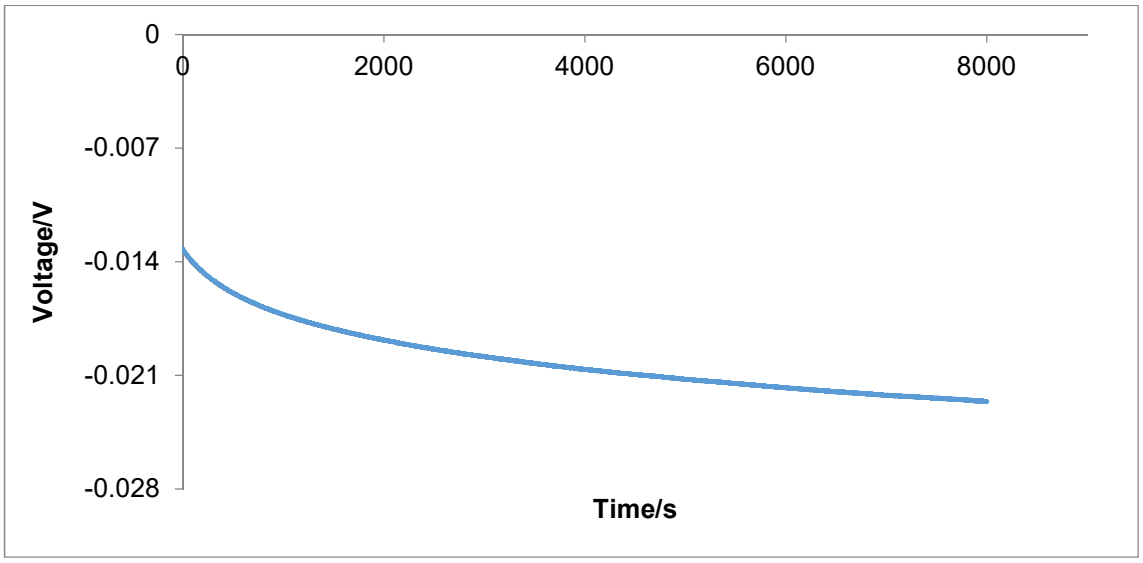


**Fig 12.** *Plot showing the recovery of the open circuit potential after a power curve measurement for 0.4M* $Fe(CN)_6^{3-/4-}$ *gel, returning towards the expected value of -0.028 V*

The overall effect is shown schematically in Figure 13, which highlights how before power is drawn, the gel contains a mixture of both redox states equally distributed across the gel. However, after a current is drawn, and redox chemistry occurs, an imbalance occurs due to frustrated migration of the species through the bulk of the gel. Repeated measurement results in an ever-greater imbalance. This has severe implications for the potential long-term use of gelled electrolyte systems, and necessitates further study.

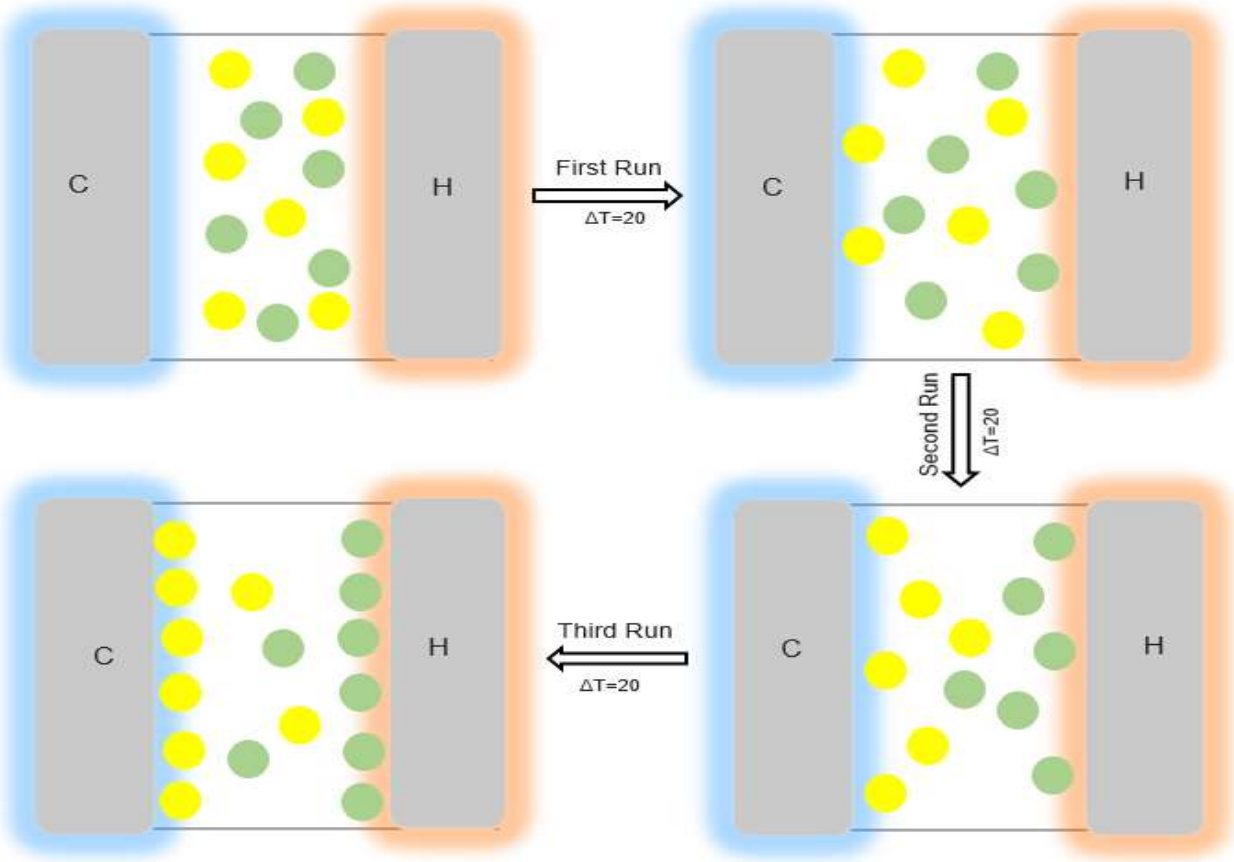


**Fig 13**. *Schematic showing the oxidation/reduction at the anode and cathodes for the thermocell for the* $[Fe(CN)_6]^{3-/4-}$ *system.*

## Conclusions

In conclusion, the thermoelectrochemistry of the conventional ferricyanide | ferrocyanide system has been investigated in single spheres of super-adsorbent sodium polyacrylate gel, as standalone thermocells (in conjunction with two electrodes). Furthermore, for the first time gold nanoparticles have been investigated, both binder-free at the gel/electrode interface, and capping-free and distributed throughout the thermocell. Impendence spectroscopy strongly indicated the benefit of including the gold nanoparticles, by virtue of significantly reduced resistance to electron transfer. However, distributing the AuNP throughout the gel did not provide any detectable enhancement in the rate of charge propagation. Futhermore, improvements in actual thermogalvanic measurements were modest; a major limitation was noted to be the instability of the AuNP themselves, which dissolved in the ferricyanide | ferrocyanide electrolyte over time; a new electrolyte is needed to achieve the potential significant improvements represented by these novel AuNP-containing systems.

## References


1 R. Hu, B. A. Cola, N. Haram, J. N. Barisci, S. Lee, S. Stoughton, G. Wallace, C. Too, M. Thomas, A. Gestos, M. E. Dela Cruz, J. P. Ferraris, A. A. Zakhidov and R. H. Baughman, *Nano Lett.*, 2010, **10**, 838–846.

2 B. Burrows, *J. Electrochem. Soc.*, 1976, **123**, 154–159.

3 A. Gunawan, C. H. Lin, D. A. Buttry, V. Mujica, R. A. Taylor, R. S. Prasher and P. E. Phelan, *Nanoscale Microscale Thermophys. Eng.*, 2013, **17**, 304–323.

4 T. I. Quickenden, *J. Electrochem. Soc.*, 1995, **142**, 3985.

5 J. Wu, J. J. Black and L. Aldous, *Electrochim. Acta*, 2017, **225**, 482–492.

6 L. Jin, G. W. Greene, D. R. MacFarlane and J. M. Pringle, *ACS Energy Lett.*, 2016, **1**, 654–658.

7 P. Yang, K. Liu, Q. Chen, X. Mo, Y. Zhou, S. Li, G. Feng and J. Zhou, *Angew. Chem. Int. Ed.*, 2016, **55**, 12050–12053.

8 M. Al Maimani, J. J. Black and L. Aldous, *Electrochem. commun.*, 2016, **72**, 181–185.

9 M. S. Romano, J. M. Razal, D. Antiohos, G. Wallace and J. Chen, *J. Nanosci. Nanotechnol.*, 2015, **15**, 1–14.

10 B. T. Huang, M. Roger, M. Bonetti, T. J. Salez, C. Wiertel-Gasquet, E. Dubois, R. Cabreira Gomes, G. Demouchy, G. Mériguet, V. Peyre, M. Kouyaté, C. L. Filomeno,

J. Depeyrot, F. A. Tourinho, R. Perzynski and S. Nakamae, *J. Chem. Phys.*, , DOI:10.1063/1.4927665.

11 T. J. Salez, B. T. Huang, M. Rietjens, M. Bonetti, C. Wiertel-Gasquet, M. Roger, C. L. Filomeno, E. Dubois, R. Perzynski and S. Nakamae, *Phys. Chem. Chem. Phys.*, 2017, **19**, 9409–9416.

12 C. Liu, H. Lee, Y. H. Chang and S. P. Feng, *J. Colloid Interface Sci.*, 2016, **469**, 17–24.

13 J. Polte, T. T. Ahner, F. Delissen, S. Sokolov, F. Emmerling, A. F. Thünemann and R. Kraehnert, *J. Am. Chem. Soc.*, 2010, **132**, 1296–1301.

14 K. S. Merza, H. D. Al-Attabi, Z. M. Abbas and H. A. Yusr, *Green Sustain. Chem.*, 2012, **02**, 26–28.

15 K. Saha, S. S. Agasti, C. Kim, X. Li and V. M. Rotello, *Chem. Rev.*, 2012, **112**, 2739–2779.

16 J. Turkevich, P. C. Stevenson and J. Hillier, *Trans. Faraday Soc.*, 1951, **11**, 55–75.

17 P. Rodriguez and M. T. M. Koper, *Phys. Chem. Chem. Phys.*, 2014, **16**, 13583–13594.

18 C. R. Susana, P. J. Jorge, H. Pablo, M. L. M. Luis and M. Paul, *Langmuir*, 2010, **26**, 1271–1277.

19 J. C. Bear, P. D. McNaughter, K. Jurkschat, A. Crossley, L. Aldous, R. G. Compton, A. G. Mayes and G. G. Wildgoose, *J. Colloid Interface Sci.*, 2012, **383**, 110–117.

20 W. Putzbach and N. J. Ronkainen, *Sensors (Switzerland)*, 2013, **13**, 4811–4840.

21 A. Gunawan, H. Li, C. H. Lin, D. A. Buttry, V. Mujica, R. A. Taylor, R. S. Prasher and P. E. Phelan, *Int. J. Heat Mass Transf.*, 2014, **78**, 423–434.

22 Y. F. Lee, F. H. Nan, M. J. Chen, H. Y. Wu, C. W. Ho, Y. Y. Chen and C. C. Huang, *Anal. Methods*, 2012, **4**, 1709–1717.

23 X. Wang, C. E. Egan, M. Zhou, K. Prince, D. R. G. Mitchell and R. A. Caruso, *Chem. Commun.*, 2007, 3060–3062.

24 D. S. Dos Santos, P. J. G. Goulet, N. P. W. Pieczonka, O. N. Oliveira and R. F. Aroca, *Langmuir*, 2004, **20**, 10273–10277.

25 D. P. Kumar, *RSC Adv.*, 2014, **4**, 45449–45457.

26 M. Kimura, S. Kobayashi, T. Kuroda, K. Hanabusa and H. Shirai, *Adv. Mater.*, 2004, **16**, 335–338.

27 E. Faoucher, P. Nativo, K. Black, J. B. Claridge, M. Gass, S. Romani, A. L. Bleloch and M. Brust, *Chem. Commun.*, 2009, 6661–6663.

28 Alzahrani, Hassan AH, et al. Success and failure in the incorporation of gold nanoparticles inside ferri/ferrocyanide thermogalvanic cells. *Electrochemistry Communications* 102 (2019): 41-45.

29 M. A. Buckingham, F. Marken and L. Aldous, *Sustain. Energy Fuels*, 2018, 2717–2726.

30 J. N. Chazalviel and P. Allongue, *J. Am. Chem. Soc.*, 2011, **133**, 762–764.

31 G. Liu, E. Luais and J. J. Gooding, *Langmuir*, 2011, **27**, 4176–4183.

32 J. Zhai, Y. Zhai, S. Dong Colloids Surf. A Physicochem. *Eng. Asp*., 335 (2009), pp. 207-210

33 S. Harish, J. Joseph, K.L.N. Phani Electrochim. *Acta,* 56 (2011), pp. 5717-5721

34 J.T. Hupp, M.J. Weaver J. Phys. *Chem*., 89 (1985), pp. 2795-2804

35 H.A.H. Alzahrani, J.J. Black, D. Goonetilleke, J. Panchompoo, L. Aldous *Electrochem. Commun*., 58 (2015), pp. 76-79

Chapter 5

# Gel-immobilised gold nanoparticles as catalysts

## Abstract

In this chapter, gelled electrolytes were also employed, following on from Chapter 3. However, in this case commercial material was employed, and novel ways of integrating gold nanoparticles with the gelled electrolyte was explored.

As such, an novel synthetic route for the formation of stabilised gold nanoparticles (AuNPs) embedded in a hydrogel via acrylate oxidation was developed and further explored. These AuNPs have been fully characterised by UV-Vis and cryo-TEM, where they were found to be have an average diameter of *ca.* 20 nm. The versatility of the AuNP-hydrogel in catalysis has been demonstrated by investigating the removal of environmentally damaging azo dyes. The AuNP hydrogels have also been demonstrated as effective catalysts for the model reduction of nitrophenol to aminophenol. The AuNP hydrogels were found to be resilient to saline environments where catalytic reduction of 4-nitrophenol is possible in a model saline solution, where citrate-capped liquid AuNPs have failed to withstand this saline environment.

## Introduction

Gold nanoparticles (AuNPs) synthesis is an area of significant interest, both in terms of synthesising stable nanoparticles, but also in controlling both the shape and size of AuNPs.[1] One of the main reasons for this exploration is due to the intensity of use of metal nanoparticles in catalysis.[2–5] Additionally, AuNPs are used extensively in both electrocatalysis,[6,7] and organic catalysis.[8,9] A model catalytic reaction is the borohydride reduction of 4-nitrophenol (4-NP) to 4-aminophenol (4-AP) (Scheme 1).[10,11] Here the AuNPs act as a facilitator for the electron transfer between the $[BH_4]^-$ and the 4-NP.[10]

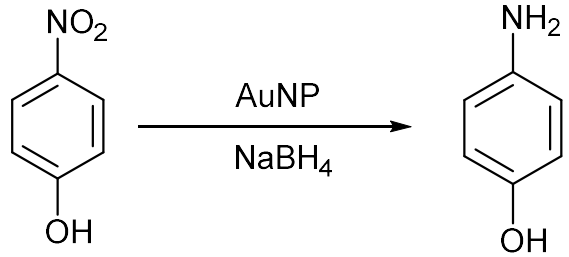


**Scheme 1 -** *Scheme representing the borohydride reduction of 4-nitrophenol (4-NP) to 4-aminophenol (4-AP) catalysed by gold nanoparticles (AuNP).*

The catalytic reduction of nitrophenols and their derivatives to amines is of particular interest, with nitrophenols produced as by-products in significant quantities from pesticide, herbicide and synthetic dye manufacturing.[12,13] In particular, 4-nitrophenol

is known to be a highly toxic.[14] The catalytic removal of organic dyes is also an area of intense research, due again in part to toxicity. However dyes are also environmentally damaging,[15] and conventional waste water treatments are not very successful at removing highly persistent organic dyes.[15,16] Dyes such as methylene blue, and congo red are produced in large quantities from many industries such as ceramics, paper, leathers and textiles. It is estimated that between 10 – 20% of manufactured dyes are lost to wastewater streams.[17,18] This results in significant environmental concern, so the removal of these strongly coloured dyes is of a high environmental priority.[19] Congo red is also classified as azo dye, which is of even greater environmental and health concerns.[18,20]

AuNPs synthesis has been demonstrated using several methods,[21–23] one such method was ascribed to Turkevisch. This method is described as a concomitant reduction of Au(III) to AuNPs, alongside the oxidation of citrate to $CO_2$.[21] Synthesised AuNPs below a certain size (1 – 100 nm) are found to require a stabilising capping agent, usually in the form of a thiol moiety.[24] In the Turkevisch synthesis the citrate molecule is in excess, and subsequently acts as a capping agent.[21]

AuNP size can be controlled via citrate oxidation based on the citrate concentration.[25] A model has been created for controlling the size of synthesised nanoparticles.[26] The coagulation concentration to form bulk gold has been found to be inversely

proportional to the size of AuNPs.[27] Other factors that affect the size of synthesised nanoparticles include introduction of co-reduction agents, such as tannic acid.[28]

Here we report novel synthetic methods for embedding AuNPs in a hydrogel, using the polymeric polyacrylate structure itself as both an Au(III) reducing agent, and a capping agent to stabilise the synthesised nanoparticles. These AuNP have been characterised by UV-Vis spectroscopy, cryo-TEM was undertaken in order to determine the dispersity in nanoparticle size within the gel. The AuNPs have been demonstrated for their catalytic reducing ability on a range of nitrophenol and dye moieties for catalytic reduction. The AuNP hydrogels have also been demonstrated to be tolerant towards a model wastewater system, this synthetic technique presents a new and interesting method for embedded nanoparticle synthesis.

# Experimental

## Chemicals

All reagent were purchased from UK and used without further purification. The chemicals are as follows; Sodium tetrachloroaurate hydrate, (98%, Acros Organics), 4-Nitrophenol (≥99%, Sigma Aldrich), 2-Nitrophenol (98% Sigma Aldrch), Sodium borohydride solution (12 wt% in 14 M NaOH, Sigma Aldrich), Sodium citrate tribasic dihydrate (ACS ≥99%, Sigma Alcrich), and commercial sodium polyacrylate spheres (Sungpunet, China).

## Aqueous gold nanoparticle synthesis using citrate

Gold nanoparticles synthesised by citrate reduction: a solution containing both 5 mM sodium citrate and 1 mM $NaAuCl_4$ was heated to boiling for ~ 30 minutes, unless otherwise specified. Subsequent nanoparticle formation was confirmed by UV-Vis. Gold nanoparticle synthesis from citrate in a polyacrylate gel was done using the previous method, only in the presence of a commercial polyacrylate spherical gel.

## Gold nanoparticle synthesis from polyacrylate gel

Gold nanoparticles embedded in polyacrylate gels were synthesised by soaking commercially bought polyacrylate gels in 4 mM sodium tetrachloroaurate solution for 1 hour. The solution was then heated to boiling for ~ 30 minutes until the gel colour changed from yellow to burgundy, indicating formation of gold nanoparticles inside the gel.

## Catalytic study

The study of AuNP-catalysed reduction of nitrophenol (NP) to aminophenol (AP) by sodium borohydride was monitored by UV-Vis. A typical procedure goes as follows: a gold nanoparticle embedded gel was placed in a solution of nitrophenol (0.1 mM), then $NaBH_4$ was added in a 1:1,000 ratio to reactant, the subsequent reaction was monitored by UV-Vis.

## UV-Vis spectroscopy

UV-Vis spectroscopy was performed using a PerkinElmer LAMBDA 465 UV-Vis Spectrophotometer with UV Lab software (UK). Spectra were recorded at 200-800 nm the reaction was monitored every 1 minute for between 30 to 60 minutes.

## UV-Vis analysis of formed nanoparticles in gel

Spectroscopy was performed using a home-built microscopy setup incorporating a Princeton Instruments isoplane spectrometer fibre-coupled to the collection optics. The nanoparticle containing spheres were placed in a quartz cuvette and gently manipulated to ensure they were not touching the faces of the cuvette. The samples were then illuminated with plane-polarised white light, with the transmitted light collected using a Mitutoyo 50X MPlan lens. Spectra were taken through the centre of each sphere, with back-reflection alignment used to ensure the beam was normal to all reflective surfaces. In addition, reference spectra through the cuvette alone and background spectra were also taken to allow the calculation of transmittance. Extinction was calculated by $-\log_{10}(T)$.

## Cryo-transmission electron microscopy

Gold embedded commercial gels were thinned, adhered to lacy carbon grids (Ted Pella) and plunge frozen into liquid ethane with a Leica GP (Leica Microsystems). Thin, peripheral areas of the hydrogels were imaged on a Talos Arctica (Thermofisher) fitted with a 4k x 4K Falcon 3EC camera with a binning of 1 in linear mode under the control of Talos Imaging and Analysis software (Thermofisher).

## Size distribution

Gold nanoparticle size distribution was analyzed in ImageJ. A total number of 568 gold nanoparticles were imaged. An average diameter of 18 nm was observed with a standard deviation of 9 nm and a median diameter of 16 nm.

## Results and Discussion

### Citrate Oxidation Synthesis in solution and hydrogel

The citrate oxidation method for synthesising AuNPs was first described by Turkevich.[21] This method was initially employed here to form AuNPs, whereby both Au(III) and citrate were dissolved in solution. To date, synthesis of AuNPs from variations of the Turkevisch[21,25] and Brust [23] methods require continuous heating and stirring to form AuNPs, unless employing a biosynthetic aid.[10] In this study, over long timescales (~24 h), gold nanoparticles were found to form in solution from Au(III) and citrate without the need for external heating. The effect of light was also tested, where in the absence of light nanoparticles were again found to form. The resultant nanoparticles were characterised by UV-Vis and are displayed in Figure 1.

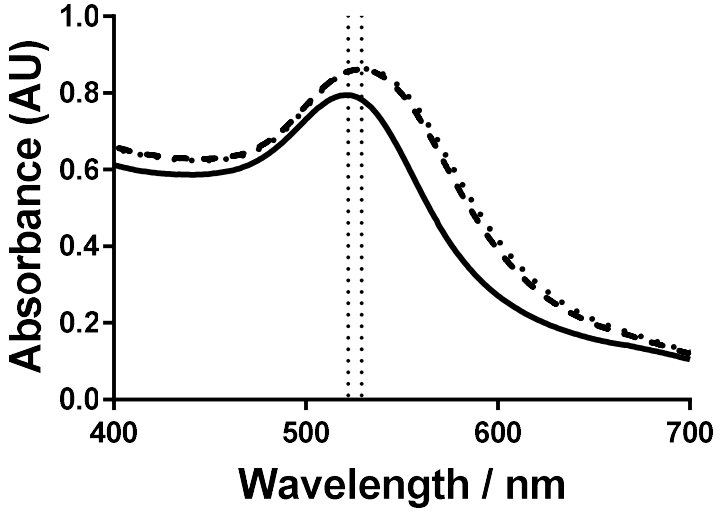


**Fig 1**. *UV-Vis spectra of gold nanoparticles formed in solution by citrate oxidation, under heated, (solid) ambient temperature with light (dashed) and ambient temperature in the dark (dotted). The dotted lines represent the two* $\lambda_{max}$ *at: 522 nm (heated) and 529 nm (ambient).*

AuNP synthesis was then investigated inside a polyacrylate gel, employing both citrate and Au(III) in a solution containing a polyacrylate hydrogel. The synthesis of nanoparticles within the gel were found to be dependent on the concentration of Au(III) and citrate. Investigating this concentration effect of both gold and citrate showed that the colour of the gel (and resultant nanoparticle formation) is significantly dependent on the Au(III) concentration. The superabsorbent polyacrylate gel was found to decrease in swelling size with increased concentration of Au(III) and citrate in solution, consistent with studies of superabsorbent polymers.[29]

The effect of citrate and gold concentrations was qualitatively tested, which showed that a low concentration of both was necessary for formation of well-defined gold nanoparticles (well-defined nanoparticle colloids being classified with systems with a strong and clear absorbance in the 520-550 nm region).

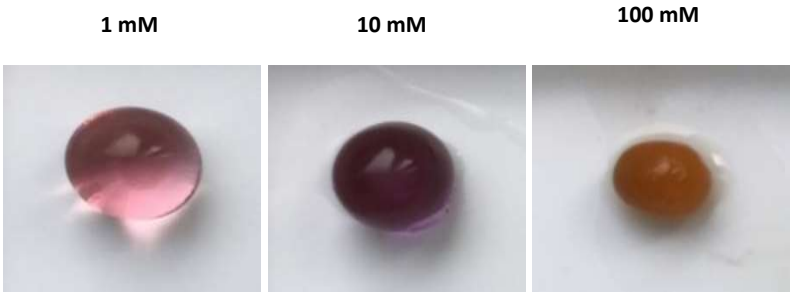


Superadsorbent spheres containing AuNP, prepared using different concentrations (1 mM, 10 mM and 100 mM of tetrachloroaurate) at a fixed [gold] : [citrate] ratio of 1 : 5

## Embedded nanoparticle formation

Gold nanoparticles were also synthesised in the absence of citrate, where the gold nanoparticles were still embedded in the polyacrylate sphere via the reduction of Au(III) by the polyacrylate gel itself. The nanoparticles were found to be synthesised at particle sizes between 5 – 40 nm. Some nanoparticles conglomerated to form larger nanoparticles at sizes >40 nm (Figure 4). The small size of the formed nanoparticles would suggest that a capping agent is required,[24] so it is assumed that the gel itself acts as a capping agent for the AuNPs in the hydrogel, analogous to citrate capping in

solution.[21] The hydrogel synthesis of AuNPs from Au(III) solution is displayed pictorially in Figure 2.

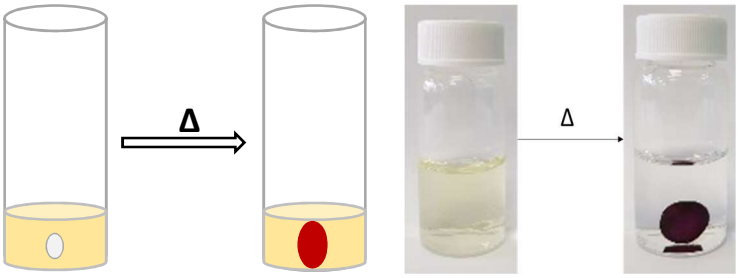


**Fig 2.** *Pictorial representation (left) and photos (right) of AuNP synthesis embedded in a commercial polyacrylate hydrogel from a $[AuCl_4]^-$ solution.*

It is assumed that the AuNPs are stabilised by the gel, and would be bound to the polymer in an analogous way to recent research into Pt nanoparticles fixed to rigid polymer of intrinsic microporosity.[30–32] In an attempt to understand the synthesis of the AuNPs within the hydrogel, AuNPs embedded in the gel were probed by UV-Vis. The λmax was found to be higher than that solution synthesised AuNPs (Figure 1). This is due to the differing refraction index of solid and liquid media.[22,33] In order to determine whether a different amount of gold present in solution resulted in different AuNP formation. AuNPs in gels were synthesised using different volumes of the same concentration of [AuCl4]- solution (Figure 3), the λmax remained approximately

constant despite this difference, indicating homogeneous formation across different volumes of present Au(III).

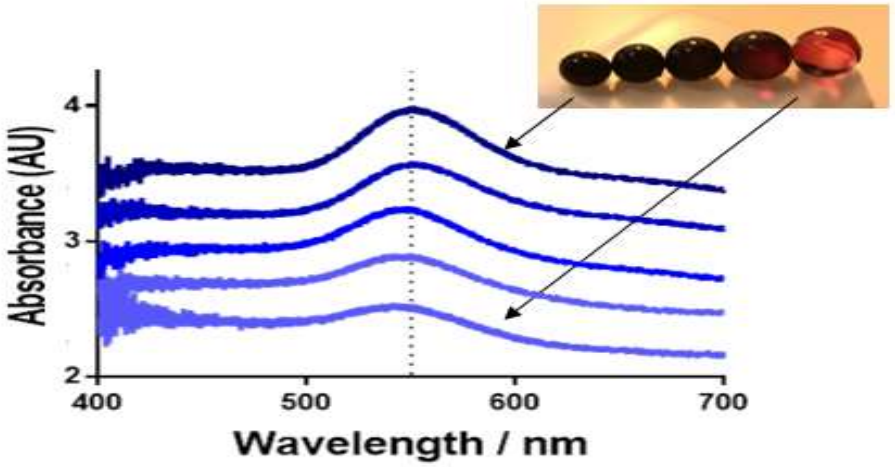


**Fig 3.** *Uv-Vis spectra of AuNPs synthesised in polyacrylate gel soaked in different volumes, (1) 2 mL (2) 4 mL (3) 6 mL (4) 8 mL (5) 10 mL of (4 mM) concentration of* $[AuCl_4]^-$*, the dotted line indicated the* $\lambda_{max}$ *at 550 nm.*

## Cryo-Tranmission electron microscopy

With the UV-Vis spectra indicating homogenous synthesis of nanoparticles across different volumes of Au(III), the homogeneity of AuNPs size within the gel was measured using cryo-TEM (Figure 4). Analysis of cryo-TEM images of cross-sections of an AuNP-containing polyacrylate gel determined that the majority of particles fell within the range of 20 – 25 nm, with an average diameter of 22 nm. This means these AuNP are larger than AuNPs previously prepared encapsulated by a metal organic

framework environment [33] and platinum, palladium and silver nanoparticles embedded in amine-based polymers,[34] but is of a comparable size to Ag nanoparticles synthesised in acrylic acid hydrogels.[35]

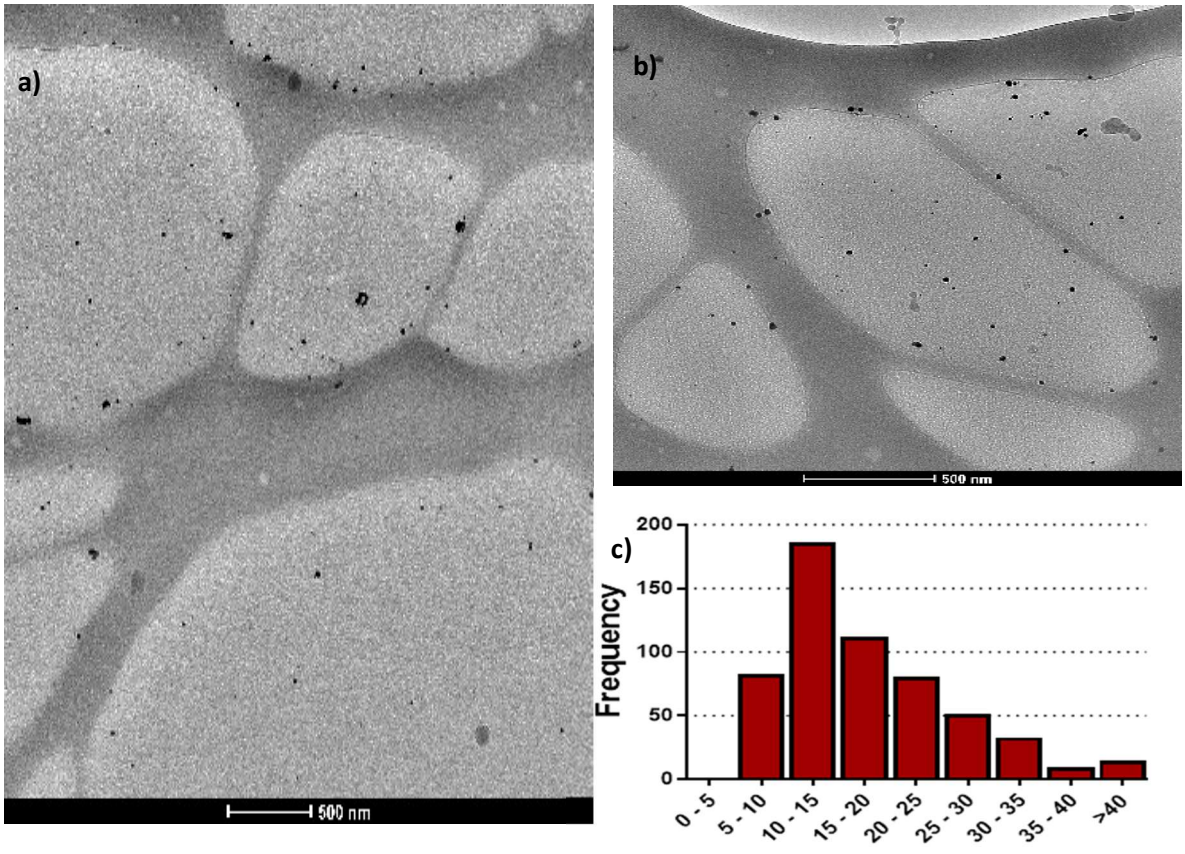


**Fig 4.** *Capping free 3 M NaCl gold nanoparticles imaged at liquid nitrogen temperatures.* ***a)*** *Lower magnification micrograph of gold nanoparticles from the hydrogel.* ***b)*** *Higher magnification micrograph demonstrating the distribution of gold nanoparticle sizes.* ***c)*** *Distribution plot of gold nanoparticle diameters.*

## Catalysis of Nitrophenol

Nitrophenol reduction is a model reaction for nanoparticle catalysis.[14,36] Therefore, the reduction of nitrophenol to aminophenol was selected to demonstrate the catalytic capability of the polyacrylate hydrogel AuNPs. Nanoparticle catalysis of nitrophenols can be monitored by UV-Vis,[11] where initially a shift in absorption wavelength is observed by the phenol to phenolate transition.[14] The subsequent nitrophenolate peak at ~ 400 nm can then be observed to decrease with time as the nitro group is reduced to an amino group. This is coupled with an increase of the aminophenol signal (Figure 5a & 5b). This reaction is known to not proceed in the absence of AuNPs, but has been demonstrated here as well (Figure 5e).[37,38] Due to a large excess of $[BH_4]^-$ with respect to the nitrophenol, a pseudo-first-order model can be applied, the apparent rate constant determined from concentration vs time are shown in Table 1.

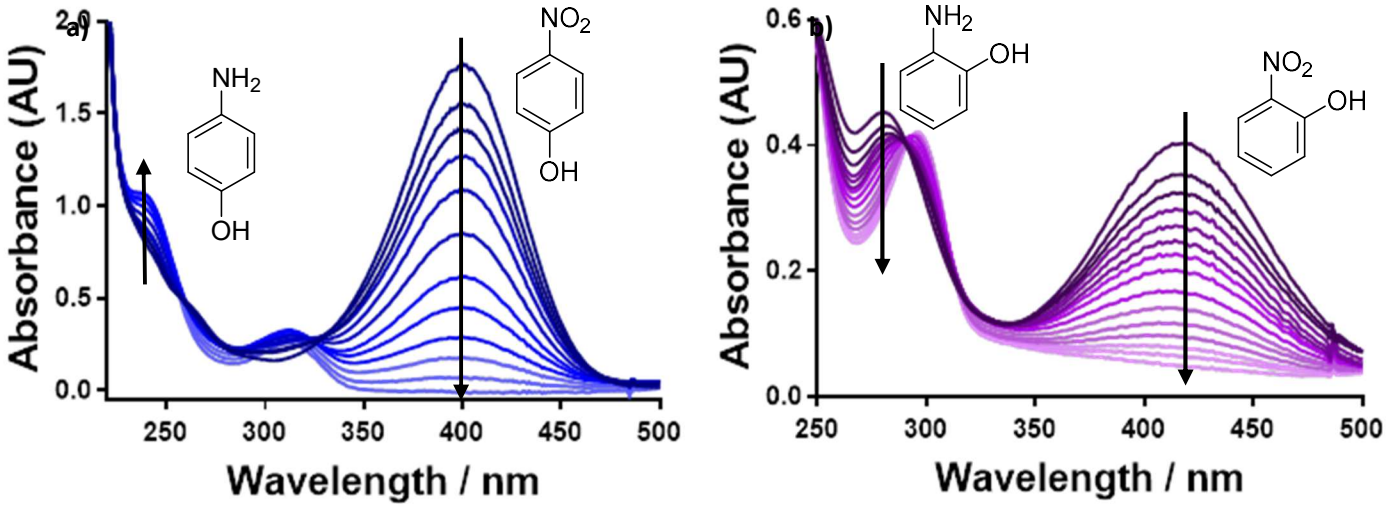

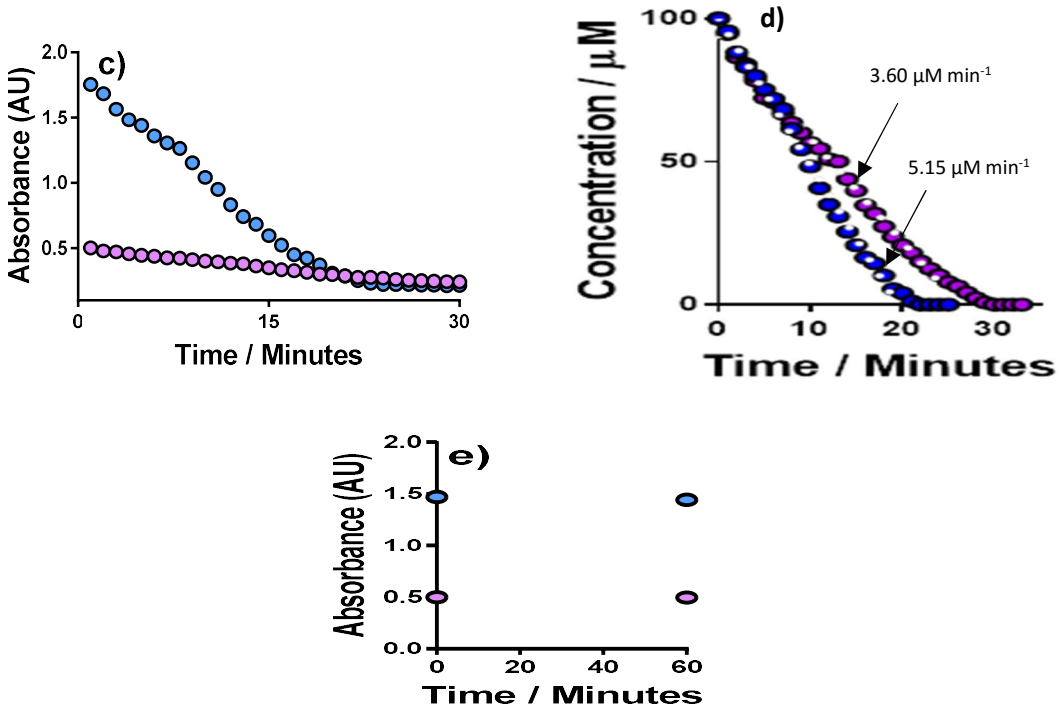


**Fig 5.** ***a)*** *UV-Vis spectra showing the concomitant decrease in 4-nitrophenol (4-NP) signal (400 nm) with the increase in 4-aminophenol (4-AP) signal (305 nm), the arrows demonstrate increasing time.* ***b)*** *concomitant 2-nitrophenol (2-NP) (418 nm) signal decrease alongside the 2-aminophenol (2-AP) (300 nm).* ***c)*** *Decrease in concentration over time for (blue) 4-nitrophenol and (purple) 2-nitrophenol signals over time..* ***d)*** *decrease in absorbance of 400 nm (4-NP, blue) and 418 nm (2-NP,purple) signals over time.* ***e)*** *absorbance of the same experiment in the absence of AuNP hydrogels.(blue) 4-NP, (purple) 2-NP.*

| **Substrate** | **Reaction rate / $min^{-1}$** |
|---|---|
| 4-nitrophenol | 5.15 |
| 2-nitrophenol | 3.60 |

**Table 1** – *Tabulated values of kinetic rates of AuNP hydrogel catalysed $[BH_4]^-$ reduction of nitrophenol and dye substrates.*

## Model waste water environment catalysis

The AuNP embedded hydrogels were investigated on a model waste effluent environment of relatively high ionic strength. Catalytic reduction of 4-NP was investigated in 0.1 M KCl solution. The AuNP hydrogel was found to be catalytically active for the reduction, as observed previously (Figure 7). The rate of catalysis was found to be roughly half that found in the pure water environment: 5.15 $min^{-1}$ for without KCl, and 3.42 $min^{-1}$ for with KCl environments, respectively. To test the effectiveness of the AuNP hydrogel, solution-based citrate capped AuNPs were tested on the same system. Due to the saline environment, the gold nanoparticles were found to coagulate to bulk gold, and were therefore immediately rendered catalytically inactive (*cf.* Figure 7b). Conversely, even soaking the AuNP hydrogel in 0.1 M KCl for extended periods of time did not remove its catalytic activity, as shown visually below in Figure 6.

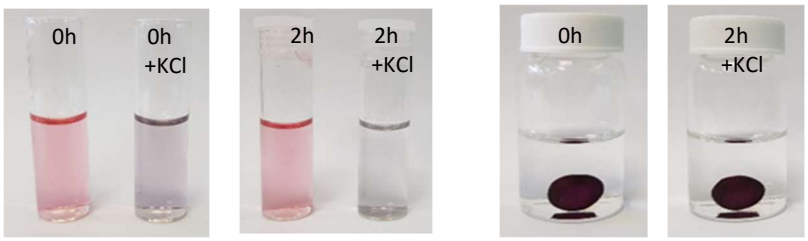


**Fig 6.** *Images showing the effect of 0.1 M KCl on citrate capped nanoparticles over 2 hours compared to the absence of KCl. And the same effect on a AuNP hydrogel in 0.1 M KCl over the same time period, both time and KCl presence is indicated in the image.*

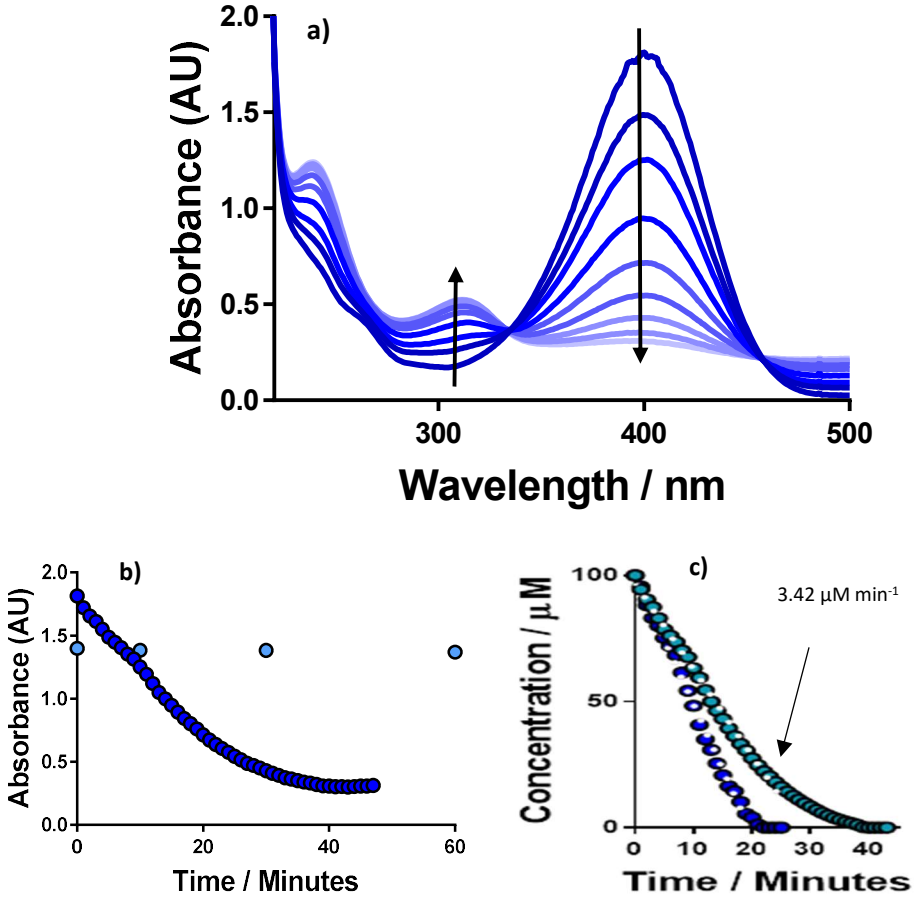


**Fig 7.** ***a)*** *UV-Vis wavelength showing the reduction of 4-NP to 4-AP via AuNP hydrogel catalysed* $BH_4^-$. ***b)*** *(dark blue) 400 nm wavelength reduction in absorbance with time. (light green) 400 nm wavelength monitoring of citrate capped AuNPs in solution in 0.1 M KCl solution.* ***c)*** *Decrease in concentration over time of 4-NP in the absence (blue) and presence (green) of 0.1 M KCl.*

## Conclusion

An elegant new synthetic route for the formation of polyacrylate hydrogel embedded gold nanoparticles (AuNPs) has been developed. Cryo-TEM has shown that the dispersion in size of these synthesised nanoparticles typically fall within the 5–25 nm range. The AuNP hydrogels have been demonstrated as effective catalysts for the model reduction of both 2- and 4-nitrophenol to 2- and 4-aminophenol. The AuNP hydrogels have been found to be resilient to saline environments where catalytic reduction of 4-nitrophenol is possible in a model saline solution, and to the best of our knowledge this saline resistance has not been demonstrated previously for this type of system.

## References


1 Grzelczak, M.; Pérez-Juste, J.; Mulvaney, P.; Liz-Marzán, L. M. Shape Control in Gold Nanoparticle Synthesis. *Chem. Soc. Rev*. 2008, 37 (9), 1783–1791.

2 Corma, A.; Garcia, H. Supported Gold Nanoparticles as Catalysts for Organic Reactions. *Chem. Soc*. Rev. 2008, 37 (9), 2096–2126.

3 Della Pina, C.; Falletta, E.; Prati, L.; Rossi, M. Selective Oxidation Using Gold. *Chem. Soc. Rev*. 2008, 37 (9), 2077–2095.

4 Johnson, B. F. G. Model Nanoparticles in Catalysis. Met. Nanoparticles Clust. Adv. *Synth. Prop.* Appl. 2017, 24 (October), 165–199.

5 Klabunde, K. J.; Mulukutla, R. S. Chemical and Catalytic Aspects of Nanocrystals; 2003; Vol. 3.

6 Leigh Sumner. Electrocatalytic Oxygen Reduction Studies on Gold Nanoparticles, 2018, Vol. 84.

7 Miola, M.; Hu, X.-M.; Brandiele, R.; Bjerlund, E. T.; Gronseth, D. K.; Durante, C.; Pedersen, S. U.; Lock, N.; Skrydstrup, T.; Daasbjerg, K. Ligand-Free Gold Nanoparticles Supported on Mesoporous Carbon as Electrocatalysts for $CO_2$ Reduction. J. $CO_2$ Util. 2018, 28 (June), 50–58.

8 Zheng, N.; Stucky, G. D. A General Synthetic Strategy for Oxide-Supported Metal Nanoparticle Catalysts. J. Am. *Chem. Soc.* 2006, 128 (44), 14278–14280.

9 Miyamura, H.; Matsubara, R.; Miyazaki, Y.; Kobayashi, S. Aerobic Oxidation of Alcohols at Room Temperature and Atmospheric Conditions Catalyzed by Reusable Gold Nanoclusters Stabilized by the Benzene Rings of Polystyrene Derivatives, 2007, Vol. 46.

10 Gangula, A.; Podila, R.; M., R.; Karanam, L.; Janardhana, C.; Rao, A. M. Catalytic Reduction of 4-Nitrophenol Using Biogenic Gold and Silver Nanoparticles Derived from Breynia Rhamnoides. *Langmuir* 2011, 27 (24), 15268–15274.

11 Pradhan, N.; Pal, A.; Pal, T. Silver Nanoparticle Catalyzed Reduction of Aromatic Nitro Compounds. *Colloids Surfaces A Physicochem. Eng. Asp.* 2002, 196, 247–257.

12 Rode, C. V.; Vaidya, M. J.; Chaudhari, R. V. Synthesis of p -Aminophenol by Catalytic Hydrogenation of Nitrobenzene . *Org. Process Res. Dev.* 2002, 3 (6), 465–470.

13 Panigrahi, S.; Basu, S.; Praharaj, S.; Pande, S.; Jana, S.; Pal, A.; Ghosh, S. K.; Pal, T. Synthesis and Size-Selective Catalysis by Supported Gold

Nanoparticles: Study on Heterogeneous and Homogeneous Catalytic Process. J. Phys. *Chem. C* 2007, 111 (12), 4596–4605.

14 Aditya, T.; Pal, A.; Pal, T. Nitroarene Reduction: A Trusted Model Reaction to Test Nanoparticle Catalysts. *Chem. Commun.* 2015, 51 (46), 9410–9431.

15 Kurtan, U.; Baykal, A.; Sözeri, H. Recyclable Fe3O4@Tween20@Ag Nanocatalyst for Catalytic Degradation of Azo Dyes. J. Inorg. *Organomet. Polym. Mater*. 2015, 25 (4), 921–929.

16 Whang, T. J.; Hsieh, M. T.; Chen, H. H. Visible-Light Photocatalytic Degradation of Methylene Blue with Laser-Induced Ag/ZnO Nanoparticles. *Appl. Surf. Sci.* 2012, 258 (7), 2796–2801.

17 Kielar, F.; Talbot, H. M.; Johnson, K. L. Oxidative Decolorization of Acid Azo Dyes by a Mn Oxide Containing Waste. *Environ. Sci. Technol. 2*010, 44 (3), 1116–1122.

18 Xiao, L.; Liu, L.; Zhu, H.-Y.; Jiang, R.; Zeng, G.-M. Efficient Decolorization of Azo Dye Solution by Visible Light-Induced Photocatalytic Process Using SnO2/ZnO Heterojunction Immobilized in Chitosan Matrix. *Chem. Eng. J.* 2011, 172 (2–3), 746–753.

19 Park, H.; Park, Y.; Kim, W.; Choi, W. Surface Modification of TiO2 Photocatalyst for Environmental Applications. J. Photochem. Photobiol. *C*

Photochem. Rev. 2013, 15 (1), 1–20.

20 Lachheb, H.; Puzenat, E.; Houas, A.; Ksibi, M.; Elaloui, E.; Guillard, C.; Herrmann, J.-M. Photocatalytic Degradation of Various Types of Dyes (Alizarin S) in Water by UV-Irradiated Titania. Appl. Catal. B Environ. 2002, Volume 39 (Issue 1), 75–90.

21 Turkevich, J.; Stevenson, P. C.; Hillier, J. A Study of the Nucleation and Growth Processes in the Synthesis of Colloidal Gold. Trans. *Faraday Soc.* 1952, 55, 23.

22 Cushing, B. L.; Kolesnichenko, V. L.; O'Connor, C. J. Recent Advances in the Liquid-Phase Syntheses of Inorganic Nanoparticles. *Chem. Rev.* 2004, 104 (9), 3893–3946.

23 Brust, M.; Walker, M.; Bethell, D.; Schiffrin, D. J.; Whyman, R. Synthesis of Thiol-Derivatised Gold Nanoparticles In. J. *Chem. Soc. Chem. Commun.* 1994, No. 7, 801–802.

24 Hutchings, G. J.; Brust, M.; Schmidbaur, H. Gold-an Introductory Perspective. *Chem. Soc. Rev*. 2008, 37 (9), 1759–1765.

25 G. Frens. Controlled Nucleation for the Regulation of the Particle Size in Monodisperse Gold Suspensions. *Nat. Phys. Sci.* 1973, 241, 20–22.

26 Kumar, S.; Gandhi, K. S.; Kumar, R. Modeling of Formation of Gold Nanoparticles by Citrate Method. Ind. Eng. *Chem. Res.* 2007, 46 (10), 3128–3136.

27 Frens, G. Particle Size and Sol Stability in Metal Colloids. Kolloid-Zeitschrift Zeitschrift für Polym. 1972, 250 (7), 736–741.

28 Mühlpfordt, H. The Preparation of Colloidal Gold Particles Using Tannic Acid as an Additional Reducing Agent. *Experientia* 1982, 38 (9), 1127–1128.

29 Chen, X.-P.; Shan, G.-R.; Huang, J.; Huang, Z.-M.; Weng, Z.-X. Synthesis and Properties of Acrylic-Based Superabsorbent**. *J. Appl. Polym. Sci.* 2004, 92 (1), 619–624.

30 Adamik, R.; Hernández-Ibáñez, N.; Iniesta, J.; Edwards, J.; Howe, A.; Armstrong, R.; Taylor, S.; Roldan, A.; Rong, Y.; Malpass-Evans, R.; et al. Platinum Nanoparticle Inclusion into a Carbonized Polymer of Intrinsic Microporosity: Electrochemical Characteristics of a Catalyst for Electroless Hydrogen Peroxide Production. *Nanomaterials* 2018, 8 (7), 542.

31 He, D.; He, D. S.; Yang, J.; Low, Z. X.; Malpass-Evans, R.; Carta, M.; McKeown, N. B.; Marken, F. Molecularly Rigid Microporous Polyamine Captures and Stabilizes Conducting Platinum Nanoparticle Networks. *ACS Appl. Mater. Interfaces* 2016, 8 (34), 22425–22430.

32 Rong, Y.; He, D.; Malpass-Evans, R.; Carta, M.; McKeown, N. B.; Gromboni, M. F.; Mascaro, L. H.; Nelson, G. W.; Foord, J. S.; Holdway, P.; et al. High-Utilisation Nanoplatinum Catalyst (Pt@cPIM) Obtained via Vacuum Carbonisation in a Molecularly Rigid Polymer of Intrinsic Microporosity. *Electrocatalysis* 2017, 8 (2), 132–143.

33 Dhakshinamoorthy, A.; Asiri, A. M.; Garcia, H. Metal Organic Frameworks as Versatile Hosts of Au Nanoparticles in Heterogeneous Catalysis. *ACS Catal.* 2017, 7 (4), 2896–2919.

34 Esumi, K.; Isono, R.; Yoshimura, T. Preparation of PAMAM- and PPI-Metal (Slver, Platinum, and Palladium) Nanocomposites and Their Catalytic Activities for Reduction of 4-Nitrophenol. *Langmuir* 2004, 20 (1), 237–243.

35 Heidari, A.; Moghimi, H.; Rashidiani, J.; Taheri, R. A. CHEMISTRY Molecular Development of Silver Nanoparticles-Loaded Poly Acrylic Acid Hydrogel as a Catalyst for Dye Degradation. *Phys. Chem. Res.* 2018, 6 (4), 857–869.

36 Lu, Y.; Pérez-Lorenzo, M.; Dzubiella, J.; Hervés, P.; Ballauff, M.; Liz-Marzán, L. M. Catalysis by Metallic Nanoparticles in Aqueous Solution: Model Reactions. *Chem. Soc. Rev*. 2012, 41 (17), 5577.

37 Deng, Y.; Cai, Y.; Sun, Z.; Liu, J.; Liu, C.; Wei, J.; Li, W.; Liu, C.; Wang, Y.;

Zhao, D. Multifunctional Mesoporous Composite Microspheres with Well-Designed Nanostructure: A Highly Integrated Catalyst System. J. Am. *Chem. Soc.* 2010, 132 (24), 8466–8473.

38 Li, L.; Niu, R.; Zhang, Y. Ag-Au Bimetallic Nanocomposites Stabilized with Organic-Inorganic Hybrid Microgels: Synthesis and Their Regulated Optical and Catalytic Properties. *RSC Adv*. 2018, 8 (22), 12428–12438.

Chapter 6

# Conclusions

Thermogalvanic (thermoelectrochemical) systems can employ heat difference for the generation of electrical power by utilising the entropy change associated with a redox process. The main objective of this thesis was to investigate novel systems for this, mainly by either the application of novel redox couples or the application of nanoparticles to enhance known systems. A key part throughout has been the development of novel experimental apparatus, required to investigate the redox system's Seebeck coefficient and the thermogalvanic cells' power density. This was achieved using using different thermogalvanic cell designs, such as homemade glass battery, coated battery casings, custom cells for gel discs, as well as self-contained spherical cell systems simply housed inside plastic washers. When novel systems found limited applications within thermogalvanic cells, they were also extended to other redox-based systems, in the case of the spherical gels.

In Chapter 2, the thermoelectrochemistry of vanadium systems were investigated for the first time. This was prompted by the current intense investigation of the vanadium V(IV) / V(V) redox couple in the contexts of electrical energy harvesting, storage and release. As such, the aqueous thermoelectrochemistry of the common all-vanadium redox couple redox flow battery electrolyte, acidified $VOSO_4$ and $NaVO_3$, was investigated. While it was found to be capable of converting a temperature gradient into electricity, insufficient thermodynamics and kinetics was observed.

Unexpectedly, the facile electrodeposition of vanadium oxide deposits was noted on glassy carbon and stainless steel when non-acidified electrolyte was used; this was capable of reversible Faradaic insertion (intercalation) and release of sodium ions in neutral, unbuffered aqueous solution. A significant observation was that intercalated $Na^+$ ions migrated from the colder electrode to the hotter electrode, with an associated thermogalvanic current generation. When the temperature gradient was removed, the re-balancing of the $Na^+$ ion content between the two intercalation electrodes resulted in a flow of current in the opposite direction. Accordingly, this demonstrates two opportunities; waste thermal energy harvesting and waste heat energy storage.

In Chapter 3, a preliminary study into gelling electrolytes for thermogalvanic cells was performed. Here, the goal was to use relatively benign (*i.e.* edible) gelling agents. While ultimately agar agar was successful, for the ferri/ferrocyanide system it required heating, and then had to be set in the desired shape. For the iodide/triiodide redox couple, this prevented gelation after heating and cooling, but gelled systems could be prepared by soaking pre-formed gels. However, this was noted to restrict the ability to vary the concentration of the materials inside the gel. Therefore further study aimed to utilise pre-formed commercial super-adsorbent gels.

In Chapters 4 and 5, gold nanoparticles were employed in conjunction with commercial super-adsorbent gels. Conventional thermogalvanic system convert a temperature gradient into electricity by utilising redox chemistry, with a resulting electron transfer followed by physical migration of ions, in order to sustain current generation. However, the kinetics of electron transfer and the physical mass transport of these redox couples are known to be major limitations. Attempts were made to overcome these limitations, such that in Chapter 4 thermogalvanic cells containing the ferricyanide/ferrocyanide redox couple were developed whereby the gold nanoparticles were either immobilised at the electrode surface or evenly distributed throughout the electrolyte. This was achieved by developing the novel synthesis of gold nanoparticles inside single spheres of super-adsorbent sodium polyacrylate gels. Both methods of utilising gold nanoparticles demonstrated electrocatalytic improvement, evidenced by significant decreases in the electron transfer resistance. However, the distribution of the gold nanoparticles throughout the gel did not contribute any detectable improvement in the rate of charge propagation. Noticeably, the improvement in the thermogalvanic measurements were only moderate, with a major shortcoming being the instability of the gold nanoparticles in contact with the ferricyanide | ferrocyanide electrolyte over time. Therefore, further improvement in this area would likely require the development of a new electrolyte which is stable in

the negatively charged polyacrylate system (i.e. the redox couple cannot be positively charged) and needs to be stable in the presence of gold nanoparticles.

Chapter 5 explored further investigation of the gold nanoparticle system. Given that the formation of polyacrylate hydrogel-embedded gold nanoparticles was established using a new synthetic route, but attempts to use these to develop stable thermogalvanic cells were unsuccessful, other catalysed redox processes were explored. As such, the AuNPs hydrogels were first characterised by UV-Vis and cryo-TEM. The AuNP hydrogels were also demonstrated to be as effective catalysts for the model (chemical) reduction of both 2- and 4-nitrophenol to 2- and 4-aminophenol, respectively. The utility of these immobilised AuNP were demonstrated by their application within artificial saline environments; the catalytic reduction of 4-nitrophenol was possible in a model potassium chloride solution, whereas colloidal AuNP were completely unstable and therefore deactivated in this environment. Such saline resistance seemed also not been demonstrated previously by other types of AuNP systems, to the best of our knowledge.